

Dissertations and Theses

7-2018

Improving Seaglider Efficiency: An Analysis of Wing Shapes, Hull Morphologies, and Propulsion Methods

Christopher James Hockley

Follow this and additional works at: <https://commons.erau.edu/edt>



Part of the [Mechanical Engineering Commons](#)

Scholarly Commons Citation

Hockley, Christopher James, "Improving Seaglider Efficiency: An Analysis of Wing Shapes, Hull Morphologies, and Propulsion Methods" (2018). *Dissertations and Theses*. 418.
<https://commons.erau.edu/edt/418>

IMPROVING SEAGLIDER EFFICIENCY: AN ANALYSIS OF WING SHAPES, HULL
MORPHOLOGIES, AND PROPULSION METHODS

by

Christopher James Hockley

A Dissertation Submitted to the College of Engineering Department of Mechanical
Engineering in Partial Fulfillment of the Requirements for the Degree of
Doctor of Philosophy in Mechanical Engineering

Embry-Riddle Aeronautical University
Daytona Beach, Florida
July 2018

IMPROVING SEAGLIDER EFFICIENCY: AN ANALYSIS OF WING SHAPES, HULL
MORPHOLOGIES AND PROPULSION METHODS

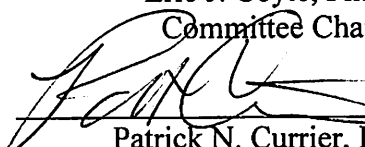
by

Christopher James Hockley

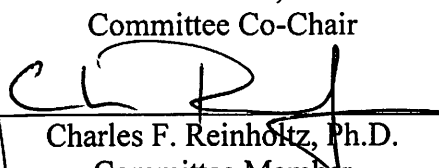
This dissertation was prepared under the direction of the candidate's Dissertation Committee Chair, Dr. Eric J. Coyle, Associate Professor, Daytona Beach Campus, the Committee Co-Chair Dr. Brian K. Butka, Associate Professor, Daytona Beach Campus, and Thesis Committee Members Dr. Patrick N. Currier, Associate Professor, Daytona Beach Campus, Dr. Charles F. Reinholtz, Professor, Daytona Beach Campus, and Dr. Snorri Gudmundsson, Associate Professor, Daytona Beach Campus, and has been approved by the Dissertation Committee. It was submitted to the Department of Mechanical Engineering in partial fulfillment of the requirements for the degree of Doctorate of Philosophy in Mechanical Engineering

Dissertation Review Committee:


Eric J. Coyle, Ph.D.
Committee Chair

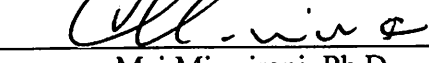

Patrick N. Currier, Ph.D.
Committee Member


Brian K. Butka, Ph.D.
Committee Co-Chair


Charles F. Reinholtz, Ph.D.
Committee Member


Snorri Gudmundsson, Ph.D.
Committee Member


Eduardo Divo, Ph.D.
Ph.D. Program Coordinator,
Mechanical Engineering


Maj Mirmirani, Ph.D.
Dean, College of Engineering


Eduardo Divo, Ph.D.
Department Chair,
Mechanical Engineering


Christopher Grant, Ph.D.
Associate Vice President of Academics

Date: 7/13/2018

Acknowledgements

If you want to go fast, go alone. If you want to go far, go together. I have said this to people on more than one occasion, and I do believe it. As many of you can attest, some more vehemently than others, this was not a fast process for me. I believe the words excruciatingly or mind-bogglingly slow have been uttered on more than a few occasions. Despite the lack of celerity, we did cover a heck of a distance, so you can deduce from that I had a lot of people help me. If I forget to thank you here, I am sorry. So by way of a blanket statement. You all have my profound and heartfelt gratitude.

This work would never have started let alone been completed without the grant from the Office of Naval Research, Contract N00014-15-1-2746. I need to thank the University, particularly the Computational Mathematics Department for the use of the Wave Tank in the Center for Nonlinear Waves, especially Dr. Ludu and M A Qayyum Mazumder for ensuring we didn't flood the building, and the College of Engineering for generally putting up with and supporting me.

To my committee: Dr. Butka, Dr. Coyle, Dr. Currier, Dr. Gudmundsson, and Dr. Reinholtz. My supervisors, advisors, councilors, consiglieri, the people who kept me plodding down the right path. I do not know how you all managed it but thank you. Thank you for your time, your patience, your wisdom, and sometimes your indulgence. Dr. Butka, I know this wasn't easy, I am sure at times you wanted to tear your hair out, but we made it. The poking, prodding, questioning, cajoling, guiding, humor, unintentionally scary emails, the meetings, oh so many meetings, and putting up with my random acts of linguistic legerdemain. It all worked. Although I am sure we both aged about a decade in the process. Dr. Coyle and Dr. Currier, good cop and bad cop. You were

both there when I needed reassurance, a kick in the behind, or some perspective. Dr. Gudmundsson, thank you for being the man who is not afraid of non-dimensional coefficients, and for having the knowledge and perspective I needed when it came to the gliding part of underwater gliders. Dr. Reinholtz, no matter how you slice it a vast majority of this is your fault. I came into robotics by happenstance, and through your personality, actions, and attitude made it so I couldn't imagine being anywhere else. Tim and Stephen, you guys sure helped make things interesting. You also helped keep me sane, and on track. Neither of these are easy things. We also had a lot of fun and I know we will never be the same after this. Thank you for being there through all the mountains, and molehills, the whole time being accepting of my myriad of quirks. James, Rebecca, Victoria without you helping, organizing, and just being there I would not have gotten this far. To all the members of RAER past and present. I would not have known as much as I do now without working with you all, it was mostly fun.

To my family. Thank you for being there, for supporting me, and not getting bored when I talk about what I am doing. To my parents thank you for all the hard work and sacrifices you made to bring us to the US and putting me through school, and to my little brother for helping in more ways than I had any right to expect, or deserve. To my extended family, thank you for the game nights, dinners, the talks, the mental health breaks, and generally just making sure I kept moving. I have always counted myself lucky to have a support group of family and friends as great as I do. Thank you.

Abstract

Researcher: Christopher James Hockley

Title: Improving Seaglider Efficiency: An Analysis of Wing Shapes, Hull Morphologies and Propulsion Methods

Institution: Embry-Riddle Aeronautical University

Degree: Doctor of Philosophy in Mechanical Engineering

Year: 2018

Autonomous underwater gliders are a family of autonomous underwater vehicles used for long-term observation of oceanic environments. These gliders leverage changes in buoyancy and the resulting vertical motion, to generate forward locomotion via hydrodynamic surfaces. In order to function for extended periods, these systems operate in a low-speed, low-drag regime. This research examines factors impacting the operational efficiencies of gliders, including morphological changes, configuration changes, and propulsion. An interesting question arises when considering the operational efficiencies of conventionally propelled systems at the operating speeds typical of gliders. Can a conventional propulsion system match the efficiency of an underwater glider buoyancy engine? A first-principles, energy-based approach to glider operations was derived and verified using real world data. The energy usage for buoyancy driven propulsion was then compared to conventional propulsion types. The results from these calculations indicate that a conventionally propelled autonomous underwater vehicle can compete with and in some cases outperform a buoyancy driven system given the proper propulsive efficiency.

I. Table of Contents

ACKNOWLEDGEMENTS	II
ABSTRACT	IV
I. TABLE OF CONTENTS.....	V
II. TABLE OF TABLES	VIII
III. TABLE OF FIGURES	IX
IV. TABLE OF EQUATIONS	XII
CHAPTER 1: INTRODUCTION.....	1
1.1 AN INTRODUCTION TO SEAGLIDERS.....	1
1.2 CHAPTER OUTLINE	6
<i>Chapter 1</i>	6
<i>Chapter 2</i>	6
<i>Chapter 3</i>	6
<i>Chapter 4</i>	7
<i>Chapter 5</i>	7
<i>Chapter 6</i>	7
1.3 THE SIGNIFICANCE OF THE STUDY - SEAGLIDERS AND THEIR APPLICATIONS	7
1.4 STATEMENT OF THE PROBLEM – HYPOTHESES STATEMENT	9
1.5 DELIMITATIONS	10
1.6 LIMITATIONS AND ASSUMPTIONS	11
1.7 AN AEROSPACE PERSPECTIVE ON SEAGLIDERS	11
1.8 ENERGY USAGE OF A SEAGLIDER	14
1.9 DEFINITIONS OF TERMS	20
1.10 LIST OF ACRONYMS	21
CHAPTER 2: REVIEW OF THE RELEVANT LITERATURE	22
2.1 INTRODUCTION	22
2.2 SEAGLIDER HISTORY	22
2.3 SEAGLIDER DESIGN, AND KEY CONCEPTS	26
2.4 CURRENT GENERATION OF SEAGLIDER	27
2.5 SEAGLIDER MORPHOLOGY	28
2.6 SURVEY OF CURRENT SEAGLIDER RESEARCH AREAS.....	29
2.7 MODELING AND CONTROL.....	30
2.8 ENERGY USAGE	31
2.9 PROPULSION	31
2.10 TESTING VERIFICATION.....	32
2.11 SUMMARY.....	33
CHAPTER 3: MORPHOLOGICAL CHANGES AND THEIR IMPACT ON AUTONOMOUS UNDERWATER GLIDER PERFORMANCE	34
3.1 INTRODUCTION	34
3.2 RESEARCH APPROACH.....	34

3.3	BODY TYPES.....	36
3.4	LEGACY TYPE.....	37
3.5	INVERSE ZIMMERMAN	38
3.6	VARIABLE INCIDENCE WING	43
3.7	INVERSE ZIMMERMAN CRANKED KITE PLANFORM.....	45
3.8	ANNULAR WINGS	47
3.9	TESTING PROCEDURE.....	48
3.10	RESULTS	50
3.11	SUMMARY.....	52

CHAPTER 4: DERIVATION OF SEAGLIDER ENERGY USAGE, AND EFFICIENCY..... 55

4.1	INTRODUCTION	55
4.2	SEAGLIDER POWER USAGE.....	57
4.3	AUV POWER USAGE	67
4.4	THRUSTER SYSTEM ANALYSIS.....	71
4.5	JET DRIVE	71
4.6	PULSATILE VORTEX THRUSTER	73
4.7	PROPELLER DRIVEN.....	75
4.8	GENERAL CASE ANALYSIS	78
4.9	AUV AND AUG RANGE VERSUS OPERATIONAL DEPTH	81
4.10	OPTIMIZING THE SURROGATE AUV FOR THRUSTER ONLY OPERATIONS.....	83
4.11	SUMMARY.....	84

CHAPTER 5: WAVE TANK TESTING..... 87

5.1	INTRODUCTION	87
5.2	DESIGN PARAMETERS	88
5.3	WAVE TANK/WATER TUNNEL	88
5.4	FORCE BALANCE DESIGN	89
5.5	LOAD CALIBRATION	93
5.6	EXPERIMENTAL SETUP.....	93
5.7	TESTING PROCEDURE.....	96
5.8	TESTING RESULTS.....	97
5.9	DISCUSSION OF RESULTS.....	99
5.10	CONCLUSION	105

CHAPTER 6: CONCLUSION AND FUTURE WORK 107

6.1	SUMMARY.....	107
6.2	CONCLUSIONS.....	110
6.3	FUTURE WORK	111
6.3.1	μ AUV	112
6.3.2	3D Printing/Bespoke Manufacturing.....	112
6.3.3	Energy Modeling	113
6.3.4	Propulsive Methodologies	113
6.3.5	Application of smart materials	114
6.3.6	Energy Harvesting.....	115
6.4	SUMMARY.....	116

REFERENCES..... 118

BIBLIOGRAPHY 125

APPENDIX A	132
APPENDIX B	133
B1 SPARKFUN OPENSCALE [82]	133
B2 MICRO LOAD CELL (0-780G) - CZL616C [83]	134
B3 MICRO LOAD CELL (0-5KG) - CZL635 [84].....	138
APPENDIX C	143
C1 ENERGY ANALYSIS MATLAB SCRIPT	143
APPENDIX D	145
D1 MANUFACTURER SUPPLIED DATA FOR THE BLUE ROBOTICS T200 THRUSTER.....	145
D2 STATIC RUN 1 OF THE BLUE ROBOTICS T200 THRUSTER***	146
D3 STATIC RUN 2 OF THE BLUE ROBOTICS T200 THRUSTER***	147
D4 STATIC RUN 3 OF THE BLUE ROBOTICS T200 THRUSTER***	148
D5 DYNAMIC RUN 1 OF THE BLUE ROBOTICS T200 THRUSTER***	149
APPENDIX E	150
E1 TEST STAND ASSEMBLY OVERVIEW	151
E2 TEST STAND BASE ASSEMBLY OVERVIEW.....	152
E3 TEST STAND BASE 5 KG SIDE SCHEMATIC	153
E4 TEST STAND BASE RIGHT SIDE SCHEMATIC	154
E5 TEST STAND BASE LEFT SIDE SCHEMATIC.....	155
E6 TEST STAND BASE TOP SCHEMATIC	156
E7 TEST STAND SWING ARM OVERVIEW	157
E8 TEST STAND SWING ARM SCHEMATIC	158
E9 TEST STAND SWING ARM GUSSET SCHEMATIC.....	159
E10 TEST STAND SWING ARM TOP 5KG SIDE SCHEMATIC	160
E11 TEST STAND SWING ARM TOP 0.780 KG SIDE SCHEMATIC	161
E12 TEST STAND MAIN SHAFT	162
E13 TEST STAND CREEP TESTING CONFIGURATION.....	163
E14 TEST STAND STRUCTURAL CALCULATIONS	164
E15 "AEREON" LIGHTER THAN AIR SHIP. RETRIEVED FROM [17].....	166

II. Table of Tables

Table 1: Differences Between Seagliders and Heavier Than Air Gliders	11
Table 2 Legacy Seaglider Analog Physical Properties	38
Table 3: Typical Slocum Glider G2 Physical Properties and Performance Characteristics Adapted From [36]	56
Table 4: Steady State Glide Data Taken from Insitu AUG Operations.....	58
Table 5: Seaglider Range Varying Efficiency and Hotel Load	66
Table 6: Typical Slocum Glider Physical Properties for Determination of Steady State Loading. Adapted from [36].....	91
Table 7: Steady State Glide Data Taken from Insitu Seaglider Operations for Determination of Steady State Loading. Adapted from [39]	92

III. Table of Figures

Figure 1: An Illustration of a Seaglider Undertaken Multiple Yos, Highlighting the Characteristic Seaglider Sawtooth Flight Profile.....	2
Figure 2: Legacy Type Glider (Slocum Seaglider Left) [2] and a Flying Wing Type Glider (Liberdade XRay1 Seaglider Right) [3]	4
Figure 3: The Indian River Lagoon, Located on Florida's Atlantic Coast. This Image Taken From an Orbiting Satellite Highlights a Large Algal Bloom, which is particularly evident when compared to the blue waters of the Atlantic Ocean [5]	5
Figure 4: Seaglider Buoyancy Engine Current Draw and Flight Profile vs Time [14]....	15
Figure 5: Buoyancy Engine Current Draw at a Depth of Approximately 12 meters [14]	16
Figure 6: Buoyancy Engine Pump Energy Usage at Depth [14]	18
Figure 7: Buoyancy Engine Total Power Usage Compared to Thruster Power Usage and Flight Profile	19
Figure 8: Buoyancy Engine Cumulative Energy Usage Compared to Thruster Cumulative Energy Usage	20
Figure 9: Dr. Solomon Andrews “Gravitation” Propelled Lighter Than Air Ship “Aereon”. In 1863, the Aereon, successfully demonstrated the utilization of the modulation of buoyancy to propel itself against the wind. (1906). Retrieved from [17]. A larger version is available in Appendix E	23
Figure 10: Slocum G2 Hybrid Autonomous Underwater Glider Retrieved from [20]....	25
Figure 11: Spray Autonomous Underwater Glider Retrieved from [21]	25
Figure 12: Kongsberg Seaglider Autonomous Underwater Glider Retrieved from [22].	26
Figure 13: Half-Yo Diagram Highlighting Slant range and its relation to glide path angle, γ and depth, h	35
Figure 14: Legacy Seaglider Analog Rendering	37
Figure 15: NACA 65(2)-415 Airfoil Cross-section Retrieved from [75]	39
Figure 16: Lift Coefficient vs Angle of Attack for the NACA 65(2)-415 Airfoil.....	39
Figure 17: Drag Coefficient vs Angle of Attack for the NACA 65(2)-415 Airfoil.....	40

Figure 18: Lift Coefficient vs Drag Coefficient of the NACA 65(2)-415 Airfoil.....	40
Figure 19: Illustration Highlighting Multiple Low Reynolds Number Planforms and their Resulting Wing Tip Vortices (dotted lines) Retrieved from [72]	41
Figure 20: Inverse Zimmerman Planform Seaglider Test Model Before Finishing	43
Figure 21: Illustration of the Angle of Incidence of an Aircrafts Wing Compared when to its Longitudinal Axis Retrieved from [74].....	44
Figure 22: Inverse Zimmerman Cranked Kite Planform Seaglider Test Model	44
Figure 23: Top Down Projection of a Cranked Kite Planform Retrieved from [72]	45
Figure 24: A Flying Wing Type Seaglider Retrieved from [30]	46
Figure 25: Annular Wing Aircraft Concept Retrieved from [77].....	47
Figure 26: An Example of an Aircraft Producing Wingtip Vortices Produced by an Aircraft Retrieved from [78].....	48
Figure 27 Seaglider Glide Path Test Tank.....	49
Figure 28 Composite Image Illustrating Inverse Zimmerman Planform featuring an Annular Wing's Glide Path	50
Figure 29: Glide Slope vs Angle of Incidence for The Inverse Zimmerman Glider and Legacy Glider Cataloguing Glide Slopes with a Conventional Wing and with an Annular Wing while Varying the Angle of Incidence. Each test consisted of 5 separate runs.....	51
Figure 30: Annotated Free-Body Diagram of a Slocum Electric Autonomous Underwater Glider in Operation	56
Figure 31: Seaglider Sawtooth Yo-Yo Flightpath	57
Figure 32: Simplified Half-Yo Descending Leg Flight Pattern	59
Figure 33: One Yo cycle Showing Distances Covered	63
Figure 34: Jet Efficiency Varying Inlet Efficiency and Vehicle to Jet Velocity Ratio	72
Figure 35: Pulsatile Vortex Thruster Schematic Showing Fluid Entrainment (Left) and Vortex Ring Formation Resulting During Ejection (Right) Retrieved from [66]	73
Figure 36: Propulsive Efficiency of a PVT vs. Duty Cycle Retrieved from [78].....	74
Figure 37: T200 Thrust vs PWM	77

Figure 38: T200 PWM vs Efficiency	77
Figure 39 Depth Variations Impact on AUV and AUG Range	83
Figure 40 ERAU Wave Tank	89
Figure 41 Final Design of the T-type Swing Arm Force Balance (Shown with the Immobilizing Rod Inserted).....	90
Figure 42: Experimental Force Balance Installed in the ERAU Wave Tank Facility.....	94
Figure 43: T200 Thruster Operating at a PWM Setting of 1600 in a Static Flow Condition.....	95
Figure 44: T200 Thruster and Force Balance Under Testing the ERAU Wave Tank with Fluid Velocity of 0.015 meters per second.....	95
Figure 45 T200 PWM Thrust Data	100
Figure 46: T200 PWM Power In Data.....	100
Figure 47: T200 PWM Power Out Data	104
Figure 48: T200 PWM Efficiency Curves for Static and Dynamic Operation Cases....	104
Figure 49: T200 Thrust Efficiency Data	105

IV. Table of Equations

Equation 1: Seaglider Propulsive Force Equivalence.....	57
Equation 2: Calculation of Glide Path Angle.....	59
Equation 3: Half Yo Distance Covered.....	60
Equation 4: Propulsive Energy Usage Per Operation	60
Equation 5: Propulsive Energy Usage Per Yo Cylce	62
Equation 6: Distance Covered Gliding Per Yo	63
Equation 7: Horizontal Distance Covered Gliding Per Yo	63
Equation 8: Time Required to Cover Horizontal Distance Covered in Multi-Yo Flight	64
Equation 9: Hotel Load Energy Calculation.....	65
Equation 10: Number of Yo Cycles for a Given Energy Usage	65
Equation 11: Seaglider Range Equation.....	65
Equation 12: Thrust Drag Equivalence.....	67
Equation 13: Drag Force.....	68
Equation 14: Buoyant Force Propulsive Component	68
Equation 15: Thruster Energy Required	69
Equation 16: AUV Thruster Efficiency Target	69
Equation 17: Waterjet Efficiency.....	72
Equation 18: Power Output for a Propeller Based Thruster	75
Equation 19: Efficiency of a Propeller Based System.....	76
Equation 20: Force to PWM Translation.....	78
Equation 21: Figure of Merit Definition.....	79
Equation 22: Buoyancy Engine Energy Usage as a Function of Depth and Efficiency.	79
Equation 23: Thruster Energy Usage as a Function of Drag Distance Covered and Efficiency	79

Equation 24: Buoyancy Motive Force.....	79
Equation 25: Thruster Energy Usage as a Function of Motive Buoyant Force Distance Covered and Efficiency	80
Equation 26: Simplified Thruster Energy Usage.....	80
Equation 27: Fully Expanded Figure of Merit.....	80
Equation 28: Simplified Figure of Merit	80
Equation 29: Final Figure of Merit.....	81
Equation 30: Final Figure of Merit with Surface Losses.....	81
Equation 31: Longitudinal Component of the Buoyant Force	92

Chapter 1: Introduction

1.1 An Introduction to Seagliders

Autonomous Underwater Gliders (AUG) as the name suggest are a subset of Autonomous Underwater Vehicles (AUV) that glide through the ocean. Often referred to as gliders or seagliders these vehicles utilize their wings to generate hydrodynamic rather than aerodynamic forces. Unlike their aerial counterparts, that rely solely on gravity, its potential, and the occasional thermal as a motive force, seagliders use the interaction of lift and buoyancy, allowing them to glide forward while either ascending or descending.

Henry Strommel first posited the concept of a buoyancy-driven seaglider in his 1989 article, “The Slocum Mission.” Intended to serve as part of an ocean sampling flotilla consisting of 1000’s of small floats called Slocums. These floats would “migrate vertically through the ocean by changing ballast, and they can be steered horizontally by gliding on wings at about a 35 degrees angle”, [1], operating for long periods of time without human interaction. The only break in this vertical migration would be the occasional respite on the surface to transmit data or gain a positional fix before diving again. Although intermediate iterations of this concept existed shortly after “The Slocum Missions” publication, the first identifiable seagliders did not exist for another decade.

Modern seagliders utilize the combination of buoyancy modulation and lifting surfaces to propel themselves in a series of sawtooth maneuvers called yos, illustrated in Figure 1. Gliders perform these yos constantly to move forward, operating at low-speed, on the order of one meter per second. As such, they are in a low-speed, low-drag regime where the hydrodynamic losses incurred via operation are at a minimum.

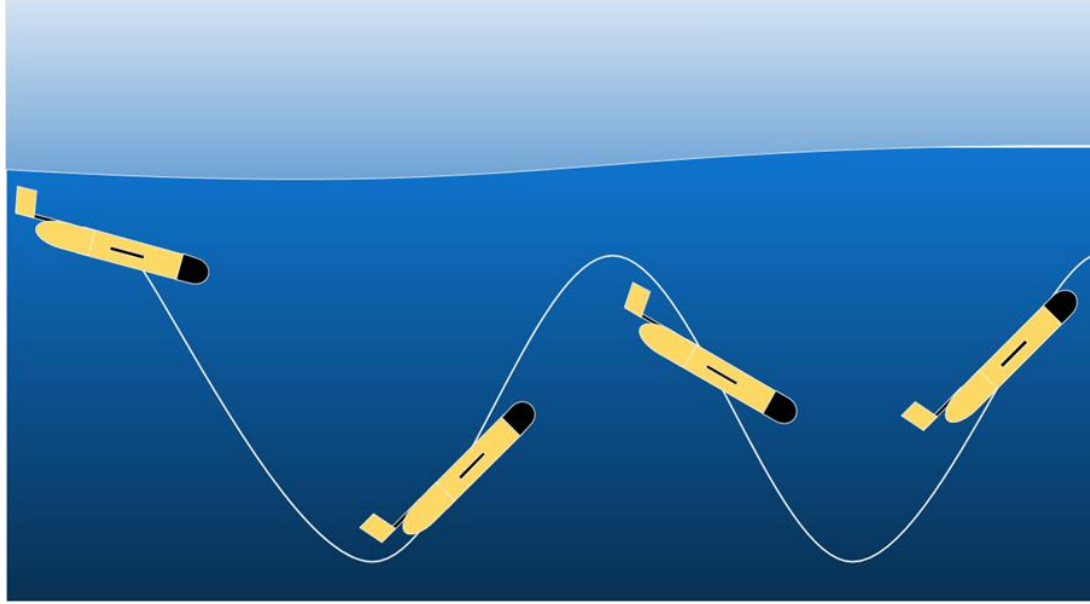


Figure 1: An Illustration of a Seaglider Undertaken Multiple Yos, Highlighting the Characteristic Seaglider Sawtooth Flight Profile

This buoyancy modulation is generated via a system known as a buoyancy engine. As with most engines, this system is run in a cyclic manner to provide propulsive force. At the top of a typical yo cycle, the vehicle needs to reduce its buoyancy in order to sink. It accomplishes this by reducing its displaced volume; the simplest approach to this is pumping fluid onboard into its buoyancy engine, thereby increasing its density. Accompanying this is the slight change in position and orientation of internal masses to fine-tune the pitch of the vehicle. This is done to optimize the system's glide slope and maximize its forward motion for each operation of the buoyancy engine. To further minimize the energy required by the engine, the change in vehicle displaced volume is small, typically no more than a few percent of total displaced volume. When the vehicle reaches the bottom of the dive, it pumps fluid out of the buoyancy engine, increasing the vehicle's displacement, and if necessary, re-adjusting its pitch. This propulsive method,

powered by the movement of a working fluid, the location of the platform's center of buoyancy, and adjustment of the vehicle's center of gravity, form the basis of the system's buoyancy engine.

The saw tooth profile seagliders fly allows them to cover many thousands of miles, remaining in the field for weeks to months at a time. This low-energy, low-noise, long-endurance method of propulsion makes underwater gliders, and platforms like them, ideally suited for long duration environmental studies. During these extended deployments, seagliders autonomously collect data on the surrounding water column, including salinity, oxygen content, and temperature. The transmission of this data gives the operator a near real-time view of the health of the biome.

Seagliders tend to fall into two familial subgroups, the traditional body of revolution design with simple lifting surfaces, referred to here as legacy types shown in

Figure 2 left, and flying wing types, shown in

Figure 2 right. These two types can either be powered electrically, which is by far the most common method, or they can be thermally powered. Thermal systems rely on the temperature gradient of the ocean stratification, to power an onboard phase-change based system, which in turn drives the buoyancy engine.

Legacy type gliders typified by the Slocum, Spray, and eponymously named Seaglider designs are most prevalently in active service. Typically measuring on the order of 2 meters in length by 1 meter in wingspan, legacy types are suited for deeper dives at lower speeds than their flying wing counterparts, which have large hydrodynamically tailored wings. Flying wing systems are both larger and faster than the

legacy types, favoring larger buoyancy engines. Despite the differences in overall design and size these legacy gliders still operate under the same principles.



Figure 2: Legacy Type Glider (Slocum Seaglider Left) [2] and a Flying Wing Type Glider (Liberdade XRay1 Seaglider Right) [3]

Regardless of its familial type, traditionally sealgliders are limited to operations in offshore environments, typically measuring hundreds of meters deep. This rules out their use in large shallow bodies of water, which would otherwise benefit from the mobile, re-taskable, near real-time sensing gliders offer. The focus of this research is the investigation of novel enabling concepts and technologies that could be leveraged to produce systems capable of operation in environments where traditional seagliders would be of limited functionality. An example of this is the Indian River Lagoon, located on the Atlantic coast of Florida. Covering almost 6000 square kilometers, and five Florida counties, the lagoon, shown in

Figure 3, is home to 35 threatened or endangered species and generates \$3.7 billion dollars for the local economy [4]. Despite this body of water's large size, it is

poorly suited for seaglider operations. This is in part due to its shallow nature, frequent traffic, and the environment being full of potential entanglements.

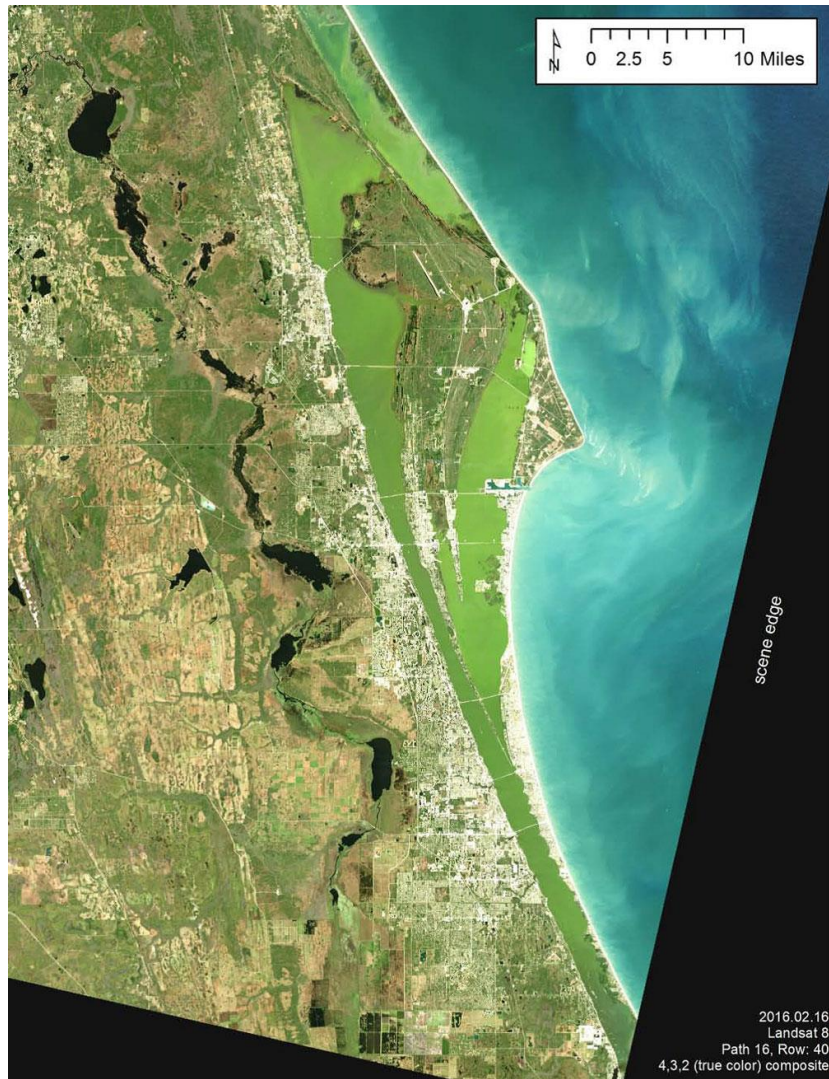


Figure 3: The Indian River Lagoon, Located on Florida's Atlantic Coast. This Image Taken From an Orbiting Satellite Highlights a Large Algal Bloom, which is particularly evident when compared to the blue waters of the Atlantic Ocean [5]

The careful management of the lift to drag ratio and propulsive energy used by any vehicle moving through a fluid, especially a vehicle relying on the dynamic

propulsion of buoyancy-lift interaction for continued operation, is critical. The research described herein is part of an effort to investigate technologies for a novel buoyancy driven winged autonomous submarine capable of operations in environments that traditional seagliders are unable to function. To do this, the research consists of two main tranches: improvement in hydrodynamic efficiency through overall configuration and wing planform and the design, evaluation, and implementation of different propulsion mechanisms. Each of these tranches consists of sub-areas, which are detailed in the following chapters.

1.2 Chapter Outline

The development of this line of questioning is multi-disciplinary in nature and is developed based on the following outline.

- | | |
|-----------|--|
| Chapter 1 | Introduces the reader to seagliders and their importance in the overall framework of autonomous remote sensing. It also briefly describes how seagliders, as buoyancy driven vehicles work, and how this functionality is investigated as part of the research questions. |
| Chapter 2 | This chapter reviews the relevant literature used in this study. It covers work spanning seaglider design and key concepts in which basic concepts of glider morphology is introduced as well as the different propulsive methods. Following this are the key areas of glider research highlighting key works covering controls, propulsion, modeling, and hydrodynamic optimization. Rounding out this chapter are sections covering energy usage, propulsive systems testing and verification. |
| Chapter 3 | Chapter 3 covers morphological changes and the impact they have on seaglider performance. Starting with the overall research approach, moving onto the definition, and anticipated benefits of variable incidence wings. The introduction of the inverse Zimmerman Cranked Kite planform and the annular wing is followed by the testing procedures and results of testing. |

- Chapter 4 Covers the derivation of equations for the estimation of a seagliders energy usage, efficiency, and range. This result is compared with other means of propulsion ranging from jet drives to conventional propeller based system. Data from a real-world conventional propeller based thruster is then used for the determination of whether or not it can operate with comparable efficiency to a seaglider.
- Chapter 5 Chapter 5 consists of the design of experiment, experimentation, and results from work undertaken in the Nonlinear Wave Tank. The results from this experimentation was used to confirm data used in the development of the results of Chapter 4. This testing carried out in phases begins with design and manufacturing of a custom force balance and moved onto static testing. Static testing was performed to confirm values supplied by the manufacturer on thruster performance.
- Chapter 6 Chapter 6 is a summary of the work along with conclusions and recommendations for future research.

1.3 The Significance Of The Study - Seagliders And Their Applications

The ocean is the largest habitat on earth, covering more than 70 percent of the planet, and making up 97 percent of its habitable volume [6]. This sprawling ecosystem and its health are key to our continued survival, as it profoundly influences the weather of the world. As such, collecting data on this biosphere is as important as collecting data on our atmosphere. However, unlike our atmosphere, where measurement can be made by all manner of sensors both direct and remote, the nature of water makes this task far more difficult. Acquiring data from all depths of the oceans requires direct measurement. Communicating this data back to an observation station is far more difficult than the same task in the atmosphere. This is where the multivalent nature of AUVs are revolutionizing oceanography. These system are allowing for the collection of data, be it physical sampling, biological health monitoring, or chemical sampling, and all this is

being done from more places than ever before in greater quantities, greater detail, and greater density.

The need for more oceanographic sampling is what motivated the concept of Autonomous Underwater Gliders to first evolve. Utilizing buoyancy as a motive force is not a new concept in and of itself, with examples of motion derived from changes in displacement being readily available in both the animal kingdom and mechanized world. In the maritime domain, changes in displacement have allowed for the change in depth for systems ranging from oceanographic profiling floats to manned submersibles. It was not until 1989 when Henry Stommel devised the concept of buoyancy modulation to be leveraged into locomotion was fully realized. A complete history of seagliders and their evolution from floats can be found in the seminal work on seaglider control and design by Joshua Graver [7].

Seagliders are near the forefront in a shift to fully autonomous remote sensing technologies for oceanography. As such, the improvement of their overall performance is of key interest to end users ranging from civilian scientists to government entities such as the Office of Naval Research (ONR), and the United States Navy. Both of these groups like the seaglider for its low cost, simplicity and low noise signature. While research on morphological adaptations for improvement in seaglider performance, primarily focusing on the implementation of a blended-wing-body phenotype already exists, the use of variable incidence wings, annular wings, and Low-Reynolds number shaping has had little prior work. The work that does exist has an aviation slant.

In the area of seaglider propulsion, work has been done investigating more efficient path planning [8], changes in actuation methods, such as compressed air, [9], or

shape memory alloys, [10], [11] for the operation of the buoyancy engine, and development of hybrid systems, [12], [13]. Hybrid gliders that use a secondary propulsive system in addition to the buoyancy engine focus on the performance benefits of such a system. These systems all look at expanding the current performance of the glider beyond its originally conceived low-speed, low-drag envelope.

1.4 Statement of the Problem – Hypotheses Statement

There are two main thrusts to this research, both of which are pursuant to the Office of Naval Research award N00014-15-1-2746 Novel Underwater Vehicle Using Buoyancy and Wings. This requires investigation and evaluation of enabling technologies for a novel, buoyancy driven, winged autonomous submersible platform. This focus was translated into investigating transformative technologies that will allow seagliders to pursue missions outside of their normal capabilities.

To do this, two different approaches have been undertaken. The first approach of the research will focus on the morphology of the glider itself. By investigating the impact of hydrodynamic changes based on concepts previously applied to aerospace systems. These approaches are the application of variable incidence wings, annular wings, and an inverse Zimmerman cranked kite planform. The second approach was the investigation of the efficiency of the buoyancy engine itself and the implications of using other propulsive methods in the seaglider low-drag, low-speed regime. It is believed that either of these technologies or the combination of the two will yield for novel systems with unique capabilities, including operation in shallow water environments, a larger speed range, and increased maneuverability.

1.5 Delimitations

To formulate a cogent research approach, a thorough understanding of seagliders is required. This, in turn, required a survey of the current state of the art and research areas for both seagliders and their operation. From this survey, certain areas of the glider design space were deemed outside the scope of this work. Chief among them was the entire family of thermally powered gliders. These systems harness the differential in thermal energy, a result of ocean stratification. The reasoning for this omission is that this family of gliders rely on large differences in the thermoclines, these large gradients are typically found in the more temperate parts of the world, and as such pose a significant limiting factor to their widespread deployment.

The maximum operational depth a glider can achieve also plays a key role in overall seaglider exploration range. This coupled with its diving characteristics determine if the glider will be partaking in a more vertical water column sensing role, or a more horizontal basin level sensing. Depths for these operations range from the tens of meters to many hundreds of meters, with some gliders aiming to operate at depths of thousands of meters for extended periods.

Another area deemed outside of the scope of this work is the sensor or system scheduling domain. This is where sensors and onboard systems activation and operation is scheduled to minimize average power draw and thusly expand available operational reserves. This approach is highly architecture and payload dependent, again limiting its overall probative value.

1.6 Limitations and Assumptions

One of the key assumptions made in this research is that the seaglider's motion is limited primarily to the longitudinal plane. As a majority of a seaglider's operation during any particular operation is limited to this plane it is felt that this assumption is of little overall impact to the study. Following this assumption is whilst in the longitudinal plane a vast majority of operational time is in a steady state or cruise configuration. This minimizes the impact of complicated higher order phenomena such as the added mass the vessel carries along with it.

1.7 An Aerospace Perspective on Seagliders

Embry-Riddle Aeronautical University has a long-standing tradition of aerospace research and education. This common thread runs throughout the community and curriculum, which often leads to problems being looked at from this very particular point of view. As shown in Table 1 there are numerous differences between seagliders and heavier than air gliders. This makes approaching seagliders and their operation from a purely aerospace standpoint somewhat counterintuitive.

Table 1: Differences Between Seagliders and Heavier Than Air Gliders

Seaglider	Heavier than air glider
Neutrally buoyant	Heavier than air
Can stop in place	Needs to move to stay aloft
Denser working fluid	Less dense working fluid
More viscous working fluid	Less viscous working fluid
Higher density working fluid	Lower density working fluid
Density is constant with depth	Density changes with altitude
Small displacement change to vary depth	Large displacement change to vary altitude
Pressure increases with depth	Pressure decreases with altitude

To begin the discussion we note that air gliders are more dense than the surrounding air and are therefore negatively buoyant. Seagliders operate by varying their buoyancy from slightly negative to slightly positive. Seagliders operate at low speeds and a key to their efficiency is that drag forces are tiny at these speeds.

The force due to gravity and the buoyant force are conservative and therefore the work done is path independent. Therefore, the work done is independent of the glide angle. In theory, for a dive down to a depth and then returning to starting depth, the net work done is zero. There are losses due to drag, but these are small at typical seaglider velocities.

When a sea glider reaches the bottom of its yo, the seaglider pressurizes a bladder to expel water and make the vehicle positively buoyant. That pressure is locked and remains throughout the vehicle's ascent. Once at the top of its yo, the pressure stored in the bladder is released to allow the vehicle to take on water and become negatively buoyant. Since the ambient pressure at the top of the yo is substantially lower than the pressure in the bladder, the work accomplished is negative and of roughly the same magnitude as the work performed at depth. This is similar to inflating a balloon and then later releasing the pressure and using it to propel the balloon about the room. However, in seagliders the energy stored in the bladder is just vented and not used in any way. In fact, because of the high-pressure that need to be vented, additional work needs to be done to prevent damage to the pump system. The fact that this stored energy is wasted is what allows a thruster based system to compete with a seaglider with respect to efficiency.

Seagliders can be neutrally buoyant, heavier than air gliders are negatively buoyant. This allows a seaglider to sit stationary at a fixed depth in a water column

without any forward motion, which is impossible for a heavier than air glider in flight.

The medium in which the systems operate in are also vastly different. Water is denser, more viscous and incompressible, when compared to air. These radically different mediums influence the vehicles operating in them. As water is 1000 times denser than air, a small change in overall displacement in water yields a 1000 times larger motive force than a comparable change in displacement in air, making it a far better working fluid for a buoyancy driven system.

The maximum takeoff weight of a Stemme S-12G is 900 kg. To be neutrally buoyant, this would have to displace 735 cubic meters of air, which is equivalent to an 11.2-meter diameter sphere at sea level. A vehicle of this displacement will have both structural and performance issues due to the excessive drag and sail area. Bodies of water have near constant density when compared to their depth. This is untrue for air, with the atmosphere showing a large non-linear variation in density from the surface to the edge space. If the 11.2-meter spherical glider were taken to an altitude of 2 km it would be negatively buoyant, being only able to support 740 kg of the vehicle's 900 kg, a net loss of 160 kg. A typical seaglider uses approximately 250 grams of buoyant force, which can carry the vehicle from the surface to the ocean floor. This assumes the vehicle is capable of achieving that depth without imploding.

The size of the system, viscosity of water and speed at which seagliders operate also has an impact on the vehicle's operational regime. The combination of these factors result in seagliders operating in a regime more akin to large lighter-than-air airships than heavier than air gliders. All of these factors combine resulting in seagliders operating in a fundamentally different way than their airborne counterparts.

1.8 Energy Usage of a Seaglider

A seaglider's energy usage can be broken up into two distinct classes; the hotel load which consists of all energy usage that is non-propulsive in nature, and the propulsive load. In the energy usage analysis presented here a notional platform, based on a Slocum electric glider is examined. This notional system operates under both buoyancy driven and thruster borne paradigms and is covered in more detail in Chapter IV. As both the buoyancy propelled system and thruster borne system are identical in all but method of propulsion, the hotel loads and the impact they have on performance are identical and for the sake of simplicity ignored here.

Typically, seagliders operate at depths on the order of 100 meters. This offers a balance of forward progress per yo, frequency of buoyancy engine operation, and energy expended fighting pressure at depth. Regardless of operational depth the propulsive energy used by a seaglider when operating in a purely buoyancy driven mode can be broken into two distinct phases, energy used to descend and energy used to ascend. This energy consumption consists of short bursts, followed by long periods of buoyancy engine inactivity while the system glides. A majority of the energy used by the buoyancy engine is in the ascent stage. This is where the seaglider undergoes an inflection moving from descending to ascending operations. This can be seen in Figure 4 which shows the current draw as a function of time for a sequence of 10-meter yos. Each of these yos take approximately 400 seconds to travel from a depth of 2 meters, down to the inflection point at 12 meters and back up to 2 meters.

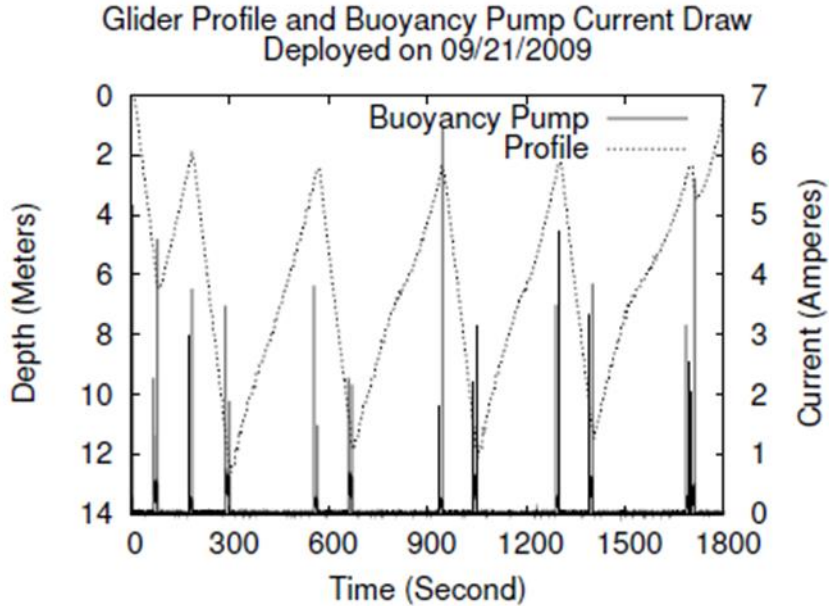


Figure 4: Seaglider Buoyancy Engine Current Draw and Flight Profile vs Time [14]

The reason for this increase is the added work required to evacuate the buoyancy engine due to the added pressure at depth. In both the ascent and descent cases, the buoyancy engine relies on a pumping system and a braking mechanism. The braking mechanism's function is to regulate the pump against external pressures when not in use, while the pumping mechanism is responsible for the change in the seagliders overall displacement. Notionally, it is easy to think that the energy used to descend, is essentially zero, consisting of nothing more than the opening of valves and allowing the water to rush in. However, like a great many things seaglider related, reality is not that simple, sinking is not free. To ready the seaglider to descend the buoyancy engine must be in the correct configuration to take on water. This requires the correct configuration of all pumping and breaking mechanisms, and is independent of the pumps efficiency at depth.

Motion of these components requires the expenditure of energy without producing any motion, or work, on the driving fluid or vessel.

The best available data for Seaglider in situ buoyancy engine energy usage comes from [14], where a Slocum seaglider was studied while undertaking a series of shallow (~10-meter) yoos. Coupling this work with [15] the energy usage for a seaglider's buoyancy engine while gliding is readily determined. This was achieved using the power drawn by the pump and the time over which it was operating, these values can be estimated from Figure 5. Each inflection at the bottom of a 10-meter yo was assumed to operate with a constant battery voltage, and current draw being proportional to the overall power consumed. Given the short nature of the missions in question, 30 minutes, it is safe to assume the onboard battery packs were functioning in a nominal manner, making these assumptions valid.

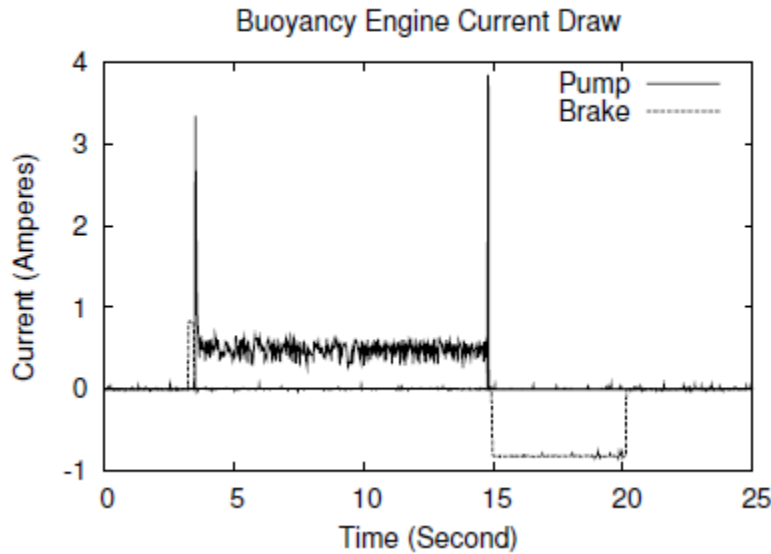


Figure 5: Buoyancy Engine Current Draw at a Depth of Approximately 12 meters [14]

Figure 5 shows the current draw vs time at the inflection point of a 10 meter yo at a depth of approximately 12 meters. Prior to, and following the activation of the pump the buoyancy engine brake must be set. This operation draws 0.85 Amps for both engagement and release. The brake operates for 0.2 seconds at the beginning of the inflection and 5.49 seconds at the end of the buoyancy engine cycle using a total of 56 Joules. It should be noted that Figure 5 shows the brake current alternates directions between engagement and release. Despite this reversal in sign, the brake does always consume power while operating. Upon activation and deactivation of the pump current draw peaks. Demand from starting and stopping the pump causes large spikes in the current draw totaling 3.4 Amps and 3.9 Amps respectively. Nominal power draw at 12 meters is smaller on the order of 0.49 Amps. During the 11.68 seconds it takes to complete an inflection at this depth the buoyancy engine pump consumes a total of 81.8 Joules. To complete one inflection at 12 meters depth, that is to change from a descending configuration to an ascending configuration takes a total of 137.8 Joules. This value will increase with depth as the buoyancy engine's pump has to expend more energy to overcome the external operating pressure.

Figure 6 plots a Slocum seaglider's buoyancy engine pump energy usage versus depth. The non-zero y-intercept is a result of the energy consumed by the systems brake totaling 32.8 Joules at the surface. The buoyancy engine pump energy required per meter of depth is 3.5 Joules/meter. When compared with the 164 Joules for the brake of the notional Slocum and the 4.1 Joules/meter for the pump depth relation there are differences. The variation in brake energy consumption values are attributable to differences in the pressure ratings between the two systems, with the deeper operating

system requiring a larger more energy intensive brake mechanism. The discrepancy in the Joules/meter value for the pump is attributable to differences in displaced volume between the two systems buoyancy engines. The buoyancy engine used in the study by Woithe has a displacement of 460 cc, whereas the system used in the analysis presented here is 488 cc. The difference between the Joule/meter values of 0.6 Joules/meter shrinks to 0.35 Joules/meter if the same displacement engine is used in both cases. Another factor could be a difference in the efficiency of the pumps used in the buoyancy engines. No good data exists on this to do the comparison.

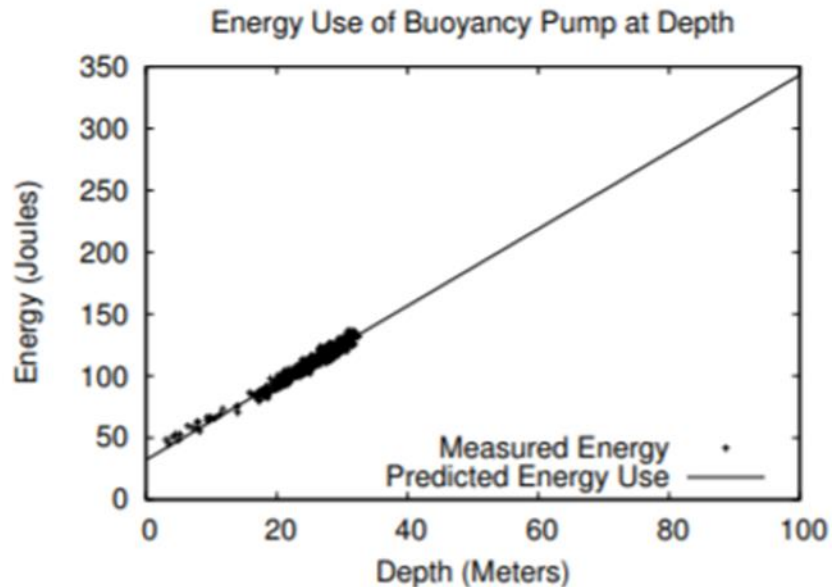


Figure 6: Buoyancy Engine Pump Energy Usage at Depth [14]

A seaglider undertaking a 25 degree glide slope, with a yo depth of 10 meters will travel 47.3 meters per yo. With an average yo time of 400 seconds the glider in the Woithe study is traveling at an average velocity of 0.11 meters per second, with a

buoyancy engine displacing 460 cc providing a total propulsive force of 0.98 Newtons.

Now consider a thruster borne vehicle travelling the same path, same distance, at the same speed. For a system with a 50% efficient thruster, providing the propulsive component of the buoyant force (0.98 Newtons), over the distance covered in a single yo (47.3 meters) yields a total energy usage of 92.4 Joules expended. This equates to an average power draw of 0.23 Watts over the 400 seconds it takes to complete a yo. The differences in energy utilization discussed here are shown in Figure 7, which highlights the power consumption of the two systems over the course of a yo, and Figure 8 which shows the cumulative energy usage over the course of a yo.

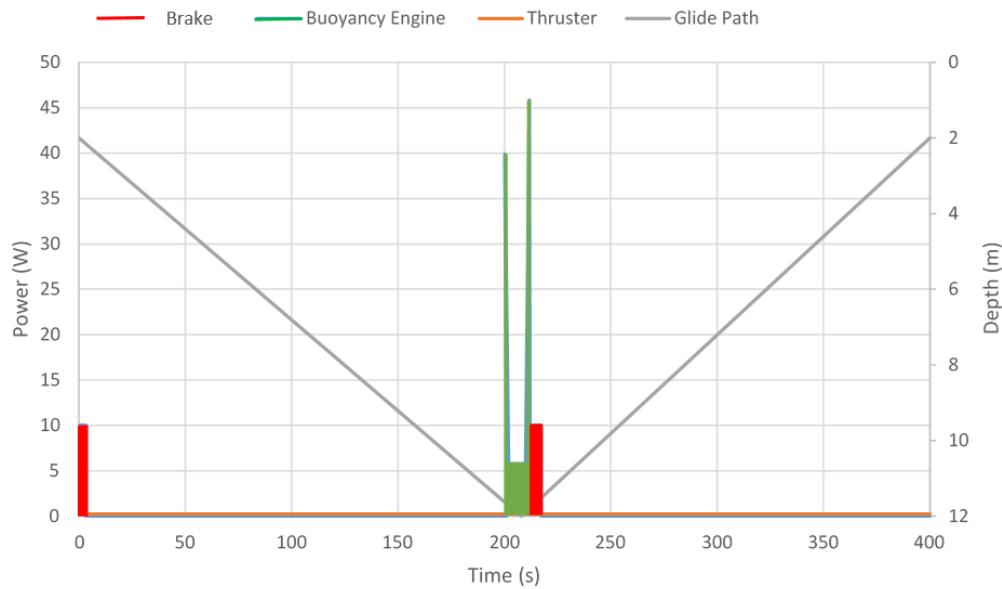


Figure 7: Buoyancy Engine Total Power Usage Compared to Thruster Power Usage and Flight Profile

Figure 7 and Figure 8 show that the thruster outperforms the buoyancy engine. Both figures also show that the buoyancy engine expends power in large discrete blocks

followed by long periods of inactivity, as opposed to the continual draw of a conventional thruster. In this case the cause for the difference between the two is primarily due to the depth of operation. Although shallower yos do benefit from not having as high an external pressure to overcome, they do have to operate more often. In this case every 47.3 meters. Exacerbating this is the fact that buoyancy engine pumps are optimized for depth. This means that not only is the system running more frequently it is doing so in a less efficient manner than it would otherwise do so if operating at a greater depth. A more detailed explanation of the issues surrounding the energy expenditure of the two systems is given in Chapter IV.

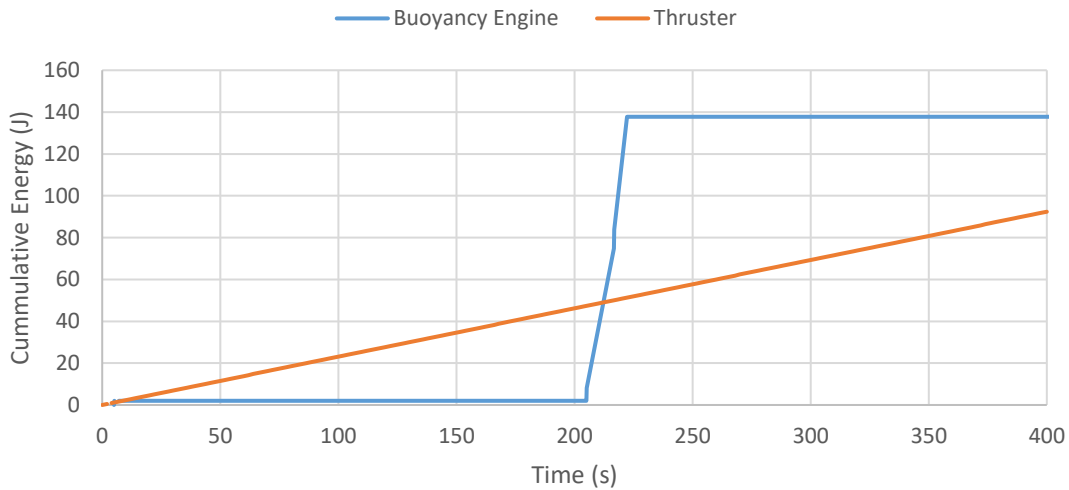


Figure 8: Buoyancy Engine Cumulative Energy Usage Compared to Thruster Cumulative Energy Usage

1.9 Definitions of Terms

Flying Wing Type Large hydrodynamically tailored seagliders whose body functions primarily as a wing.

Legacy Type	Seagliders whose consisting of a streamlined body of revolution with smaller hydrodynamic surface
Yo	A Yo is a single down/up cycle of a seaglider's operation

1.10 List of Acronyms

ABS	Acrylonitrile Butadiene Styrene
AoA	Angle of Attack
AUG	Autonomous Underwater Glider
AUV	Autonomous Underwater Vehicle
COTS	Commercial Off-the-Shelf
DDM	Direct Digital Manufacturing
ERAU	Embry-Riddle Aeronautical University
FDM	Fused Deposition Modelling
FOM	Figure of Merit
NACA	National Advisory Committee for Aeronautics
NEMO	Nature in Engineering for Monitoring the Oceans
ONR	Office of Naval Research
PVC	Polyvinyl Chloride
PVT	Pulsatile Vortex Thruster
PWM	Pulse Width Modulation
RC	Remote Control
RPM	Revolutions Per Minute
VaCAS	Virginia Center for Autonomous Systems
μ AUV	Micro Autonomous Underwater Vehicle

Chapter 2: Review of the Relevant LiteratureIntroduction

In this chapter, themes central to the exploration of seagliders and their performance are examined. Starting first with a brief overview of seaglider history, from the birth of buoyancy driven vehicles, through to ideation and on to realization, followed by design features and concepts. Following this, the design, modeling, and issues associated with buoyancy driven winged autonomous underwater vehicles are presented. Next, a review of the energy used in their operation and methods of maximizing its utilization is discussed. This is followed by sections covering propulsive methods, and analysis. Finally, a brief review of testing methods and concepts is undertaken.

2.2 Seaglider History

A vehicle moving through a fluid using nothing but a change in buoyancy is not a new concept. In 1862 Dr. Solomon Andrews unveiled a concept using the motive power of “gravitation”. In June of 1863 he tested his lighter than air ship, the Aereon, seen in

Figure 9, and by venting hydrogen gas, for descent, or throwing ballast overboard, for ascent, he successfully flew against the wind with sufficient celerity to cause the streamer behind the vessel to remain taut [16]. Despite the success of the Aereon and its sister ships, the idea of a lighter than air ship using “gravitation” as the motive force, fell into obscurity, along with the company he founded for their production in the turmoil of the post-civil war United States. The idea of using “gravitation” as a means of propulsion, the interaction of buoyancy and gravity, to propel a vehicle through a fluid did not surface again for nearly 130 years.

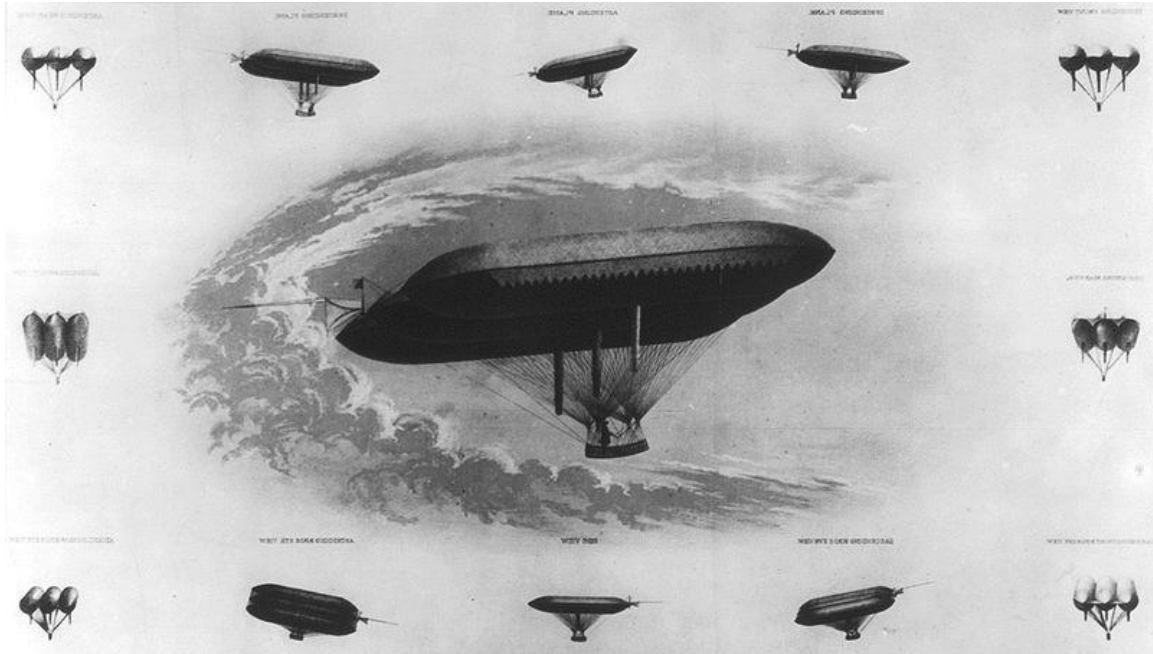


Figure 9: Dr. Solomon Andrews “Gravitation” Propelled Lighter Than Air Ship “Aereon”. In 1863, the Aereon, successfully demonstrated the utilization of the modulation of buoyancy to propel itself against the wind. (1906). Retrieved from [17]. A larger version is available in Appendix E 15

In 1989, an article titled, “The Slocum Mission”, penned by Henry Strommel [1], detailed what would become the template for the modern oceanographic seaglider. His intent, to deploy an ocean sampling flotilla, comprised of multitudinous small autonomous floats called Slocums. Each Slocum uses the changing of ballast to induce vertical displacement, which results in a gliding motion through the ocean on wings. The first tests of an electrically powered glider took place two years later. It took another decade for this idea to come to fruition with the development of a readily deployable, functional, oceanographic seaglider. Three separate research groups spearheaded this work, funded by ONR as part of their Autonomous Oceanographic Sampling Network development, over the decade following the publication of the Slocum Mission. The Slocum glider, developed by the Webb Research Corporation, continued development

with an electrical version being tested, while work progressed on a thermally powered wax based phase change material buoyancy engine. At the same time work was progressing on the Slocum electric prototype, work was also underway on the eponymously named Seaglider at the University of Washington, and the Spray glider at the Scripps Institute of Oceanography [18].

All three of these early gliders are streamlined bodies of revolution with simple lifting surfaces attached to the body. The Slocum glider,

Figure 10, has the simplest hull form consisting of a cylindrical hull with hemispherical endcaps, thin highly aft-swept wings of moderate aspect ratio, and a conventional T-tail empennage. The Spray glider,

Figure 11, developed by the Scripps Institute of Oceanography features a similar overall configuration to that of the Slocum. The Spray glider shares the cylindrical hull of the Slocum, but eschews the hemi-spherical endcaps for a more slender elliptical profile, thin slightly aft-swept wings of moderate aspect ratio, and a large vertical stabilizer. The Seaglider,

Figure 12, developed by the University of Washington, features a teardrop-like ogival outer hull, with short trapezoidal wings mounted in front of a vertical stabilizer, trailing this hull is a large pole which houses antennas for surface communication.

Congruent to this effort was the development and deployment of the ALBAC glider [18] by the University of Tokyo, in 1992. Unlike the Slocum, Spray, or Seaglider, the ALBAC carries with it a single disposable mass, allowing for a single descent, and subsequent ascent per mission, similar to the manner in which the Aereon operated. By

2002 gliders were being sold commercially and operating for extended periods around the globe.



Figure 10: Slocum G2 Hybrid Autonomous Underwater Glider Retrieved from [20]



Figure 11: Spray Autonomous Underwater Glider Retrieved from [21]



Figure 12: Kongsberg Seaglider Autonomous Underwater Glider Retrieved from [22]

2.3 Seaglider Design, and Key Concepts

There is a large body of work covering the multitudinous aspects of seaglider design. This work ranges from general hull morphology to hydrodynamics and wing design. Due to the overlap in both form and function, at least on a conceptual level, a large portion of this information lies in the area associated with the design of aircraft and lighter than air ships. These resources range from basic sources on hydrodynamics to airfoils, and hydrofoils [19], [20], [21]. Furthermore, a large number of resources exist on the design of aircraft, and aviation structures that, can inform and inspire new approaches to the design of seagliders. This includes resources covering the broad area of aircraft design [22], [23], [24].

Gliding through air and gliding through water is inherently different and brings with it a unique set of challenges and requirements, resulting from the density, viscosity, and salinity. This, in turn, requires a broadening of conceptual horizons, and the need to address issues foreign to aeronautical designs. Chief among these factors is the added mass of the fluid dragged along by the glider, which even at the low-speeds seagliders operate at can degrade the performance of a system a significant amount if it is not taken

into account. The paper Agile Design of Low-Cost Autonomous Underwater Vehicles [25] provides a high-level overview of the design issues influencing submersible systems like seagliders, though tilted toward conventionally propelled autonomous underwater vehicles. A key resource for understanding this wide and varied landscape of seaglider design is provided by the Underwater Glider System Study written by the Scripps Institution of Oceanography [26]. Information in the SCRIPPS study is further bolstered by [27], [7] which also cover design aspects of gliders in a general high-level manner, as well as key concepts in their operation. It then tackles contemporary glider design issues and challenges faced by the types of systems currently fielded before going further into future systems and mission types. This is of interest as it is a window into how oceanographers plan on utilizing these systems and their perceived deficiencies in those aspects. Other key concepts covered in the study are the interdependent nature of the overall hull configuration, its propulsive system, and sensor package. The morphology of seagliders is a growing area of research with other works covering various intricacies of morphology including blended wing body form factors [28], [29], flying wing types [30], and hybridized systems [13]. Further work on wing design and actuation is found in the 2009 Masters Thesis by Cheryl Skibski, focusing on external wing control surfaces [31].

2.4 Current Generation of Seaglider

The current generation of seagliders can be broken into two primary propulsive types, systems that use an electrically operated pump to move a working fluid to change displacement [32], [33], [34], [35] and those that use thermal energy from the ocean to change their displacement. These gliders typically operate at speeds ranging from 0.25

meters per second to 1.5 meters per second and depths up to 1.2 kilometers [36].

Thermally driven gliders utilize a phase change material to prime and operate their buoyancy engine, the result is extended operation times and ranges, which are ultimately measured in the thousands of kilometers, and years deployed [37]. However, their operation is limited to areas where the ocean has a high enough temperature variance to allow for the operation of their unique mode of buoyancy drive.

2.5 Seaglider Morphology

Similar to the buoyancy engines used, the seagliders overall shape, or morphology, can be broadly categorized into two groups, streamlined bodies of revolution with wings, or the blended wing body/flying wing configuration. Streamlined bodies of revolution with faired-in wings are the more prevalent, and exemplified by systems such as the Slocum, and Spray. These systems are primarily aimed at water column sensing with deep plunging dives [38], [39], [26], [40]. The blended wing body or flying wing configuration exemplified by the Liberdade gliders offer a wide platform, capable of high-speed shallow diving operations [26], [7]. It does this at the expense of being readily reconfigurable [26]. Control of the directional motion of these platforms is achieved using conventional moveable control surfaces, moving weights, or a combination of the two [31], [41].

A majority of work into seaglider morphology has come in the area of improving the flying wing, or blended wing body type. Typified by the work done in the design and development of the Liberdade flying wing type seaglider, [30].

2.6 Survey of current seaglider research areas

Current research focuses primarily on the areas of new control scheme design [7], [42], [43], [44], [8] actuation of buoyancy engines [45], [9], overall platform configuration [46] [31] [47], [26] and material usage [48]. The large majority of controls based papers focus on the development of a model for the seaglider and control schemes of both conventional gliders and hybrid gliders [13], [45]. Researchers at the National Taiwan University developed a model investigating the performance of a seaglider with fore and aft buoyancy engines [49]. This simplified model allows for the sizing of the buoyancy engines based on the desired velocity and glide slope. The results of this are yet to be tested with a glider meeting these specifications.

Actuation of the buoyancy engine is a key factor in the efficiency of the overall system. Multiple methods to achieve this displacement change have been investigated. The Virginia Center for Autonomous Systems (VaCAS) group at Virginia Polytechnic Institute & State University developed a pneumatically propelled underwater glider [9]. This platform leveraged large pneumatically driven buoyancy engines for operation in shallow water and currents. Despite achieving rapid changes in displacement, the glider was limited to achieve only 6 hours of operation due to the onboard air reservoir. Other systems such as the Massachusetts Institute of Technologies Nitinol seaglider uses a shape memory alloy actuator to move a plunger that modulates the displacement of the glider. This smart material system is similar in operation to the numerous syringe/stepper motor combination used by many smaller educational gliders such as the SeaGlide system [50], and the GUPPIE from Michigan Technological University [51].

Study of seaglider configurations varies from in-depth computational fluid dynamic investigations of revolute bodies, and optimizations on wing body interactions, to the design of blended wing body configurations and biomimetic designs. Examples of these studies include the development of the MOTH biomimetic glider from the HGF alliance [52] and the parametric optimization of a blended wing body [29]. Both of these systems heavily emphasize the hydrodynamic configuration of the platform. This emphasis can be detrimental to the overall configuration requiring the use of pressure compensated hardware, and specially shaped pressure vessels.

Research into the manufacturing of these platforms focuses on the use of novel hull forms and new manufacturing technologies. The NEMO project from the University of Southampton focused on the use of a biologically inspired isopycnal hull [48]. This hull used a combination of soft fluid-filled hull material a pressure compensating “organ” and a hardened skeletal structure, allowing for the hull to adapt to the variations in water density and pressure to a greater degree than a conventional hull.

2.7 Modeling and Control

Numerous works exist on the modeling and control of buoyancy-driven gliders. Chief among these works is [40], [53] which focus on the derivation and confirmation of both a longitudinally constrained model and full degree of freedom systems. Furthermore, these works also use real-world data for development and verification [39]. Similar work for hybridized systems can be found in, [54], [31], [12], and [55]. Although not a central thrust of this dissertation, this body of literature was key in gaining an

understanding of the impact of form, function, and operation, with its associated impact on a gliders performance.

2.8 Energy Usage

Little work currently exists focusing directly on seaglider energy usage and the work that does exist primarily focuses on enhancing the range of existing gliders through improvements in the path optimization as previously stated, or via sensor scheduling algorithms [56]. Works focused on the development of energy usage models can be found in [13], [57], and are focused on the development of extended range platforms, or conversely in the hybridization of the seaglider in which an auxiliary propulsion system is added. All of these works revolve around moving the seaglider into a high-speed, high-drag operational envelope, to overcome perceived deficiencies in the velocity achievable of the system.

2.9 Propulsion

Outside of the buoyancy-driven model which is highlighted in [40], [53], [26], [13], [57], [9], [42] AUVs can also be propelled in a more conventional manner. Numerous works focus on the design of propulsors, in both the aeronautical and maritime space [58], [59], [60]. Research focusing on the unique requirements of low-Reynolds number operation inherent to AUV's operating in a seaglider regime, covering conventional propellers, jets, and biologically inspired pulsatile vortex thrusters can be found in [60], [61], [62], [63]. However, work covering the application of these systems as a primary means of propulsion in the seaglider operational regime is nonexistent.

Achieving efficient transitory motion by operating in the low-speed, low-drag regime is not a new idea. Numerous biological organisms have successfully employed this strategy for eons. Among these organisms are those belonging to the groups Cephalopods (Squids, Octopodes, and Nautiluses) and Medusozoan (Jellyfish, and Salps). To operate in this efficient zone these organisms have eschewed more conventional methods of marine motion, such as flippers, flapping, and flukes and instead rely on a unique method of momentum transfer referred to as pulsatile vortex thrusters (PVT). This is an unsteady method of propulsion relying on the interactions of the near quiescent external fluid and the momentum transfer made possible by the interaction of the fluid, system being propelled, and a toroidal vortex. Work on the basic concepts behind pulsatile vortices, and how they are leveraged for propulsion can be found in [64], [65], [66]. The utilization of such a system as part of a maneuvering mechanism for an Autonomous Underwater Vehicle is referenced in [65] whereby a cluster of thrusters was used to allow an otherwise conventionally propelled AUV to affect zero radius turns and athwart motion. Despite being mechanically simple, these thrusters require complex tuning to both correctly integrate into the system, and operational regimes [66], [67]. This fact has led to limited use in only a few platforms [68], and only as a maneuvering thruster.

2.10 Testing verification

Verification of performance and estimates and modeling methods is essential to the completion of any work. This area is well encapsulated with work undertaken both in

wind tunnels, [69], [70], and captive model work such as, [13] highlighting methods for water tunnel based testing. Parameter identification at sea is highlighted by [39].

2.11 Summary

These buoyancy driven autonomous underwater vehicles are relatively new type of system when compared to other conventionally propelled systems. This fact means that unlike a majority of other autonomous underwater systems, whose design spaces are well understood, seagliders are in comparison fertile ground. The result of this is research within areas such as hull morphology, propulsion, control and path planning are being rapidly explored in multiple directions. However, one key aspect that makes the seaglider an efficient a platform its reliance on operating in a low-speed, low-drag environment. This is seen as a deficiency by some and is in need of correction. As with any young platform, time will tell.

Chapter 3: Morphological Changes and Their Impact on Autonomous Underwater Glider Performance

3.1 Introduction

A large body of work already exists on the benefits and drawbacks of submersible design, configuration, and hydrodynamics, as does a similarly significant body of work on aircraft design, configurations, and aerodynamics. With the exception of the brief overlap in the realm of the design of dirigibles, the two schools of thought rarely intersect or inform one another. This is primarily due to the difference in operating regime, with submersibles moving much slower through a far denser fluid than the vast majority of aviation applications. However, concepts from one can be used to influence design decisions in the other. With this in mind, this section leverages the use of aerospace concepts in the development of glider planforms and overall morphologies for the purpose of improvement in glider performance. Areas examined here included the change in the wing's angle of incidence, the use of an annular wing planform, the utilization of an inverse Zimmerman planform, and the cranked kite configuration that emerged as a result. The data taken in this study is of a preliminary nature and as such, it is intended to be a bellwether as to the usefulness of this line of research in the improvement of seaglider performance in areas where their operation would be considered atypical.

3.2 Research Approach

In keeping with the nature of this section of research, a simple experimental approach was first used to determine whether concepts found in the design of aerospace

systems were applicable to the design of Autonomous Underwater Gliders (AUG). This involved the setting of a single readily observed metric upon which to determine the overall improvement if any of a vehicle's performance. This was necessary as the modifications being suggested, namely the variable angle of incidence wing and the annular wing, had to accommodate two very different starting platforms, namely the legacy type (

Figure 14), and flying wing type, in this case, represented by the inverse Zimmerman configuration, (Figure 22). In the case of the overall morphology of a seaglider's hull, and hydrodynamic surfaces, the key metric was chosen to be slant range. This distance is the hypotenuse of the triangle formed by *yos* performed by the glider, denoted by s_{glide} . In order to improve the overall range efficiency of the glider, an improvement of its hydrodynamic qualities was required. This improvement in overall range efficiency would then allow the system to operate in shallower environments for comparable periods, or actuate its buoyancy engine more often to overcome inclement environmental factors, without suffering a degradation in performance.

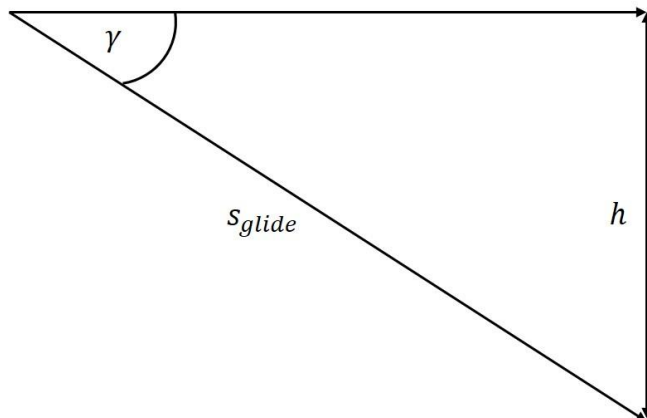


Figure 13: Half-Yo Diagram Highlighting Slant range and its relation to glide path angle, γ and depth, h

For a modification to be considered worthwhile it would have to take the same starting energy, in the case of the glider the available buoyant force after being placed at the bottom of a test tank, and use that to traverse as far a distance as possible in the test tank before surfacing. The vehicle's vertical distance covered (starting depth to the surface) and horizontal distance covered were recorded. With the application of simple trigonometry, the resulting glideslope angle was determined. This glide slope was used as a metric to determine the impact of the changes being implemented and the performance of the system as a whole.

The morphological changes investigated here are the inclusion of a variable incidence wing, Section 3.6, the utilization of an annular wing, Section 3.8, and the adoption of an inverse Zimmerman planform, Section 3.7, in lieu of a pure flying wing configuration. Each of these changes offers an improvement in hydrodynamic performance through improvement in the gliders lift to drag ratio.

These tests were conducted on two different morphological types, a legacy type glider consisting of a streamlined simple cylindrical body of revolution, and an inverse Zimmerman planform. Both of these hull types were fitted with a rectangular wing of the same aspect ratio, span, and overall wing area, which was varied through a range of angles of incidence, along with an annular wing of the same size.

3.3 Body Types

The two body types tested in this phase of research were a small, streamlined body of revolution, representing the streamlined body of revolution, legacy type gliders, and the inverse Zimmerman and cranked kite planform representing the flying wing

types. Both test articles had sufficient ballast to deliver the same amount of resultant buoyant force allowing for a one to one comparison. However, the direct comparison was only one metric of interest, with the expansion of the glider's overall operational envelope being the other.

3.4 Legacy Type

Originally, a small-scale model of a Slocum glider was produced for the experiments involving the legacy type gliders. After initial testing, it was found this test article proved difficult to ballast reliably and wholly unreliable when it came to consistent gliding operation without any of the modifications planned for the experiment. Replacing this model was a simplified system consisting of a PVC body and an acrylic wing and empennage,

Figure 14. The test results for this vehicle are in Figure 29 and Section 3.10.

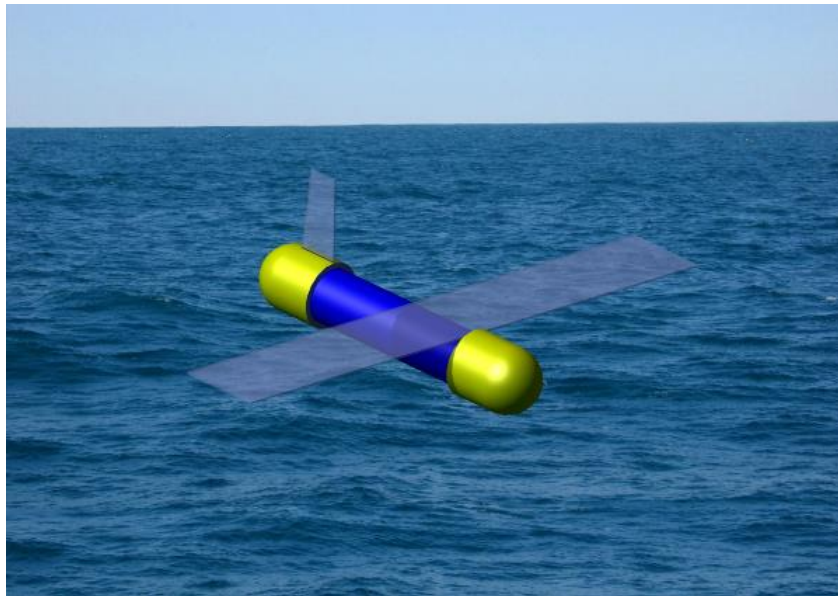


Figure 14: Legacy Seaglider Analog Rendering

Table 2 Legacy Seaglider Analog Physical Properties

Property	Value
Length (m)	0.127
Body Diameter (m)	0.021
Wingspan (m)	0.200
Mass (g)	62
Water Displaced (g)	72

3.5 Inverse Zimmerman

For a second vehicle, it was decided to develop an improved base seaglider configuration, in keeping with the flying wing style gliders. Flying wing type gliders operate at higher speeds and have a larger internal usable volume inside of their hydrodynamically tailored shells, making them an attractive starting point for a new design.

Operating at such low-speeds, where viscous forces begin to play a major part in fluid flow, and taking into account the requirements for an improved lift-to-drag ratio and large internal volume a thick airfoil was chosen as the cross-section of the gliders main body. This airfoil had to have good performance at the lower Reynolds Numbers experienced by gliders while maintaining good internal volume and desirable hydrodynamic characteristics. The result of an extensive search was that a NACA 65(2)-415, Figure 15, was selected as the hydrodynamic cross-section of the glider body for reasons referenced below.

The performance polars for the NACA 65(2)-415 geometry is shown in, Figure 16, Figure 17, Figure 18. Of key interest is the wide angle of attack (-9° to 7°) over which a high lift coefficient (-0.6 to 1) and low drag coefficient are available.

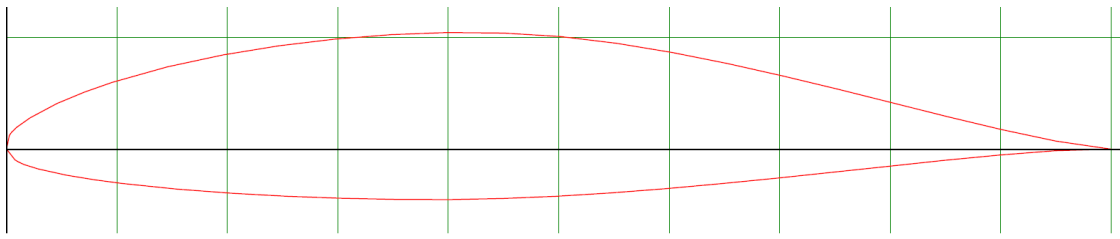


Figure 15: NACA 65(2)-415 Airfoil Cross-section Retrieved from [75]

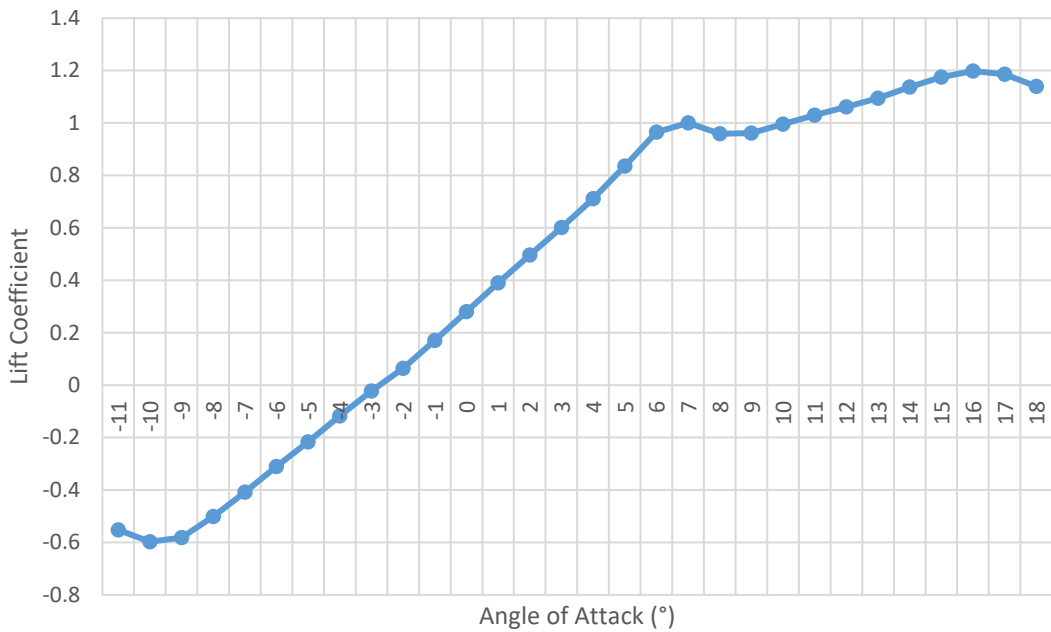


Figure 16: Lift Coefficient vs Angle of Attack for the NACA 65(2)-415 Airfoil Retrieved [75]

Once the airfoil had been selected based on useable internal space and hydrodynamic concerns, a suitable planform for the new configuration was required. Looking at the requirement for low Reynolds number operation, and the desire for a hydrodynamic design only a small subset of planforms were deemed suitable, many of which had previously been investigated for use on micro aerial vehicles.

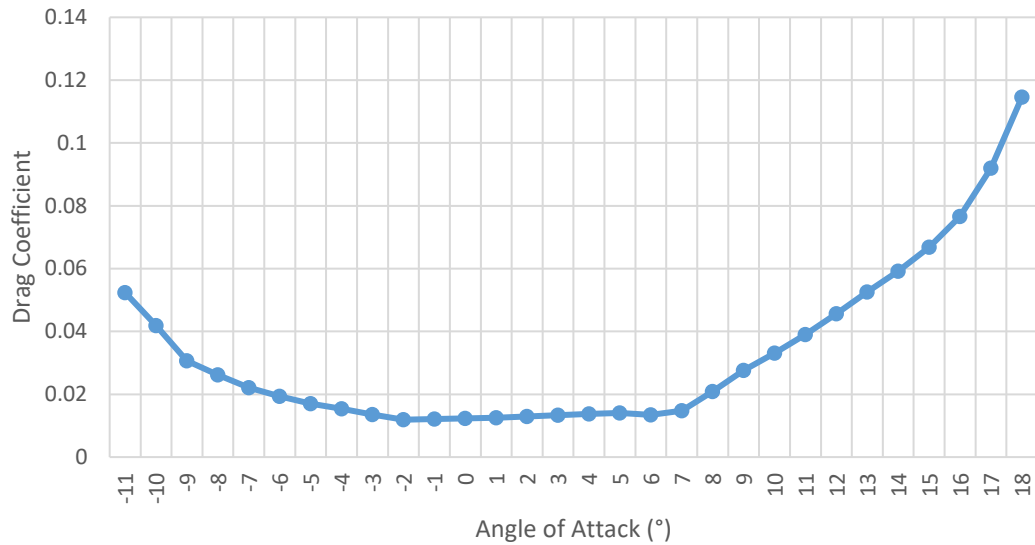


Figure 17: Drag Coefficient vs Angle of Attack for the NACA 65(2)-415 Airfoil
Retrieved from [75]

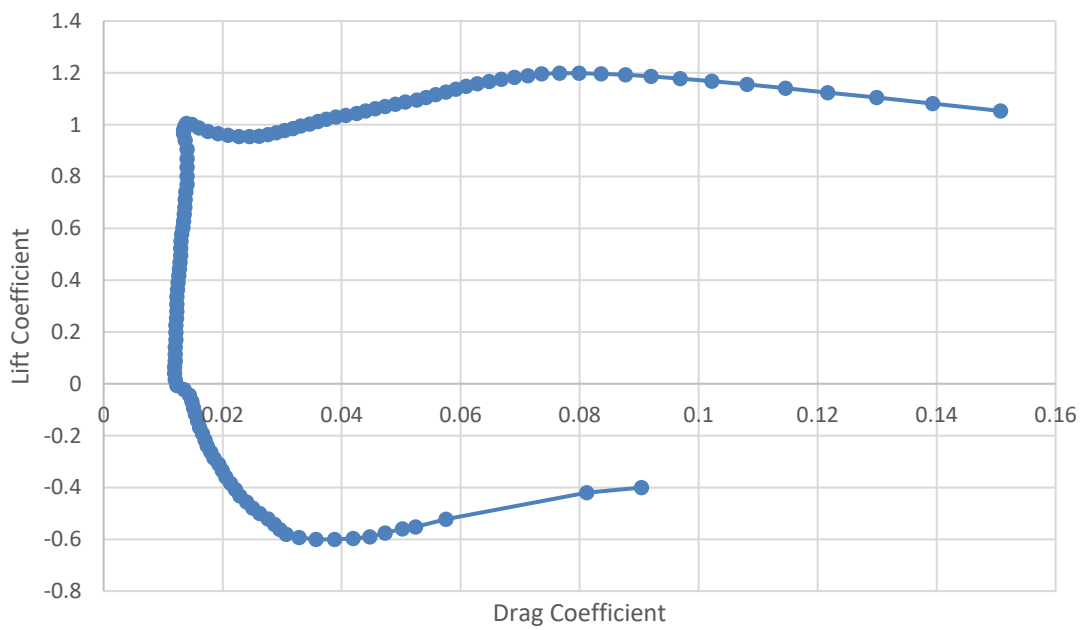


Figure 18: Lift Coefficient vs Drag Coefficient of the NACA 65(2)-415 Airfoil
Retrieved from [75]

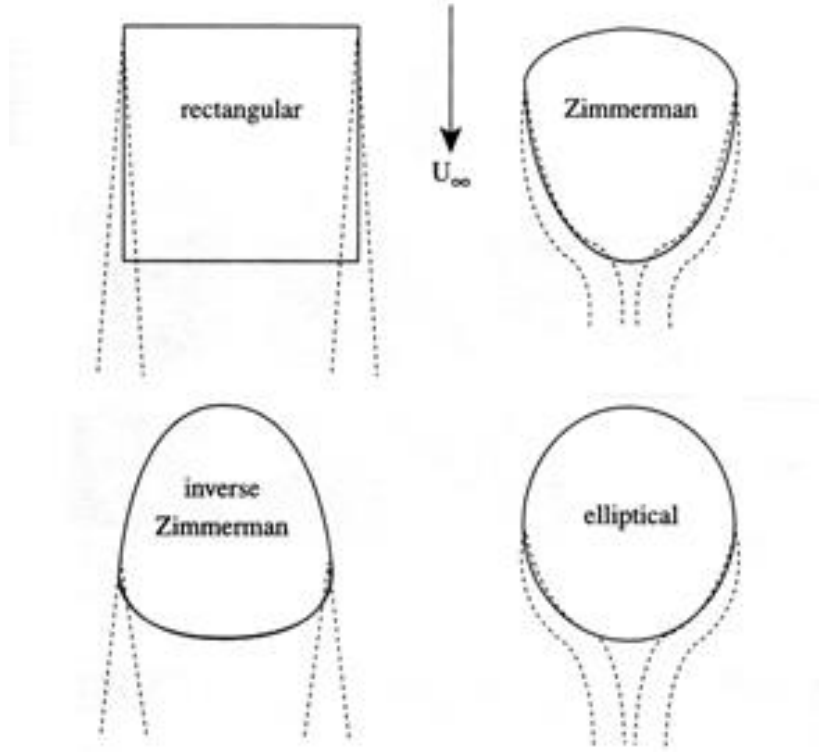


Figure 19: Illustration Highlighting Multiple Low Reynolds Number Planforms and their Resulting Wing Tip Vortices (dotted lines) Retrieved from [72]

The last component in planform selection was the nature of the wingtip vortices and their impact on the wing, this is qualitatively shown in Figure 19. When a seaglider is in steady state operation it experiences four major forces, thrust, weight, lift, and drag. The drag around an object moving through a fluid is complex, but can be broken down into three main types: viscous drag, pressure drag, and induced drag. Of the three, induced drag, a byproduct of lift, is of key concern. Lift is produced by the differential of low pressure above a lifting surface and high pressure below. However, pressure acts in all directions, and nature abhors imbalance, so at the tip of the lifting surface the high-pressure fluid curls around the tip to counteract the low pressure above. This spins the fluid and creates a wingtip vortex. The creation of a wingtip vortex is a substantial loss

of energy, and their minimization or elimination is an area of great study in aeronautics. Taking all these requirements in hand, in conjunction with the results of work on Micro Aerial Vehicle planform design and performance at low-Reynolds numbers performed by Torres and Mueller [71], an inverse Zimmerman planform was selected as it offered the combination of straight forward manufacturability, good hydrodynamic performance, and stability. However, in early testing it was found that the inverse Zimmerman planform on its own would not always glide in predictable a manner. Occasionally on ascent it would, flatten its trajectory; halt forward motion and then proceed toward the surface in an undulating fore-aft motion. The most likely cause of this behavior is the separation of flow across the gliders surfaces, similar in nature to stalling a conventional aircraft. A wing of the same specifications as that on the legacy glider was attached aft of the cross section's maximum thickness, to ensure pitch stability. This had the added benefit of allowing the later testing of a variable incidence wing. Owing to the complex nature of the geometry, and the exactness with which it needed to be produced this test article was produced using the Fused Deposition Modeling (FDM) method of Direct Digital Manufacturing (DDM). The FDM DDM process consists of a small layer of plastic, in this case, Acrylonitrile Butadiene Styrene, ABS, is extruded through a heated nozzle onto a build plate. This process results in porous parts, which in turn needed to be sealed. To seal these porous printed parts melted wax was applied to the surface in layers of varying colors. This surface was then sanded back to a smooth finish.



Figure 20: Inverse Zimmerman Planform Seaglider Test Model Before Finishing

3.6 Variable incidence wing

A variable incidence wing is a surface that can vary its angle relative to the body of the vehicle, Figure 21. Varying this angle enables the glider to optimize the wings glide slope while maintaining an overall body attitude necessary to meet mission payload requirements, e.g. sensor directionality, and field of view. This allows for the maintaining of an optimal lift to drag ratio for the wing, but also the optimization of flow and sensor view, and control over the glide slope of the overall platform with regard to the oncoming flow. In this case, the variable angle of incidence wing allowed the carrier based interceptor to land at lower speeds with a higher angle of attack while keeping a more nose down landing profile.

Two different models were tested in conjunction with a variable incidence wing. One a legacy type glider,

Figure 14, consisting of a high mounted wing, vertical tail, and body of revolution. The other a compound body using an inverse Zimmerman planform with conventional shoulder mounted straight wing. This configuration closely resembles a

cranked kite configuration, currently being used on the Northrup Grumman X-47 demonstrator aircraft shown in Figure 23 below.

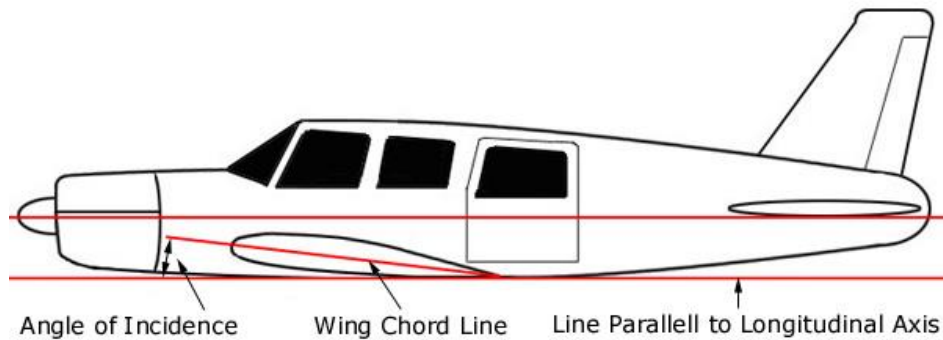


Figure 21: Illustration of the Angle of Incidence of an Aircraft's Wing Compared when to its Longitudinal Axis Retrieved from [74]

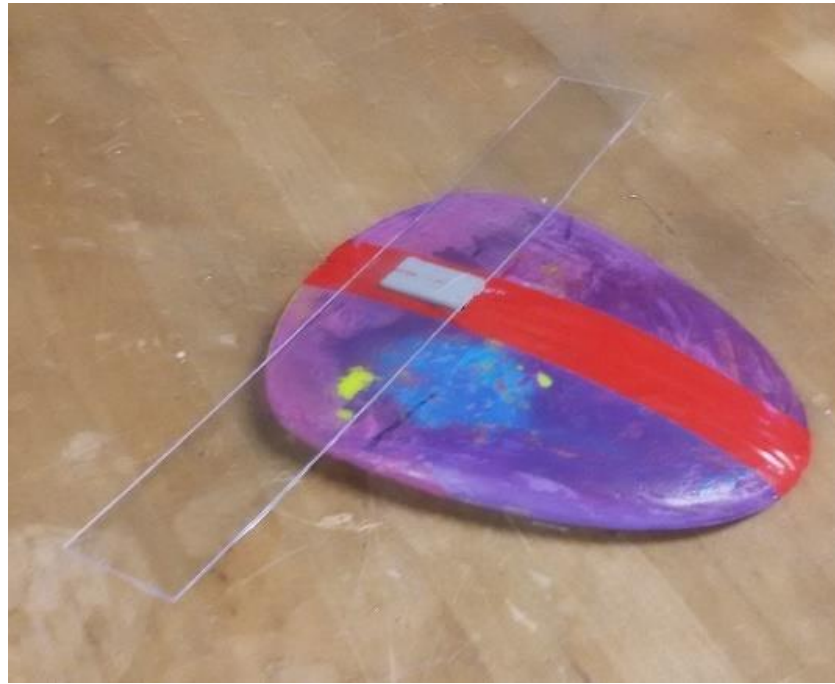


Figure 22: Inverse Zimmerman Cranked Kite Planform Seaglider Test Model

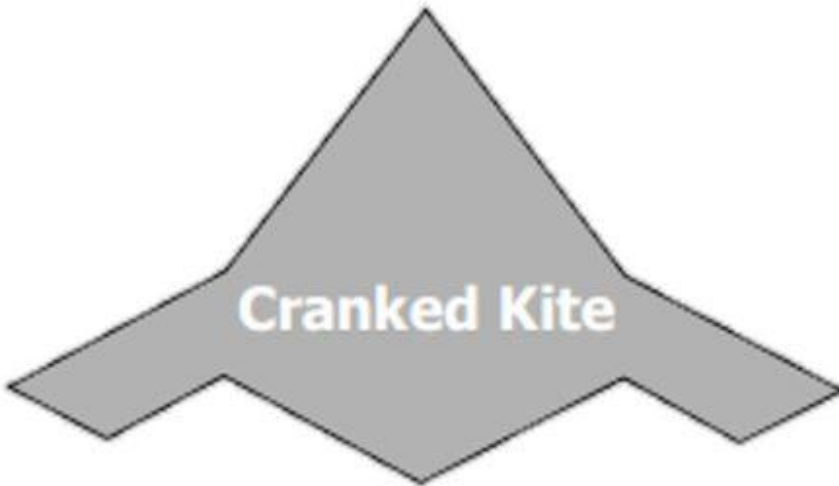


Figure 23: Top Down Projection of a Cranked Kite Planform Retrieved from [72]

3.7 Inverse Zimmerman Cranked Kite Planform

The inverse Zimmerman Cranked Kite design is intended to meet multiple design criteria including, maximization of lift-to-drag ratio, and optimization of the ratio of the wing to body, all while trying to optimize available internal volume, and wetted area. The main body consists of an inverse Zimmerman forebody with a simple un-tapered, unswept wing placed aft of the location of maximum thickness. The Cranked Kite planform is distinct from relatives such as the flying wing, and blended wing body type craft, both of which are exemplified in the Liberdade family of gliders.

Pure flying wings have excellent hydrodynamic properties but suffer due to a short body length, degrading longitudinal stability, the center of gravity placement, and the complicated installation of different payloads, which in turn drives the requirement for a higher degree of wing sweep. Of particular concern is the degree of wing sweep and its impact on overall performance. In aviation, wing sweep is used to delay the onset

of shockwaves in high-speed flight, which is of no concern in the incompressible flow found around a seaglider. Wing sweep can assist in the correct location of the center of gravity which is beneficial depending on the system in question. In general, at low-speeds, an increase in wing sweep has a deleterious effect on wing performance and often comes with an added structural penalty when compared with a constant chord unswept wing. A Cranked Kite planform, however, has similar hydrodynamic benefits of a flying wing while retaining an elongated forebody suitable for more conventional payload configurations, is far less sensitive to center of gravity changes, and has the added benefit of decoupling the outer wing panels from the center body allowing optimization of the wing and body separately [72].



Figure 24: A Flying Wing Type Seaglider Retrieved from [30]

3.8 Annular wings

Annular wings, Figure 25, are a concept which shows great promise in the improvement of performance of an object passing through a fluid. This is achieved by moving the wingtip vortices up and away from the main body. These vortices are generated whenever there is a difference in pressure between two surfaces moving through a viscous fluid, Figure 6. These wingtip vortices are responsible for induced drag, the elimination of which has the potential to improve overall hydrodynamic performance. This configuration purports to offer improved performance at higher angles of attack, including station keeping maneuvers and improve both stowage and structural strength when applied to a slocum type glider [73]. The research undertaken here investigated the method of implementation of an annular wing on a both a slocum type glider and an inverse Zimmerman planform seaglider as well as its impact in terms of overall performance.



Figure 25: Annular Wing Aircraft Concept Retrieved from [77]



Figure 26: An Example of an Aircraft Producing Wingtip Vortices Produced by an Aircraft Retrieved from [78]

3.9 Testing Procedure

Testing for the legacy type glider was conducted in a large freshwater tank measuring 1.22 meters long, by 0.457 meters wide, filled with 0.406 meters of water. This was done in order to eliminate transients caused by currents, thermoclines, and foreign bodies. Behind this transparent tank was a 0.032 meter square grid to aid in measurement of glider travel, Figure 27.

Measurements of the distance traveled by each glider configuration was taken from footage recorded for each of the trials. This footage was taken from the same location with the same camera in order to mitigate the impact distortions from refraction or reflection due to the tank would incur. Each trial consisted of the vehicle being placed horizontally at the base of the tank, at a predesignated starting point and then released. This allowed the glider to utilize its inherent buoyancy (which is the same between both systems) to float toward the surface while the hydrodynamics of the system prolonged the

glide as much as possible. Each configuration of the glider, with wing angles of incidence ranging from -7.5 degrees to 7.5 degrees and 2.5 degree increments, were launched, the gliders time to surface was measured, along with distance traveled prior to surfacing, mass, displacement, and wing configuration. The legacy typed showed a high degree of instability with the wing at a negative angle of incidence. This often resulting in tumbling, or reversal of direction while ascending.

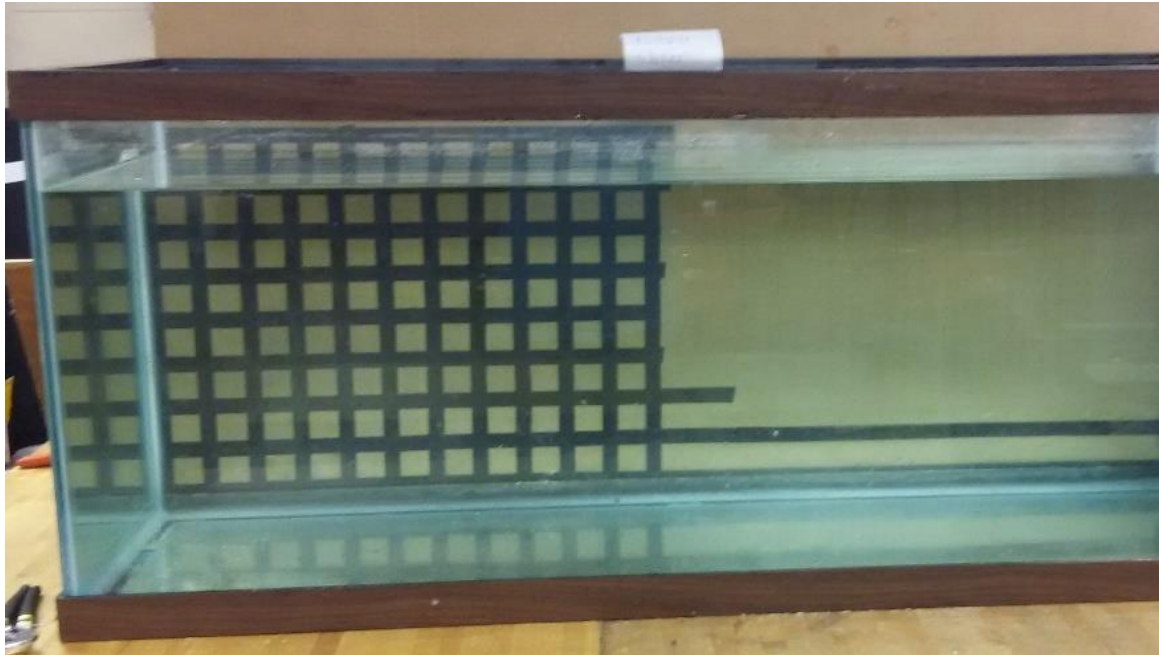


Figure 27 Seaglider Glide Path Test Tank

Using the same methodology as the legacy platform a direct digitally manufactured, inverse Zimmerman planform was tested, Figure 28. As with the streamlined body of revolution multiple runs from a depth of 0.406 meters and with a variation in the angle of incidence. This was most likely due to better flow attachment across the inverse Zimmerman's surface.



Figure 28 Composite Image Illustrating Inverse Zimmerman Planform featuring an Annular Wing's Glide Path

The inverse Zimmerman Planform, Figure 22, was then tested in the same manner using the same equipment as the legacy type glider model. Again a strong trend can be seen between the angle of incidence and the glide slope, with higher angles of incidence correlating to shallower glide slopes. However, unlike the legacy platform, the inverse Zimmerman was stable in both positive and negative wing angle of incidence producing reliable gliding data in both regimes. The results for this can be seen in Figure 29.

3.10 Results

A series of experiments in which the impact of a change in the wing angle of incidence versus the glideslope was investigated, with a wider glide slope range being preferable. This wider glide slope range allows the system to do both deep plunging dives and basin level operations. In conjunction with this testing, the investigation of an annular wing on the glide slope was also performed. Testing of the Legacy type glider showed a correlation between wing angle of incidence and glide slope performance. A clear negative trend can be seen for angles of incidence ranging between 0.0 and 7.5

degrees. This negative trend indicates that for an increase in the wing's angle of incidence a corresponding decrease in glide slope occurs. When the angle of incidence became negative a tendency for the platforms nose to pitch up occurred and the platform became unstable. The data from these experiments was used to inform the design of the inverse Zimmerman vehicle planform, and the cranked kite platform that occurred as a result.

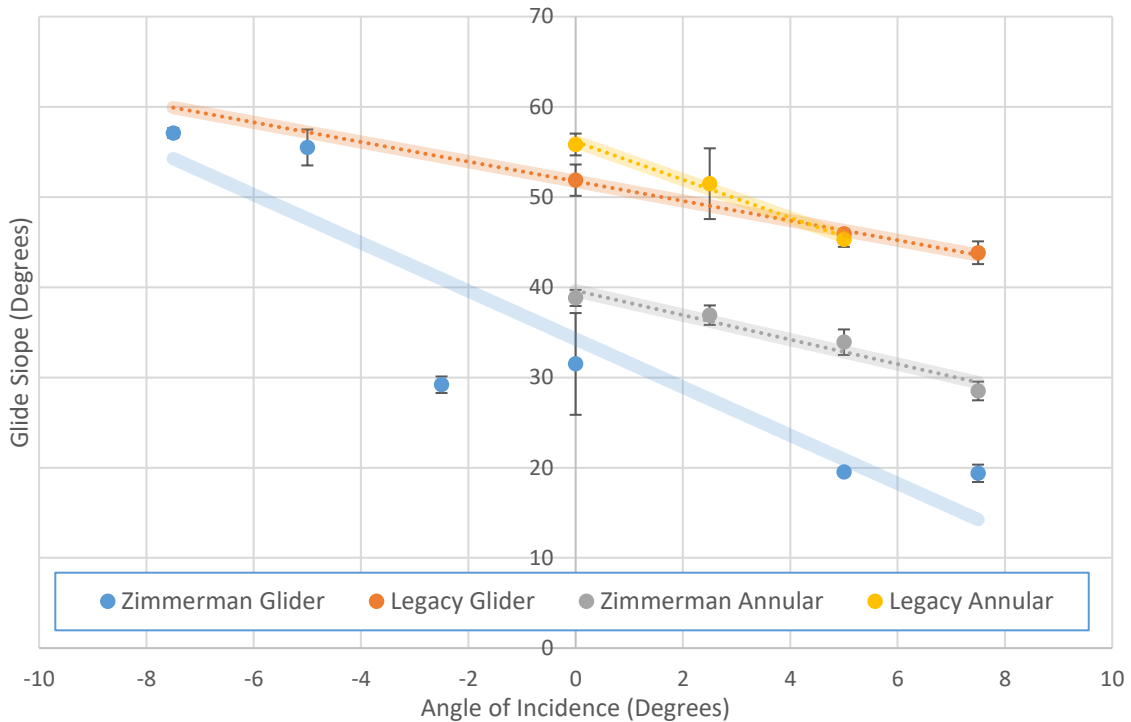


Figure 29: Glide Slope vs Angle of Incidence for The Inverse Zimmerman Glider and Legacy Glider Cataloguing Glide Slopes with a Conventional Wing and with an Annular Wing while Varying the Angle of Incidence. Each test consisted of 5 separate runs.

As a result of this research, the impact of the variation of the angle of incidence upon both a streamlined body of revolution and NACA 65(2)-415 based Zimmerman planform was investigated, utilizing both a conventional straight wing and an annular

wing of the symmetric cross section. Angle of incidence was proven to have an impact on the glide slope of both the legacy type revolute bodies and the inverse Zimmerman planform, allowing for a variation from steep plunging dives to shallower dives as shown in Figure 29. In both cases, the Zimmerman planform outperformed the legacy type, in terms of glide slope and velocity. The annular wing proved to afford the platform a significant speed improvement but did so while operating at the steeper glider angles. Overall, an inverse Zimmerman planform, coupled with a conventional symmetric planar variable angle of incidence wing afforded the best combination of operation envelope expansion.

3.11 Summary

The current generation of fielded gliders offers numerous areas for improvement. Key areas of focus are on control of the glider and improvement in performance through enhancements in efficiency in the buoyancy engine and the gliders configuration. Current gliders feature conventional control surfaces, such as rudders for maneuvering. These control surfaces are augmented in some platforms via moving masses inside of the glider. Furthermore, the nature of these control methods does not allow the gliders to perform highly dynamic maneuvers, which would allow them to operate in more dynamic environments, or more tightly survey a single area.

The dearth of variation in seaglider design leads to a largely one size fits all approach to in-situ sensing. This leads to a system that is intended for low-speed, low-drag, deep diving operations, being tasked to perform at high-speeds in shallower waters, at the expense of endurance and sensing. A chief cause of this is the way in which gliders

are shaped. Gliders featuring a streamlined body of revolution with faired-in wings features a disproportionately large body when compared to the flight surfaces. This mismatch, in turn, results in the poor lift to drag ratios when compared to a flying wing type glider, and subsequently a reduction in range, payload, and operating time. The wings on these revolute bodied gliders are also fixed, giving the platform no ability to leverage the optimal lift to drag ratios during ascent or descent. An increase in the wing to body ratio, requires the hull mass be evenly redistributed along the more planar configuration. With the increase in wing to body ratio and the associated mass redistribution occurs the system moves from a legacy type and begins to exhibit behaviors associated with the flying wing type gliders, having superior transit economy but at the expense of profiling operation [74]. Although being more hydrodynamically tailored than a revolute bodied glider, the blended wing body/flying wing configuration also suffer shortcomings associated with their shape. By their very nature, the flying wing design does not allow for the center of gravity to move a great deal either forward or aft before the platform becomes unstable. This hampers the ability of this type of glider to readily accept payload changes without the tedium of extensive and accurate weight and balance calculations.

Regardless of the overall configuration other areas in which gliders could gain efficiency from hull design include the development of low-cost isopycnal hulls. This allows the hull to adjust its displacement in response to the change in density of the surrounding water. Currently, the few systems that implement this do so using complex and expensively machined pressure hulls which rely heavily on high fidelity modeling and high precision manufacturing.

However, the overarching conclusion to this branch of research is that the hull morphology, be it the implementation of a variable angle of incidence wing, or the utilization of an annular, on either a conventional streamlined body of revolution or inverse Zimmerman planform does have a beneficial impact on glider performance. It is though, by definition a point solution that would meet a single set of design criteria, for velocity and glide angle, and whatever solution was chosen would have to be modified to work with the buoyancy engine. At this point, it was decided that despite showing improvement in performance of seagliders, in both available angle of attack, and velocity it was not the enabling technology that had been hoped for, and as such a new research path was pursued.

Chapter 4: Derivation of Seaglider Energy Usage, and Efficiency

4.1 Introduction

This section compares the efficiency of a buoyancy-propelled seaglider with that of a conventionally propelled autonomous underwater vehicle of the same design. In order to compare efficiency, a metric that fits both propulsive paradigms must first be determined. With the myriad of variables available and their interdependencies, this is not a simple task. However, once distilled, the most readily understood metric for a propulsive system's fitness, as applied to the types of missions typically undertaken by a Seaglider, is its endurance. The overall endurance of an autonomous underwater glider is dependent on the system's size, operational speed, diving depth, cruising velocity, glide angle, hydrodynamic coefficients, propulsive systems power usage, and onboard systems power usage. To determine and compare the overall energy usage of both a seaglider and a conventionally propelled AUV, a first-principles energy-based analysis was developed. The energy used by both buoyancy driven seagliders and conventionally propelled AUVs can be broken into two distinct functional groups, propulsive energy usage, and the energy lost to hotel loads. In this analysis, the propulsive energy is defined as the energy used to operate the vehicles propulsion system, and the hotel load is the energy consumed by all non-propulsive systems, including attitude control, onboard communications, and both proprioceptive and exteroceptive sensors. In order to compare the two disparate modes of propulsion, and their associated impact on endurance, a notional candidate system is based on the Slocum Electric AUG. This concept is employed to ensure that variables not directly related to the propulsive system i.e. hull morphology do not

influence the results. Table 3 contains physical and operational characteristics of this vehicle and Figure 30 shows a free-body diagram while in steady state operation.

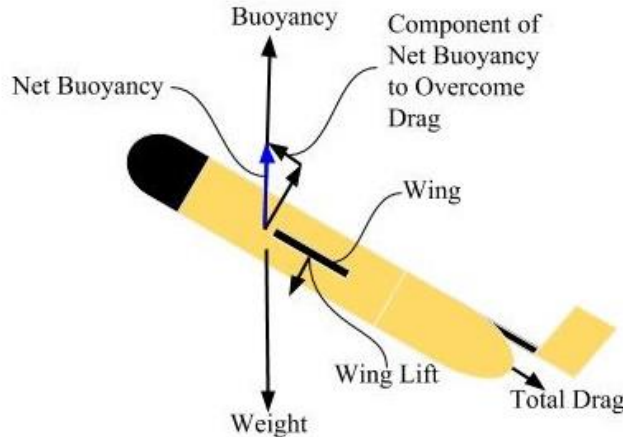


Figure 30: Annotated Free-Body Diagram of a Slocum Electric Autonomous Underwater Glider in Operation

Table 3: Typical Slocum Glider G2 Physical Properties and Performance Characteristics
Adapted From [36]

Hull Length	1.50 m
Hull Diameter	0.21 m
Hull Frontal Area, (S)	0.038 m ²
Wingspan	1.01 m
Mass	52 kg
Maximum Volume Change	0.000521 m ³
Drag Coefficient, C_D	0.27
Buoyancy Engine Efficiency	50%
Maximum Depth	200 m
Maximum Speed	.40 ms ⁻¹
Endurance Speed	.25 ms ⁻¹
Endurance Glide Angle	20°
Endurance Buoyancy Change	.26 kg
Endurance Range (estimated)	1500 km

4.2 Seaglider Power Usage

Recall that the propulsive energy of a seaglider results from the change in the system's net buoyancy which is the difference between the buoyant force and the system's weight. This change in buoyancy when referenced against a neutrally buoyant system makes the AUG ascend in the case of increased buoyancy (buoyant force is larger than the system's weight), or descend in the case of decreased buoyancy (buoyant force is less than the system's weight). In either case, this change in buoyancy, in conjunction with the seaglider's wings result in a series of approximately triangular translations through the ocean (each called a yo), Figure 31.

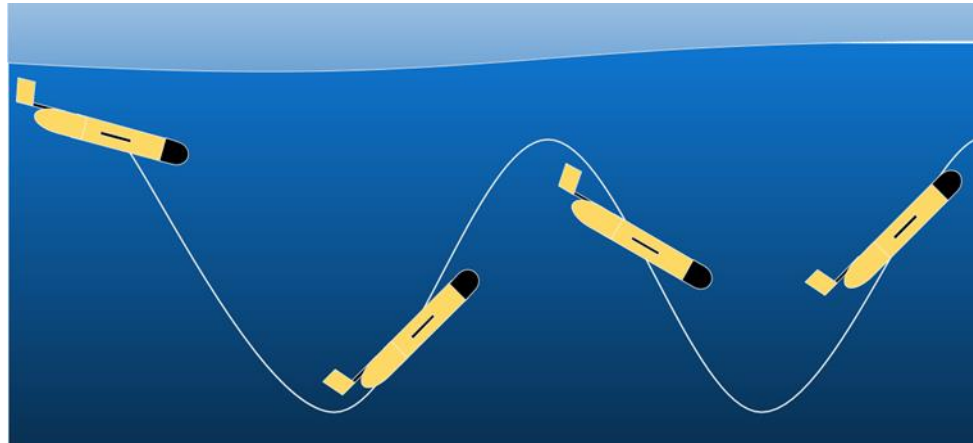


Figure 31: Seaglider Sawtooth Yo-Yo Flightpath

When the vehicle is operating at steady state, Equation 1, the component of the buoyant force utilized to propel the seaglider equals the forces associated with hydrodynamic drag, and steady state forward locomotion occurs as a result.

$$F_{buoyancy,propulsive} = F_{Drag} \quad (1)$$

For the remainder of this analysis, the values used in ensuing calculations utilize the data from Table 4 Glide 1 from, Graver's work [39]. The selected data was collected in the course of parameterizing a Slocum AUG while operating in the open ocean and is believed to be the best available published data.

In order to ensure this energy analysis is true regardless of direction or path taken the motive force from buoyancy must be conservative. This, in turn, requires that the work done moving the object between two points is not path dependent. This is stated clearly in [75].

Table 4: Steady State Glide Data Taken from Insitu AUG Operations (Glide 1 is a descending glide)

Value	Glide 1
Pitch Angle θ (deg)	-22.77
Depth rate \dot{z} (m/s)	0.168
Ballast (m ³)	-0.000244
AoA α (deg)	2.7
Speed V (m/s)	0.388
Drag Coefficient, C_D	0.27

Figure 32 depicts the descending leg of a seaglider's gliding operation, including the depth achieved, h , and the glide path angle, γ (Equation 2). It should be noted that γ is the sum of the pitch angle (θ) and angle of attack (AoA) (α). While the glide path angle calculated in Equation 2 is based on measured parameters, it should be noted that if the lift to drag ratio of the vehicle is known, the glide path angle could also be expressed as the inverse tangent of the quotient of lift to drag ratio [76].

$$\begin{aligned}\gamma &= \theta - \alpha \\ \gamma &= -22.77^\circ - 2.7^\circ \\ \gamma &= -25.47^\circ\end{aligned}\tag{2}$$

As endurance is being used as a metric, we are interested in the distance covered in a descending leg which will be called s_{glide} . This is calculated using the trigonometric relation shown in Equation 3. This leg is constructed using the glide path angle of 25.47° and a maximum depth of 200 meters . Both the glide path angle and maximum dive depth values are representative of seaglider operational capabilities, and as such are taken from Table 3, which contains the physical properties of the Slocum seaglider as well as performance characteristics.

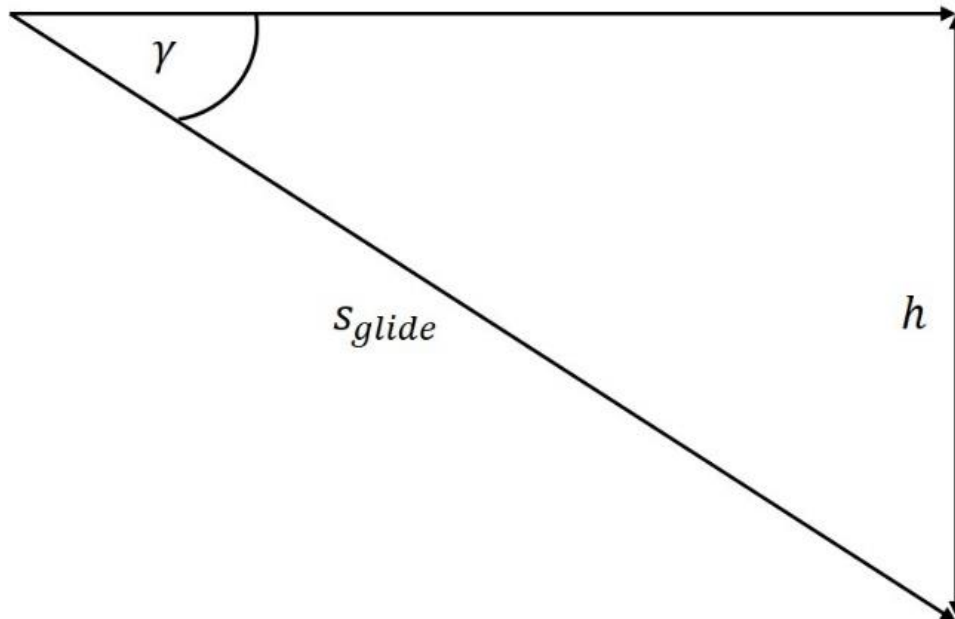


Figure 32: Simplified Half-Yo Descending Leg Flight Pattern

$$\begin{aligned}
 s_{glide} &= \frac{h}{\sin \gamma} \\
 s_{glide} &= \frac{200 \text{ m}}{\sin 25.47} \\
 s_{glide} &= 465.07 \text{ meters}
 \end{aligned} \tag{3}$$

Endurance is determined not only by the distance traveled per yo, but also by the energy consumed. While during most of a yo the seaglider consumes no propulsive energy, energy is consumed by the pump when the vehicle changes its net buoyancy at the top and bottom of the yo flight path. The amount of energy required consists of three components: the external hydrostatic pressure, the change of volume, and the motor efficiency. The external hydrostatic pressure at depth is a function of the fluid density (ρ), the acceleration due to gravity (g), and the depth at which the operation occurs (h). It should be noted that the numerical value of h increases with depth. The volume exchanged $|\Delta V|$, is determined by the design of the glider, its buoyancy engine's capacity, and capability to operate at depth. From Table 2 for the nominal glider $|\Delta V| = 0.000521 \text{ m}^3$ or 521 cc. The efficiency of the buoyancy engines pump at depth h denoted as η_{pump} . Equation 4 gives the total propulsive energy expended by the pump.

$$E_{pump} = \rho g h |\Delta V| \left(\frac{1}{\eta_{pump}} \right) \tag{4}$$

To complete one full yo, the pump must operate twice, once at the surface and once at depth, Equation 5 calculates the buoyancy based gravitational propulsive

potential energy used during a yo cycle. In order to clarify the analysis at this point, the buoyancy engine is assumed to be 100% efficient; therefore, η_{pump} , is set to one. This is done to make the initial development and implementation of this analysis method clearer to the reader. Using the maximum depth of 200 meters from Table 3, and ballast pump power consumption from [13], the overall energy per cycle is readily calculated, using Equation 5.

It should be noted that in operation a buoyancy engine must cycle between nearly full and nearly empty. However, this only results in half of the ballast being usable for the creation of any propulsive force, despite twice that amount of displacement change occurring. This is due to the system having to cycle from an ascent configuration, through neutral buoyancy, to a descent configuration, or vice-versa. The energy used by the pump near the surface is significantly less than that of a pump operating at depth and at first glance, it may appear that it should be free. It should be noted, that on the surface the delicate bellows pump used by the Slocum AUG, upon which our notional platform is based, requires both a brake and regulated exhaust of stored fluid to prevent damage to the buoyancy engine's systems. Published data on pump efficiency at the surface varies widely. To stay consistent with previous data, for the Slocum AUG a best estimate of 164 Joules is used. This information is retrieved from the work on the development of auxiliary propulsion systems by Claus [13]. Equation 5 takes the pump energy required at the surface (164 Joules) and adds the pump energy required at a target depth of 200 meters. The pump energy required at depth is given by the density of water 1023.6 kg/m³, the acceleration due to gravity (9.81 m/s²), the dive depth of 200 meters and the

total displaced volume of the buoyancy engine, 0.000488 m^3 , which is twice the ballast given in Table 4 of 0.00244 m^3 .

$$\begin{aligned} E_{cycle} &= \rho g h |\Delta V| \left(\frac{1}{\eta} \right)_{descent} + \rho g h |\Delta V| \left(\frac{1}{\eta} \right)_{ascent} \\ E_{cycle} &= 164J + \left(1023.6 \frac{kg}{m^3} \right) \left(9.81 \frac{m}{s^2} \right) (200m) (0.000488m^3) \frac{1}{1} \\ E_{cycle} &= 1144 \text{ Joules} \end{aligned} \quad (5)$$

Taking the operational depth of 200 meters and a glide angle of 25.47° a distance covered per cycle is determined. This distance can be either the glide distance, s_{glide} , Equation 6, or the horizontal distance, $s_{horizontal}$, Equation 7. These two range equations allow for the determination of the system's overall system range, as well as the testing of non-buoyancy driven systems on a seaglider's longer flight path. By selection these values will be the same in this analysis, as the glide path angle is being held constant. The glide distance is the total distance traveled during a yo and inversely proportional to the sin of the glide slope angle.

Letting h be the dive depth of 200 meters, we find that the glide distance is 930.15 meters, Equation 6. The distance covered per yo is determined by the glide slope, γ and the depth, h . Figure 33, below shows a simplified diagram of a yo, taking the seaglider from a neutrally buoyant state, through a descent cycle, and back to the surface.

In comparing the performance of a non-buoyancy propelled AUV to a seaglider the distance travelled has implications on the overall system efficiency and the resulting

mission performance. Having the AUV operate in a purely horizontal basis has its departure and destination points at the same locations as the gliders without transecting the same particular ocean segments vertically. In the case of the seaglider, this distance is akin to the systems net displacement rather than its path traveled. This occurs when- the system is transiting between areas of operation. Using the glide distance has both systems undertaking the same path required by the seaglider for forward motion and any impact it has skews the results in favor of buoyancy-driven system.

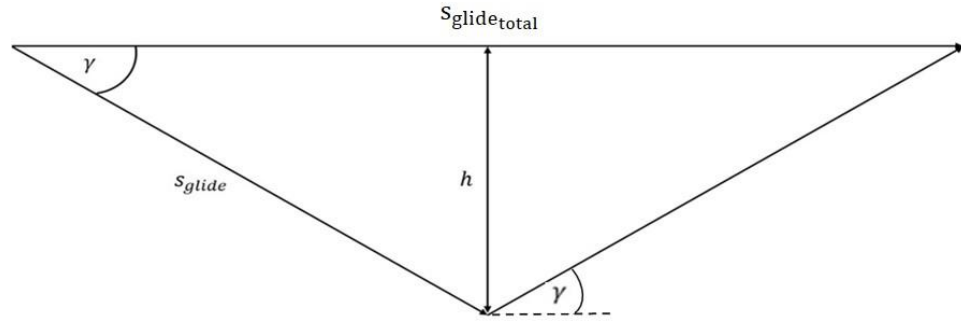


Figure 33: One Yo cycle Showing Distances Covered

$$\begin{aligned}
 s_{\text{glide}_{\text{total}}} &= \frac{2h}{\sin \gamma} \\
 s_{\text{glide}_{\text{total}}} &= \frac{2(200m)}{\sin(25.47^\circ)} \\
 s_{\text{glide}_{\text{total}}} &= 930.15 \text{ meters}
 \end{aligned} \tag{6}$$

$$\begin{aligned}
 s_{\text{horizontal}_{\text{total}}} &= s_{\text{glide}_{\text{total}}} \cos \gamma \\
 s_{\text{horizontal}_{\text{total}}} &= 930.15m \cos(25.47^\circ) \\
 s_{\text{horizontal}_{\text{total}}} &= 839.75 \text{ meters}
 \end{aligned} \tag{7}$$

The time taken to cover the horizontal distance, $s_{horizontal}$ can then be determined as the result of the distance covered divided by the average velocity at which it was covered, shown in Equation 8. The horizontal velocity of 0.349 m/s was determined by completing the velocity triangle formed by the forward speed of 0.388 m/s from Table 3 and rate of descent of 0.168 m/s from Table 3 and then using the Pythagorean theorem. Thus, the time during glide is estimated using Equation 8.

$$t_{glide} = \left(\frac{s_{horizontal}}{v_{horizontal}} \right)$$

$$t_{glide} = \left(\frac{839.75 \text{ m}}{0.349 \frac{\text{m}}{\text{s}}} \right) \quad (8)$$

$$t_{glide} = 2409 \text{ s (40 minutes)}$$

In order to determine the hotel load, E_{hotel} , of the glider during operation, average power data from [13] is used in conjunction with the overall glide time of the platform per cycle. Taking this data, the onboard electrical load, $P_{onboard}$ (0.2W), sensor load, $P_{sensors}$ (1W), and adding them together the hotel load, P_{hotel} , are computed (equation 9). The result of this shows that the sensor load, which is on the order of 2.9 kJ (Equation 9) is the dominant load, when compared to the approximately 1.14 kJ (Equation 5) propulsive load. However, this data does not take into account the impact of sensor scheduling, wherein sensors are selectively operated. The analysis below uses the full sensor load as a worst-case condition in the calculation of efficiency and range estimates.

$$\begin{aligned}
E_{hotel} &= (P_{onboard} + P_{sensors})t_{horizontal} \\
E_{hotel} &= (0.2W + 1W)2408.92 \text{ s} \\
E_{hotel} &= 2890.70 \text{ Joules}
\end{aligned} \tag{9}$$

Once the energy use per cycle by the buoyancy engine is evaluated, the hotel load is added, yielding the total system energy usage per yo. After this has been determined, this value can be divided into the storage capacity of the battery, in this case, 8 MJ per [13], Equation 10. This yields the gross number of cycles the system is capable of achieving before complete battery depletion. As there is no published data on the number of cycles achievable per battery charge, as a check of this method, this value will be used to compute a range estimate (see Equation 11). This can then be checked against published range data.

$$\begin{aligned}
Cycles &= \left(\frac{E_{battery}}{E_{cycle} + E_{hotel}} \right) \\
Cycles &= \left(\frac{8000000 \text{ J}}{1144.05 \text{ J} + 2890.70 \text{ J}} \right) \\
Cycles &= 1982
\end{aligned} \tag{10}$$

$$\begin{aligned}
Range_{km} &= (Cycles) \left(\frac{s_{horizontal}}{1000 \text{ m/km}} \right) \\
Range_{km} &= (1982) \left(\frac{839.75 \text{ m}}{1000 \text{ km}} \right) \\
Range_{km} &= 1664.38 \text{ km}
\end{aligned} \tag{11}$$

Table 5: Seaglider Range Varying Efficiency and Hotel Load

	$\eta=1$ No Hotel Load	$\eta=0.5$ No Hotel Load	$\eta=0.5$ with Hotel Load
Glide Range (km)	6506	3253	1298
Horizontal Range (km)	5874	2973	1172

Table 5 highlights both a theoretical glide range and horizontal range, Row 1 and Row 2 respectively. It does this using varying system configurations. Column 1 highlights range, while the seaglider is operating with a 100% efficient buoyancy engine, and no hotel load. As previously stated the hotel load is defined as energy being used by systems that are non-propulsive in nature. Similarly, Column 2 shows a seaglider with a 50% efficient engine operating with no hotel load. Column 3 shows a glider. As expected using an estimate of the buoyancy pump efficiency of $\eta=0.5$ substantially reduces the predicted range as shown in Table 5 Column 2. Including the hotel load in addition the buoyancy pump efficiency (Table 5, Column 3) yields a total horizontal range of 1172 kilometers.

It has been suggested that the glide path angle plays a significant factor in determining the target efficiency of the thruster. As a check of this overall method, the range was calculated using the optimal glide path angle of 20° from Table 3, and the data the ballast data from Table 4, glide 1. The result of this analysis is a horizontal range of 1448.44 kilometers, which is within 3.5% of the estimated Slocum range of 1500 kilometers.

It is interesting to note that we can also estimate the maximum mission time. Taking the glide time of an individual yo (2408 s) and the number of yo cycles (1982),

we estimate that the maximum mission time is 4.78×10^6 seconds or slightly over 55 days of continuous operation.

4.3 AUV Power Usage

A glider powered by a buoyancy engine spends the majority of a glide at a drag limited maximum velocity. We wish to compare a thruster driven AUV operating in conditions identical to the buoyancy driven glider of the last section. In this condition, the drag force must be equal to the propulsive force from buoyancy engine. This relationship is shown in Equation 12. While a seaglider utilizes the buoyancy-gravity interaction for propulsive power, the AUV leverages the momentum imparted onto the fluid by a mechanical device such as a propeller or jet thruster.

$$F_{thruster} = F_{Drag} = F_{propulsive} \quad (12)$$

To determine the energy required by the thruster, the drag force, F_{Drag} , needs to be determined. The standard drag equation from Theory of Wing Sections by Abbot and Von Doenhoff [19] is shown in Equation 13, where ρ is the fluid density at operating depth, equal to 1023.6 kilograms per cubic meter, S is the vehicle's frontal area, in this case 0.038 m taken from Table 3, V the operating velocity, and C_D is the vehicles drag coefficient. Despite the relatively simple shape of a seaglider, the low-speed operation makes their drag coefficients extremely sensitive to numerous factors including surface roughness, attitude relative to oncoming flow, and relative velocity. As such, there is a wide variation in published drag coefficient values with little agreement between

theoretical and empirical data. The value of the drag coefficient utilized here, 0.27, is taken from the data found in Table 4, glide 1 [39], and is of the same order as data from [77], making it a reasonable value with which to start the calculation of the systems overall drag. This value was non-dimensionalized using frontal area and is assumed to represent the total drag on the seaglider while in operation.

In steady state, the force produced by the thruster should equal to the force produced by the buoyancy engine in the longitudinal or propulsive direction. Therefore, we expect the results of Equation 13 and Equation 14, to be equal.

$$F_{Drag} = \frac{1}{2} \rho V^2 S C_D$$

$$F_{Drag} = \frac{1}{2} \left(1023.6 \frac{kg}{m^3} \right) \left(0.388 \frac{m}{s} \right)^2 (0.038m^2)(0.27) \quad (13)$$

$$F_{Drag} = 0.79 N$$

$$F_{buoyancy_{Longitudinal}} = \rho g \frac{|\Delta V|}{2} \sin \gamma$$

$$F_{buoyancy_{Longitudinal}} = \left(1023.6 \frac{kg}{m^3} \right) \left(9.81 \frac{m}{s^2} \right) \frac{|0.000488m^3|}{2} \sin(25.47) \quad (14)$$

$$F_{buoyancy_{Longitudinal}} = 1.05 N$$

It is readily apparent that the results of Equation 13 and Equation 14 are not equal. There are manifold reasons for this inequality. The primary reason would appear to be that C_D is underestimated. Variations in the velocity are also of great concern. These variations can occur due to unaccounted for currents, tidal activity, or wave motion.

Even small variations in the velocity can have a large impact on the drag produced. In addition to this, the systems surface finish and degree of biofouling also play a role in the drag produced. Furthermore, changes in the AoA would cause changes in the induced drag of the overall system. The resulting 20% discrepancy is coming from the variability in the drag data is the reason the propulsive component of the buoyant force is being used instead of the system's drag.

The overall energy used per cycle serves as a target value for calculating an efficiency range for an AUV thruster. In order to do this, the required thrust, distance traveled, and the thruster efficiency need to be determined. The total propulsive energy required by the thruster is ascertained by multiplying the propulsive force, $F_{Propulsive}$ which in this case is the longitudinal component of the buoyant force, by the distance covered, s_{thrust} , and dividing by the thruster efficiency, $\eta_{thruster}$, Equation 15.

$$E_{thruster} = F_{Propulsive} s_{thrust} \left(\frac{1}{\eta_{thruster}} \right) \quad (15)$$

$$\begin{aligned} \eta_{target} &= \frac{F_{Propulsive} s_{glide}}{\left(\frac{E_{cycle}}{\eta_{pump}} \right)} \\ \eta_{target} &= \frac{(1.05N)(930.15m)}{\left(\frac{1144.05J}{1} \right)} \\ \eta_{target} &= 85.66\% \end{aligned} \quad (16)$$

Equation 16 shows that even if the thruster follows the same glide path as the 100% efficient buoyancy engine, the required thruster energy is 85.66% of the buoyancy engine's energy. The use of an electric thruster in this manner does not appear to have been researched and as such this result is unique. **Simply put, this analysis highlights that for the same vehicle, operating the same mission, under the same low-speed, low-drag conditions a correctly sized thruster must be only 86% efficient when compared with a 100% efficient buoyancy engine.** Expanding on this result and applying real world efficiencies further reinforces that given the correct design considerations a conventionally propelled system can meet or exceed the performance of a buoyancy driven system. As a typical Slocum type system buoyancy engine has an efficiency of 50% [77], the above analysis indicates that the thruster only needs to have an efficiency of 43%. In addition, if the non-buoyancy propelled system is performing a transiting maneuver it can improve its efficiency by taking the shorter path, $s_{horizontal_{total}}$. In this case, the efficiency requirement is 40%. These target thruster efficiencies are readily achievable. Work on developing high efficiency propulsions systems for long-rang AUVs has been undertaken with some of these systems already being fielded. These works focus on systems with higher operational speeds than those readily achievable by a seaglider under normal operating conditions. However, some systems operate at speeds very close to those achievable by a buoyancy driven system. One such system is the Tethys long-range AUV, [60]. This system designed for extended deployments operates at velocities on the order of 1 meter per second. To achieve the desired endurance this system has a specially designed aft-body and propulsion system. Through design, simulation, and testing the overall efficiency of the

propulsion system on the Tethys AUV was determined to be 53% from actual fielded data [60].

4.4 Thruster System Analysis

Having determined that a thruster driven AUV can have similar endurance to a buoyancy engine driven sea glider. However, the operational speed of a glider is much slower than that of most thruster-propelled vehicles. Three thruster paradigms were selected for analysis to answer the question of whether or not a non-buoyancy propelled AUV can compete in terms of operational endurance and range with a seaglider. These paradigms were: jet-based propulsion, a biologically inspired Pulsatile Vortex Thruster, and a conventional propeller based system. Examination of these thruster paradigms for the design space of low-speed AUVs was undertaken and their efficiencies estimated. If the estimated efficiency of any of these paradigms is close to or greater than the efficiency target calculated in the previous section, then with some certainty, a conventionally non-buoyancy propelled AUV can be competitive with a seaglider.

4.5 Jet Drive

Jet drive efficiencies were determined using the Froude Efficiency model, Equation 17 from [59], this model takes into account variations in the ratio of vehicle velocity to jet velocity, R_v , and duct inlet efficiency, ζ . Both of these values range from zero to one for propulsive applications. However, they do not take into account losses arising from the electromotive force required to spin the impeller of the jet which would lower the overall system efficiency.

$$\eta_j = \frac{2R_v(1 - R_v)}{1 - R_v^2(1 - \zeta)} \quad (17)$$

The graph produced for jet propulsion, Figure 34, shows that with an increase in inlet efficiency, ζ , and a decrease in the velocity ratio a corresponding increase in overall efficiency can be seen peaking at maximum theoretical value of 100% on the right-hand side of the graph. Similarly, as the vehicle to jet velocity ratio approaches one on the right-hand side of the graph the efficiency again increases peaking to approximately 75%. Taken together, the interplay of inlet efficiency and vehicle to jet speed ratio skews the efficiency curves as the inlet efficiency increase toward one. As for operation in the low speed environment favored by gliders, this pulls the vehicle to jet velocity ratio down and therefore, dropping overall efficiency toward the 20% range making jet propulsion system less efficient than a buoyancy engine.

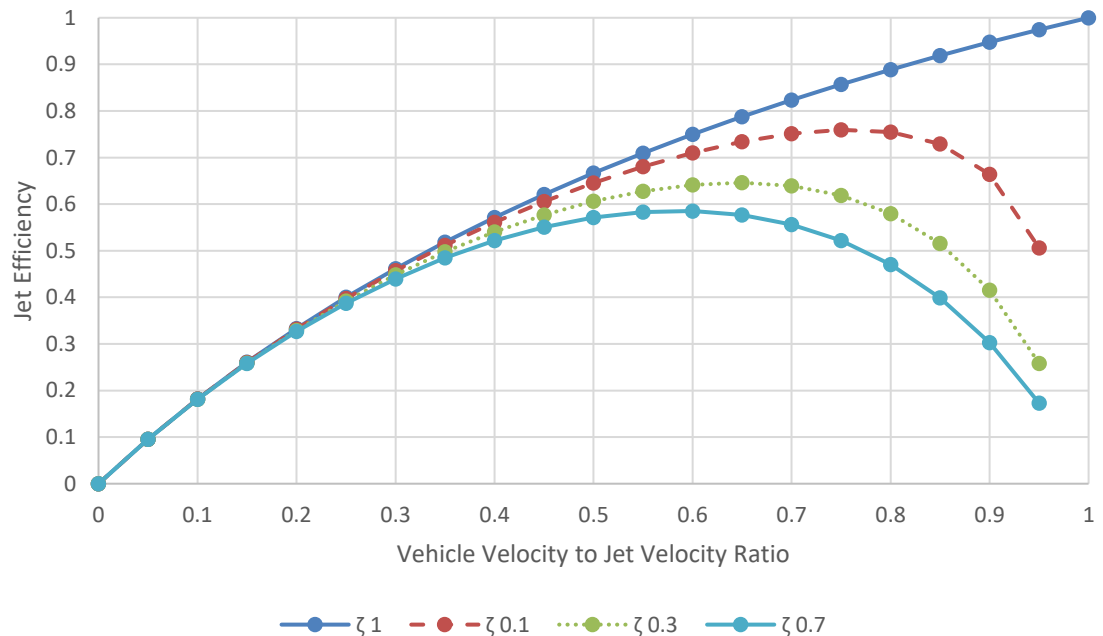


Figure 34: Jet Efficiency Varying Inlet Efficiency and Vehicle to Jet Velocity Ratio

4.6 Pulsatile Vortex Thruster

The Pulsatile Vortex Thruster (PVT) is a bioinspired and unsteady thruster.

Inspired by the propulsive methodology employed by squid and jellyfish, this synthetic jet consists of a deformable diaphragm, chamber, plunger, and single orifice. Imparting a cyclic motion to the diaphragm results in slugs of fluid leaving the orifice with fresh fluid then being ingested through the same orifice. Upon ejection the fluid slug is moving at a higher velocity than the near quiescent external fluid, this coupled with the act of leaving the orifice adds vorticity to the ejected mass causing a toroidal vortex to form. This vortex, if sized correctly, helps impart added momentum to the fluid, a result of the vortex expansion and the resulting overpressure propels the vehicle forward more efficiently than the fluid slug alone. More information on their design and function can be found in [66], [67], [68].

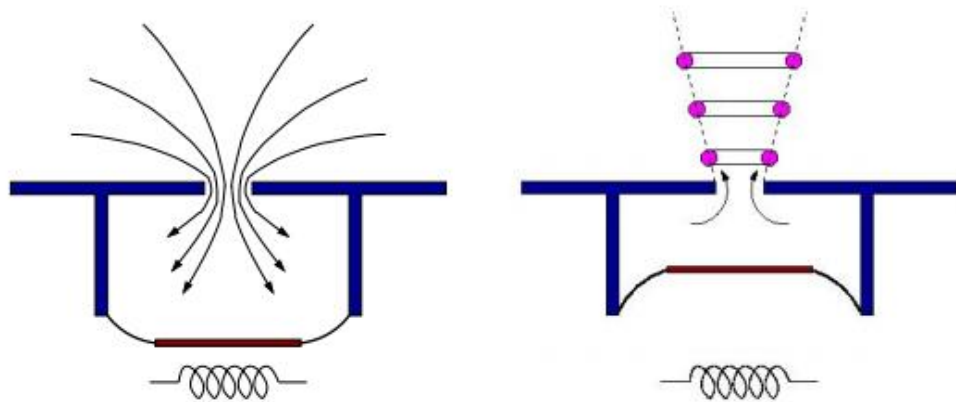


Figure 35: Pulsatile Vortex Thruster Schematic Showing Fluid Entrainment (Left) and Vortex Ring Formation Resulting During Ejection (Right) Retrieved from [66]

PVT efficiency is a complex multivariate problem, that depends on parameters such as jet-to-vehicle velocity ratio, cycle rate, shaft work, and impulse imparted to the fluid. However, work done by Krieg and Mohseni [78] indicate that for duty cycles in the 40-50% range, efficiencies in the 35-40% range are possible, as shown in

Figure 36. This implies that, a correctly designed AUV propelled by a PVT would be able to compete favorably with a seaglider.

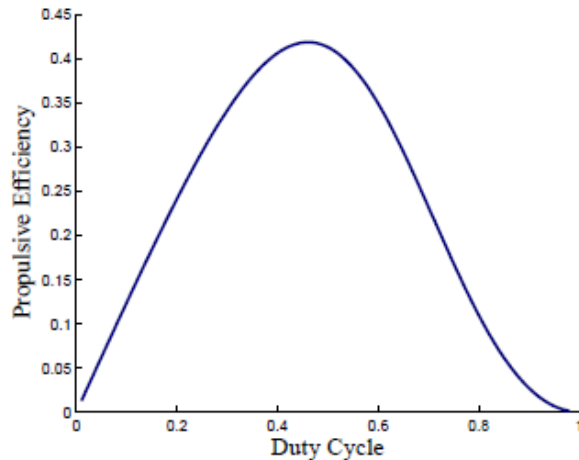


Figure 36: Propulsive Efficiency of a PVT vs. Duty Cycle Retrieved from [78]

With its mechanical simplicity, high-efficiency, and predisposition for operations in slow moving fluids the PVT was expected to be the better candidate for a propulsion system able to compete effectively with a buoyancy engine. However, with the result from section 4.3, showing that a propulsion system need only be on the order of 43% efficient to compete with a buoyancy drive, commercially available methods of propulsion become viable, chief among these are the conventional propeller based system.

4.7 Propeller Driven

Propulsive efficiencies for a propeller based drive system were investigated using a data set from a commercially available candidate thruster. The T200, from Blue Robotics is more powerful than necessary to move the candidate Slocum type vehicle. However, unlike many commercially available AUV propulsions systems, it has a plethora of available performance data. The manufacturer provided data, is given in Appendix D Table D1. This data was used to determine the overall propulsive efficiency of the system while operating in the low-speed regime required for seaglider operation. In order to determine the power output of the system, the momentum imparted to the fluid had to be ascertained, which in turn, required the calculation of a reasonable estimate for the thruster's efflux. An initial estimate of thruster's efflux was determined by taking the geometric pitch of the propeller and multiplying it by the RPM of the motor to determine the velocity of the fluid leaving the propeller. Multiplying this efflux velocity with the thrust produced by the system yields the power out, Equation 18. Dividing the power out by the measured supplied power results in the overall propulsive efficiency, Equation 19. Assuming a no-slip condition for the propeller, which given the quasi-quiescent state of the fluid being operated in was deemed acceptable based on the near quiescent nature of the flows involved, these estimates are considered a good initial estimate of propulsive efficiency. The results of Equation 18 and Equation 19 can be seen in Appendix D Table D1.

$$Power_{out} = Pitch \left(\frac{RPM}{60} \right) Thrust \quad (18)$$

$$\eta_{propeller} = \frac{Power_{out}}{Power_{in}} \quad (19)$$

Much of the data in Appendix D is given in terms of Pulse Width Modulation or PWM. Figure 37 and Figure 38 plot thrust and efficiency in terms of PWM. As its name suggests PWM is a modulation technique using the width of pulses typically found in the control of electronic motors and thrusters. Typically, for radio control (RC) type hardware, a pulse is expected every 20 milliseconds, with a pulse width varying between one and two milliseconds. The amplitude of the pulse correlates to the commanded throttle for motors. In the case of the Blue Robotics T200, a range of pulse widths from 1000 to 2000 milliseconds correspond to a command full reverse thrust to full forward thrust, with zero throttle at a command of 1500 microseconds. For example, a PWM of 1750 microseconds relates to a throttle setting of approximately 50% of maximum forward thrust.

The efficiencies for the T200 operating at 12 volts is tabulated Appendix D Table D1 and graphed in Figure 38.

At steady state operation, a vehicle's thrust equals its drag. This allows for the use of the linear trend line found using the data displayed in Figure 37, equating thrust to a specific PWM value, Equation 20. This was determined by calculating the thrust required to move the candidate AUV of 1.05 Newtons from Equation 14.

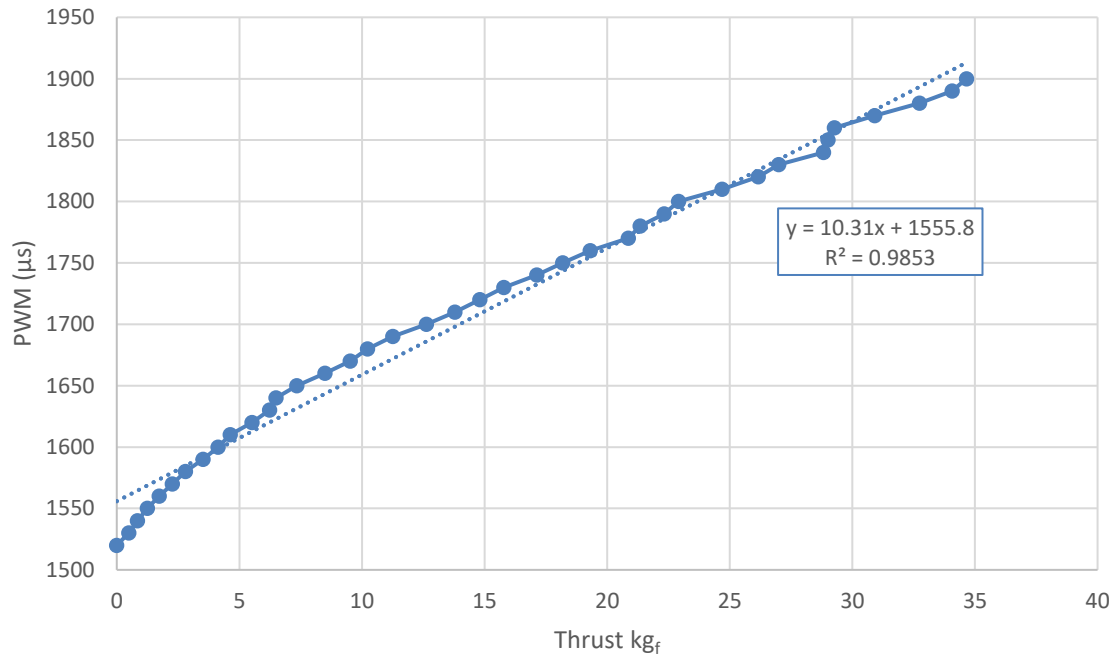


Figure 37: T200 Thrust vs PWM

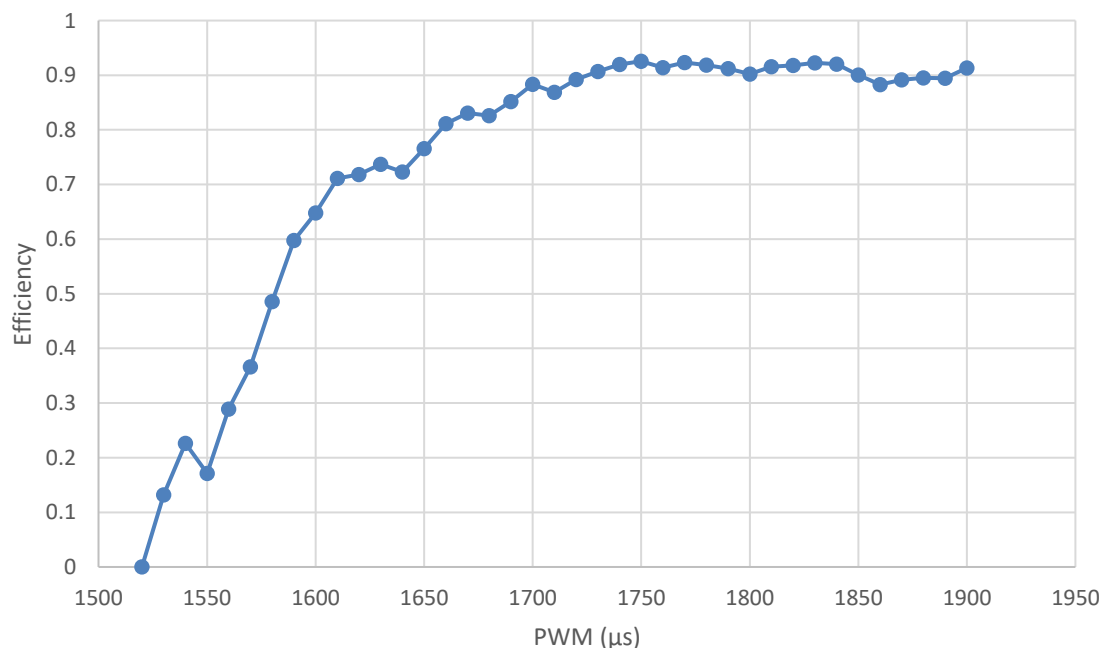


Figure 38: T200 PWM vs Efficiency

$$\begin{aligned}
 PWM &= 10.31F_{propulsive} + 1555.8 \\
 PWM &= 10.31(1.05) + 1555.8 \\
 PWM &\cong 1566 \mu s
 \end{aligned} \tag{20}$$

Taking the PWM value of 1566 and the data from [79] the resulting efficiency for the T200 thruster ranges from 28.87% to 36.64% for the PWM values of 1560 microseconds and 1570 microseconds respectively. Although these efficiencies are less than what is required to equal the efficiency of a buoyancy engine, the maximum efficiency achieved by thruster at higher RPMs is sufficient to do so. This indicates that it is possible to design a thruster that achieves the required efficiencies at the required thrust levels.

4.8 General Case Analysis

Having established that a thruster can be more efficient than a buoyancy engine we now extend the analysis from Section 4.3 to an arbitrary propulsion system. The determination of a more general energy usage case of seagliders when compared conventional AUVs can be undertaken using equations already derived in this chapter. We define a Figure of Merit (FOM) by dividing the seaglider energy usage per cycle by the equivalent equation for AUV power usage, arriving at an energy ratio. The resulting energy ratio indicates which method of transport is more efficient. If the number is greater than one seagliders use more energy, less than one a conventional system uses more energy. The derivation of this is laid out below in Equation 21 through Equation 29.

$$FOM = Energy\ Ratio = \frac{E_{cycle}}{E_{thruster}} \quad (21)$$

Taking the buoyancy engine per cycle energy use equation, Equation 5, and adding subscripts for ascent and descent allows for the impact of varying depth between surfacing and non-surfacing to be adequately captured, the result of this is displayed in Equation 22. As in Equation 5 the density of the working fluid is, ρ , the acceleration due to gravity, g , and the volume of the buoyancy engine, ΔV , with the efficiency of the buoyancy engine at the associated depth represented by, η .

$$E_{cycle} = \rho g h_{descent} |\Delta V| \left(\frac{1}{\eta} \right)_{descent} + \rho g h_{ascent} |\Delta V| \left(\frac{1}{\eta} \right)_{ascent} \quad (22)$$

Equation 23 serves as the basis for the denominator in the FOM. Using the fact that the drag force on the system is equivalent to the component of the buoyant force in the drag direction, Equation 24 can be substituted into Equation 23.

$$E_{thruster} = F_{Drag} s_{travelled} \left(\frac{1}{\eta_{thruster}} \right) \quad (23)$$

$$F_{buoyancy_{DragDirection}} = \rho g \frac{|\Delta V|}{2} \sin \gamma \quad (24)$$

Similarly, taking Equation 15 and setting the distance thrusted equal to the gliders distance travelled, which in this case is equal to Equation 6, total glide distance results in Equation 25.

$$E_{thruster} = \rho g \frac{|\Delta V|}{2} \sin \gamma \frac{2h_{ascent}}{\sin \gamma} \left(\frac{1}{\eta_{thruster}} \right) \quad (25)$$

Cancelling terms and collecting the remaining variables the simplified form of the thruster's energy usage can be seen in Equation 26 which serves as the denominator of the FOM.

$$E_{thruster} = \rho g |\Delta V| h_{ascent} \left(\frac{1}{\eta_{thruster}} \right) \quad (26)$$

The assembly of Equation 25 and Equation 26 into our energy ratio equation yields Equation 27. Collecting terms and simplifying Equation 27 yields the final version of our energy ratio Equation 29.

$$FOM = \frac{E_{buoyancy}}{E_{thruster}} = \frac{\rho g h_{descent} |\Delta V| \left(\frac{1}{\eta} \right)_{descent} + \rho g h_{ascent} |\Delta V| \left(\frac{1}{\eta} \right)_{ascent}}{\rho g |\Delta V| h_{ascent} \left(\frac{1}{\eta_{thruster}} \right)} \quad (27)$$

$$FOM = \frac{h_{descent} \left(\frac{1}{\eta_{pump}} \right)_{descent} + h_{ascent} \left(\frac{1}{\eta_{pump}} \right)_{ascent}}{h_{ascent} \left(\frac{1}{\eta_{thruster}} \right)} \quad (28)$$

If we consider a dive from the surface $h_{descent} = 0$ to some depth h_{ascent} Equation 29 becomes just the ratio of the thruster and pump efficiencies (Equation 29).

$$FOM = \frac{h_{ascent} \left(\frac{1}{\eta_{pump}} \right)_{ascent}}{h_{ascent} \left(\frac{1}{\eta_{thruster}} \right)} = \frac{\eta_{thruster}}{\eta_{pump}} \quad (29)$$

However, from, Claus and Bachmeyer's [13] work on gliders, it is known that running the pump at/near the surface requires a fixed non-zero amount of energy of roughly 164J. Including the energy consumed at the surface the energy ratio becomes Equation 30.

$$FOM = \frac{SurfaceLosses + h_{ascent} \left(\frac{1}{\eta_{pump}} \right)_{ascent}}{h_{ascent} \left(\frac{1}{\eta_{thruster}} \right)} \quad (30)$$

It becomes clear that even if one were to assume the thruster and pump systems are equally efficient, that the numerator is larger than the denominator and that the buoyancy engine based vehicle will consume more energy than a thruster based vehicle. This is due to the fact that at the surface a seaglider expends energy to ready its pump to dive, which in the case of a Slocum glider this is 164 Joules. Therefore, a thruster borne vehicle designed to operate in a seagliders low-speed, low-drag regime will use less energy than a buoyancy driven seaglider.

4.9 AUV and AUG range versus operational depth

Having a method of determining the energy use as function of dive depth, an investigation of AUV and AUG range versus operational depth was conducted. Autonomous Underwater Gliders operate efficiently by utilizing their propulsive systems for a short period compared to the time at which they are in motion resulting from this action. Typically, to complete one cycle, or yo, an AUGs buoyancy engine operates for approximately one minute. When operating at a lower depth of 200 meters with a glide path angle of 25.47 degrees this one minute of work results in 40 minutes of forward motion. An analysis was conducted to compare the AUV and seaglider range for the full range of potential dive depths.

Due to the constant load at the surface, seagliders consume more energy when operating in shallow waters, which requires the more frequent cycling of their buoyancy engine. This is a result of the optimization of the buoyancy engine's pump for operation at depth. As the seaglider approaches the surface, its buoyancy engine is run more often in a lower efficiency mode resulting in an increased power draw. In addition to this decrease in efficiency of the pump, due to the shallow nature of the operating environment the pump is forced to run more frequently. Figure 39, shows both the seaglider and conventionally propelled AUV system operating with no sensor load. This would be equivalent to the system transiting from one location to another, or if run in this configuration until the battery is depleted a maximum theoretical range. Using the efficiency target of 42% this equates to an AUV having equal to or better performance than an AUG up to a depth of approximately 200 meters. This encompasses all the worlds' littoral and riverine areas as well as a majority of the planets continental shelf. In the scenario posited in Figure 39, it would take an increase in the AUVs energy storage of

only 6.25% to equal the range of the AUG to the 1000 meter operational depth. This would be readily achievable by placing batteries in the volume previously occupied by the buoyancy engine, or a reduction in the size of the vehicle which would improve its drag characteristics.

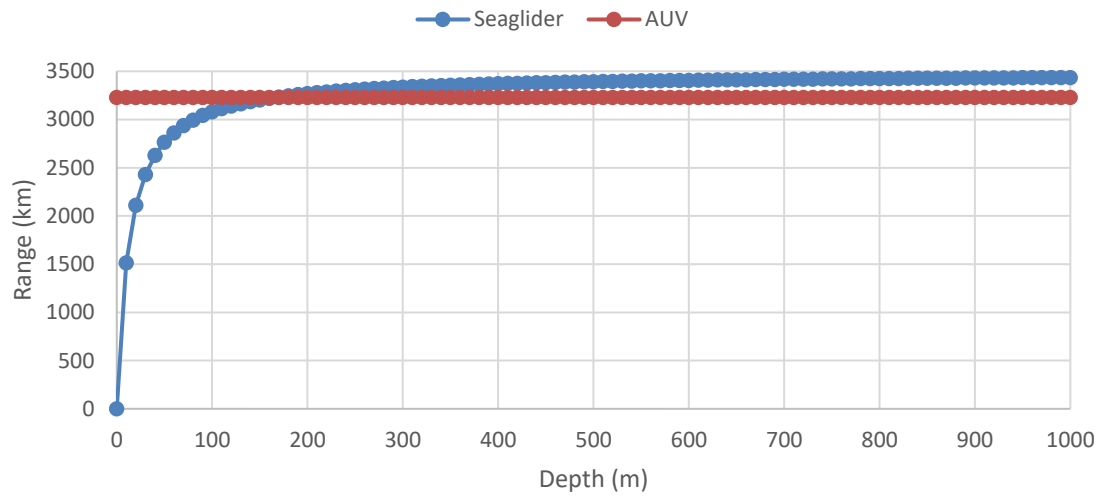


Figure 39 Depth Variations Impact on AUV and AUG Range

4.10 Optimizing the Surrogate AUV for Thruster Only Operations

Up to this point in the comparison of propulsion systems, the analysis has intentionally favored the buoyancy driven system. This is evident in the use of the notional surrogate, which is functionally a legacy seaglider with an additional thruster. It should be evident that the surrogate, as it is essentially a seaglider is optimized for buoyancy driven operations as opposed to thruster borne operations. What would happen if the buoyancy-propelled system were optimized for thruster borne operation instead? Without the undertaking of a full systems trade study a simple thought experiment can be

used to see the benefits of switching propulsive types while maintaining the low-speed, low-drag operational regime.

The external encumbrances required for buoyancy driven operation become redundant under solely thruster borne operation. Removal of the wings and empennage from the glider decrease its hydrodynamic losses through a reduction in both wetted area and removal of the wings which cause lift induced drag. The removal of the buoyancy engine and its associated systems allow for hull optimization for thruster borne operations. This optimization can leverage the internal volume gained through the removal of the bulky buoyancy engine through either an overall reduction in size or the addition of batteries or sensing systems. With the further reduction in volume, and wetted area, the entire propulsion system can be reevaluated, as to propel a smaller, lighter, and lower drag system at the same speed as a larger heavier, higher drag system, less thrust is required. This in turn would decrease power requirements further, allowing for either an additional reduction in overall system size, or all things being equal a longer ranged system using the existing onboard energy stores.

4.11 Summary

A simple first principles energy-based approach to seaglider operation was developed and then verified using real-world data. This was done to determine if a conventionally propelled AUV operating in the low-speed, low-drag regime of a seaglider could perform in a comparable manner, something which had previously not been investigated. The resulting AUV propulsion system target efficiency of approximately 43% was determined. This method was then generalized to prove that in general a

properly sized propulsion system can compete with a buoyancy engine throughout the seaglider operational regime. Three separate propulsion paradigms were selected for study in this regard, a jet based system, a pulsatile vortex thruster, and a propeller.

Jet propulsion resulted in a propulsive efficiency on the order of 20%. Once coupled with a mechanical drive system and controller it is felt this option would drop below the desirable efficiency thresholds. To do otherwise would take a highly optimized system, this coupled with the long-term nature of glider missions and the likelihood of an impeller-based system being fouled this was deemed a poor choice for further investigation.

Efficiency data for the PVT shown in,

Figure 36, indicates that for duty cycles ranging between 40-60% the estimated efficiency of the system overlaps the AUV target efficiency. Further benefits of a PVT propulsion system are its minimal impact on overall system hydrodynamics, compact form factor, and the preference for operation at low speed. However, the intricacies of design and manufacturing of such a system when compared with the better-understood propeller based systems left it as an interesting concept, and one worthy of future investigation.

The analysis of the electric Blue Robotics T200 commercially available thruster yielded results indicating peak efficiencies of 28.87% to 36.64% for the 94 millimeter geometric pitch. These efficiencies correspond to the very lowest thrusts that the thruster is able to produce and an area in which it is not particularly efficient. This result indicates the high likelihood of designing around this inefficiency via a larger internal

energy store, streamlining, or planform change, in conjunction with a suitably designed propulsion unit.

The key result of this chapter is that although a seagliders propulsion system has a low average power-draw its overall efficiency is not outside the realm of feasible operation for a more conventional propulsion method operating in the same low-speed regime. Furthermore, the overall efficiency of a seaglider's, buoyancy based propulsion paradigm is impacted by the depth of operation. Deeper dives drive the time between buoyancy engine pump operation up. With less frequent cycling leading to less energy lost to pumping at the surface, however, this is offset by the increased work required to pump at depth. An added handicap that faces buoyancy based propulsion is the sawtooth yo path required for operation. Unless the specific mission requires that exact path be taken, shorter straight line paths are available. This decrease in distance results in a less operational runtime on the conventional propulsor, which in turn leads to less energy draw, and an improvement in overall endurance.

Chapter 5: Wave tank testing

5.1 Introduction

Chapter IV discussed the efficiency of a conventional buoyancy driven system and compared it with that of other propulsive paradigms. It was asserted that propeller based propulsion systems are able to attain efficiency values exceeding the 43% required to meet or exceed the performance of a buoyancy engine. It was also stated that if properly designed a conventional propeller based propulsion could achieve these high efficiencies in the low-drag, low speed environment in which seagliders operate. In Chapter IV, this was accomplished using manufacturer supplied data for the Blue Robotics T200 thruster. However, in the development of this data set, especially the efflux velocity of the thruster and its ensuing power output, assumptions were made such as the no-slip condition for viscous fluids. This assumed that fluid contact with a solid boundary has zero velocity. In the complex flow environment present around a propeller this is inaccurate, and leads to an overestimation of thruster efflux velocity, and therefore power output. To prove the assumptions made in the propeller model are sufficiently accurate, real-world data is required. This data was collected using the non-linear wave tank facility, a force balance, to measure the thrust produced by the thruster, and a fluid velocity measurement system. The data needs to be collected in two distinct flow regimes, static, and dynamic. Data taken in the static regime, in which the fluid surrounding the propulsion system is in a quiescent state, will act as a verification set, validating assumptions made in Chapter IV and improve the estimates made therein. The dynamic data, where the fluid is moving around the thruster will serve to indicate the amount of efficiency lost to operating the thruster in such an environment, simulating a

moving vehicle. As with the static data set, the dynamic data set will be used to examine the efflux of the Blue Robotics T200 thruster and its dynamic performance.

5.2 Design parameters

In order to verify assumptions and estimates made in the efficiency of the Blue Robotics T200 thruster in Chapter IV real-world data is required. This, in turn, dictates the development of an apparatus capable of measuring the loads generated by a propeller operating in the seaglider's low-speed, low-drag regime as the efficiency estimates previously made in Chapter IV. In order to do this a force balance producing meaningful hydrodynamic data in the regime in question is required. This balance must also be able to integrate into existing testing facilities, and not require any special mounting or storage equipment. This will be done using a custom designed force balance and the Wave Tank located in the Center for Nonlinear Waves in the College of Arts and Sciences.

5.3 Wave Tank/Water tunnel

The Wave Tank Laboratory located in the Center for Nonlinear Waves in the College of Arts and Sciences, shown in Figure 40, contains a large state-of-the-art wave tank and its associated data acquisition hardware. Measuring 9.75 meters x 1.22 meters x 1.22 meters, and able to hold upwards of 11,350 liters of water and is equipped with a modern wave maker system. Additionally, the wave tank is equipped with six 5.2 kW pumps, able to sustain flows of up to 1 meter per second, and has a suite of, anemometers, hotwire anemometers, and pitot tubes and gauges for velocity

measurement. This equipment is supplemented by high-speed cameras capable of taking detailed images of fluid phenomena at 1000 frames per second.



Figure 40 ERAU Wave Tank

5.4 Force Balance Design

As a commercial-off-the-shelf, force balance does not exist at the ERAU Wave Tank Facility, and was not going to be readily available in a timeframe conducive to the completion of this research, a custom unit had to be designed and manufactured. To do this the force balance's structure and the data acquisition system had to first be sized to confirm desired operation. Due to the longitudinal nature of the data being collected a 2-dimensional balance was deemed adequate. As for the overall design of the balance, a simple swing-arm assembly was chosen over other designs, such as pyramidal or sting balance types, primarily due to the swing-arm's simplicity, portability, and robustness. A

diagram of the finalized balance is shown below in Figure 41, with more detailed schematics shown in Appendix E.

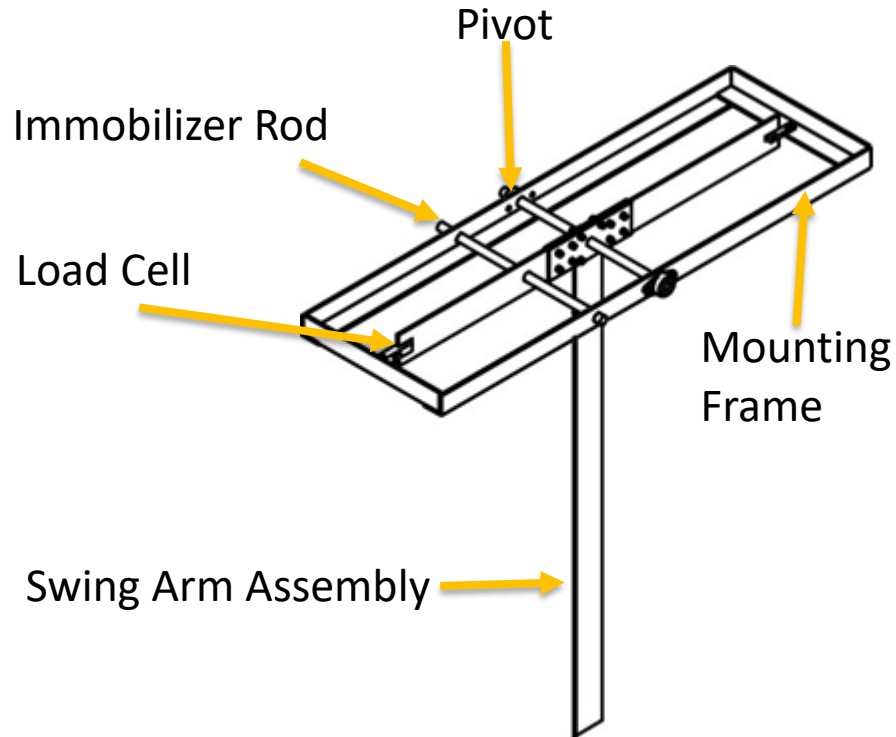


Figure 41 Final Design of the T-type Swing Arm Force Balance (Shown with the Immobilizing Rod Inserted)

The system is designed around a primary “T-type” swing arm that transmits loads from the thruster up through a pivot and onto a 5 Kg load cell, located at the top of the “T”. Using a simple static moment equivalence about the rotation point, the swing arm also imparts a 2.236 mechanical amplification of the input load. This amplification was deemed acceptable as it was a compromise between manufacturability and transportability. A set of bearings ensure that the swing arm’s motion is fluid. The load cell communicates to the Arduino Mega via a load cell amplifier. The OpenScale load

cell amplifier features an HX711 differential sensing circuit with a gain of 128, reading directly from a four wire Wheatstone bridge. Detailed specifications for this load cell can be found in Appendix C. This amplifier allows for simple communication via USB to an Arduino Mega, which acts as the data collection and transmission system. When the force balance is not in use an immobilizing rod is inserted through the assembly ensuring the load cells are not subjected to a freely swinging swing arm.

For this study, the loads are kept on the order of those experienced by a slocum type glider during normal steady-state operations. Determination of the steady-state loading was accomplished in the same manner as in Chapter IV, leveraging the propulsive component of buoyant force. The resulting load is on the order of one Newton. With the baseline maximum nominal loading for the thruster providing the operational envelope, sizing of the primary structural members is able to take place.

Table 6: Typical Slocum Glider Physical Properties for Determination of Steady State Loading. Adapted from [36]

Hull Length	1.50 m
Hull Diameter	0.21 m
Hull Frontal Area	0.038 m ²
Mass	52 kg
Volume Change	0.000521 m ³

Table 7: Steady State Glide Data Taken from Insitu Seaglider Operations for Determination of Steady State Loading. Adapted from [39]

Value	Glide 1	Glide 2	Glide 3	Glide 4
Pitch θ (deg)	-22.77	23.74	-25.78	24.03
Depth rate \dot{z} (m/s)	0.168	-0.224	0.2	-0.228
Ballast (m³)	-0.000244	0.000237	-0.00025	0.000238
AoA α (deg)	2.7	-2.9	2.3	-2.9
Speed V (m/s)	0.388	0.499	0.425	0.503
Drag Coefficient CD	0.27	0.31	0.25	0.31

Longitudinal Component of the Buoyant Force

$$F_{buoyancy_{Longitudinal}} = \rho g \frac{|\Delta A|}{2} \sin \gamma$$

$$F_{buoyancy_{Longitudinal}} = \left(1023.6 \frac{kg}{m^3}\right) \left(9.81 \frac{m}{s^2}\right) \frac{|.000488m^3|}{2} \sin(25.47) \quad (31)$$

$$F_{buoyancy_{Longitudinal}} = 1.05 N$$

Of prime concern for failure is the single longest member of the swing arm assembly. Measuring 0.8128 meters the long arm of the swing arm assembly, not only has the longest unsupported span of any single component, but is also the single component with the highest length to cross-sectional thickness ratio, and is subjected to the loads directly from the equipment, and water in the wave tank. As such, loads were analyzed for failure before moving onto the rest of the structure. These calculations can be found in Appendix E14. Despite, the long-slender moment arm the aluminum structure has a high factor of safety of at least 4 across all its structural members. The only area in which the structure is marginal is in lateral bending. However, at the time of

design and manufacturing, it was deemed a low priority as the flow and primary loads of the system are in the longitudinal plane.

5.5 Load Calibration

To ensure accurate and repeatable operation of the force balance the load cells needed to be calibrated. This was done by applying a load via a pulley ensuring that it is applied at the extreme end of the swing arm, as the thrust from the Blue Robotics T200 thruster would be. A diagram of this arrangement can be seen in Appendix E Figure E13. The load was left applied to the structure for 30 minutes, to check the system for creep, and once removed, hysteresis. These loads are detailed in Appendix E Figure E13. After running this experiment multiple times with calibration loads up to 1 kilogram (9.81 Newtons) a steady offset of .020 kg (0.1962 Newton) was determined. Each time a new data set was collected the load cell and amplifier was re-tared in air with the offset included in the calibration at software startup.

5.6 Experimental Setup

The force balance and its mounting hardware is shown mounted in the wave tank in Figure 42. Figure 43 shows the T200 thruster mounted to the force balance and the water level at a height sufficient for testing. Figure 44, shows the data acquisition system including the Arduino and PC. The force balance designed to capture the loads resulting from the drag and thrust of the propulsion system. The fluid velocity measurement equipment, featuring a screw type anemometer to accurately measure both the free stream velocity and the efflux from the thruster.

The equipment, excluding the wave tank, is electrically powered by two separate systems. This was done for simplicity, and to reduce the likelihood of noise interfering with the data acquisition process as a commutating motor was present. Powering the system's low voltage side is a single USB power supply regulated via a laptop computer's internal USB system. This operates the Arduino, amplifier, and load cell. The motor is supplied by a 360 Watt power supply, which is connected to the Blue Robotics T200 thruster via a 30 Ampere electronic speed controller. To ensure consistent operation the power supply was configured in such a way that it delivered a constant 12 Volts while supplying up to 3 Amps to operate the motor at the desired PWM rating.

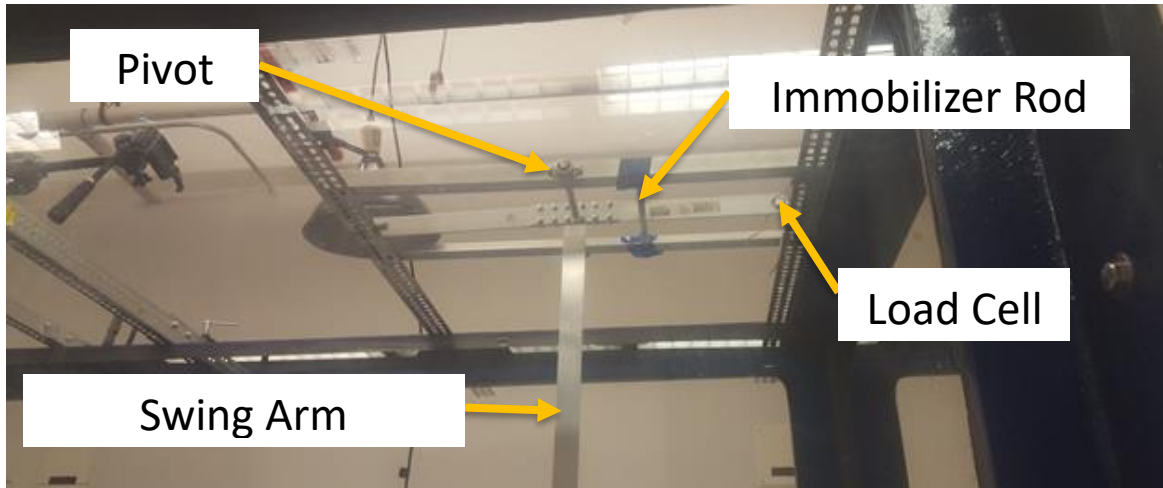


Figure 42: Experimental Force Balance Installed in the ERAU Wave Tank Facility

The thrust produced by the thruster is controlled via a laptop communicating to an electronic speed controller. To vary the thrust output, a serial command, in this case, the desired PWM value of the thruster, was sent over a serial terminal to the electronic speed

controller. This activated the data acquisition systems and the thruster, ensuring whenever the thruster was active, data was also being recorded.

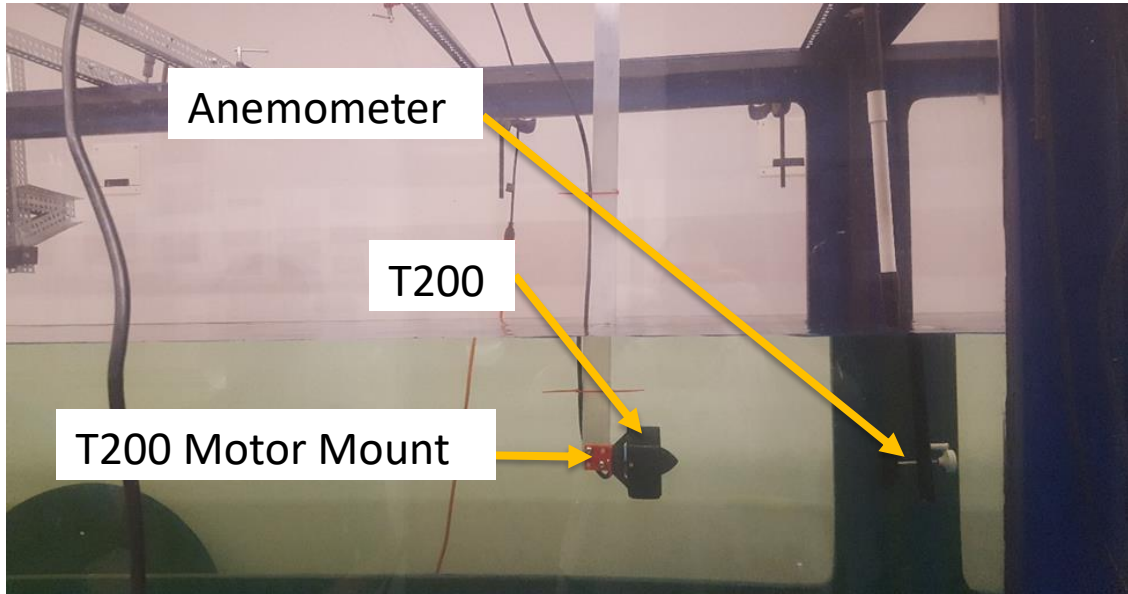


Figure 43: T200 Thruster Operating at a PWM Setting of 1600 in a Static Flow Condition

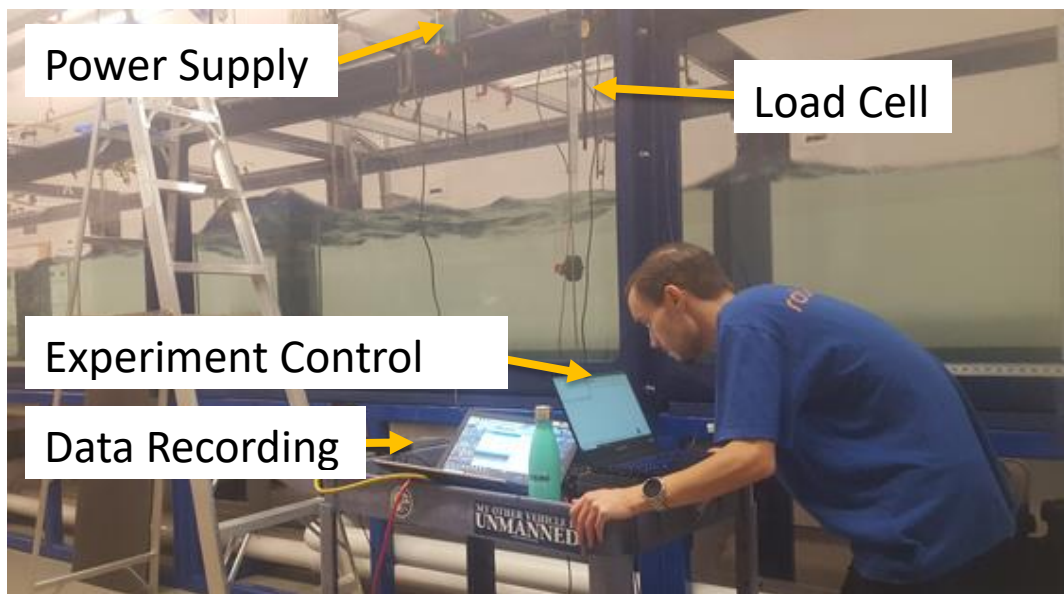


Figure 44: T200 Thruster and Force Balance Under Testing the ERAU Wave Tank with Fluid Velocity of 0.015 meters per second

5.7 Testing Procedure

The testing procedure for this experiment is dependent on what phase of experimentation was being executed. Phase 0 involved the testing and validation of the force balance in laboratory settings. This was done in the absence of the wave tank, and water in order to simplify the initial calibration and verification. Bench testing was also conducted to ensure the laptop to Arduino to electronic speed controller to thruster toolchain was reliable before it was placed in the water. Phase 0 also included the calibration of the load cells to determine the overall system offset and hysteresis.

In phase 1, testing took place in the wave tank and was done as a verification of the overall function of the data acquisition system, and the experiment design as a whole. This experiment validated the form, function, and fit of the equipment in the non-linear wave tank, its ability to collect data while installed, and its ability to collect data while the tank is pushing fluid over the experimental assembly. Once the equipment was installed, its ability to record both data and command the thruster was tested and confirmed to meet requirements. After this an initial data set was collected manually. The dataset consisted of a sweep of thrusts from 0 to 1 kilogram-force. This corresponds to PWM settings ranging from 1500 (0 thrust) to 1566 (1 kilogram force). Two chief concerns for accurate measurement are the avoidance of the ingestion of vortices from the surface and the minimizing the vibration of the system. The ingestion of vortices through the thruster was observed to occur at higher thrust levels and low water heights. This problem was corrected by the increase in overall water depth in the wave tank.

The final phase of testing involved taking a full PWM sweep data set in both static and dynamic conditions. The load data and flow velocity data was matched via

zeroing the load from the thruster between each data point, and having the PWM command and data logging software start at the same time.

5.8 Testing Results

As previously stated the results of the Phase 0 testing was the determination of the overall load offset of the system, which was 0.020 Kg_f. This experiment also confirmed the repeatability of the data collection system and the structural integrity of the system under anticipated experimental loads.

Phase 1 of experimentation resulted in both load and flow velocity data being captured through a sweep of PWM settings. Testing conditions were restricted such that the thruster would not ingest vortices during operation. The final piece of information collected during this experiment was the operational qualities of the experimental equipment itself. Originally it was planned to use either a hot-wire anemometer or pitot-static to collect flow velocity data. Both the pitot-static probe and the hotwire anemometer were preferred systems for the function of measuring the fluid velocities involved in this experiment due to their compact nature, and ease of which they can be traversed through the test section. However, these systems were unable to reliably meet the accuracy required in this experiment. In the case of the pitot-static probes, the pressure gauges were unable to read the small pressure changes resulting from the operation of a thruster at such low speeds. The hotwire anemometer was able to read changes in flow speed. The readings taken by this system were volatile at the low speeds which result from low-speed thruster operation. This is due to the probe head used being

designed for use in air. It was believed that it could be recalibrated for use in water but this was not the case.

As a result of this, a more conventional screw-type anemometer was utilized for flow velocity data acquisition. Another result of this test was the determination that at higher thrust levels, and close proximity (within 0.20 meters), the anemometer used vibrated in the longitudinal plane. This phenomenon was only exacerbated with the activation of the wave tanks pumping system. Furthermore, upon activation of the pump the oscillation of the water in the tank caused the arm on the force balance to oscillate in the lateral direction. These oscillations resulted in significant swings in the recorded efflux velocity. This was due to the anemometer measuring not only the velocity of the thruster efflux, but also the component of the tank velocity regardless of the direction the flow was going.

The final experimental run included modifications intended to correct some deficiencies discovered during the execution of the phase 1, experiments. High tensile strength monofilament guy wires were added to both the force balance and the anemometer. This retrofit decreased the magnitude of the oscillations experienced by both the force balance and anemometer arm under all stages of operation. Data collection proceeded the same as the previous experiment, with data from the static and dynamic runs shown below in the results section.

The tabulated static data for the second phase of the experiment can be seen below in table Appendix D Table D2-D4, alongside the data from the manufacturer Table D1, as well as Figure 45 and Figure 46, in which the two data sets are compared one atop the other.

5.9 Discussion of results

The purpose of this experiment was to validate the values calculated using data provided by the manufacturer of the T200 thruster. This data shown in Figure 45 and Figure 46 is shown in a tabular format in Appendix D Table D1 contains manufacturer provided data such as PWM, Voltage, Amperage, Wattage, and Load in Kilogram force. This table also contains the data derived from the manufacturers data including the Flow Rate, Load in Newtons, Power Output, and the systems overall efficiency. This derived data is highlighted in orange. The theoretical flow rate was determined by taking the RPM data from Table 3, dividing it by 60 converting it to revolutions per second, and then multiplying that by the thruster's propeller geometric pitch, of 0.094 meters [79]. Multiplying this flow rate by the PWM derived thrust output yields the theoretical power output of the entire propulsion system. From this data, it can be seen that according to this analysis at maximum thrust a theoretical efficiency of 82.59% is possible. However, at the output requirements for the extremely low-speed, low-drag regime in which seagliders operate this thrust requirement drops significantly, and along with it the overall efficiency.

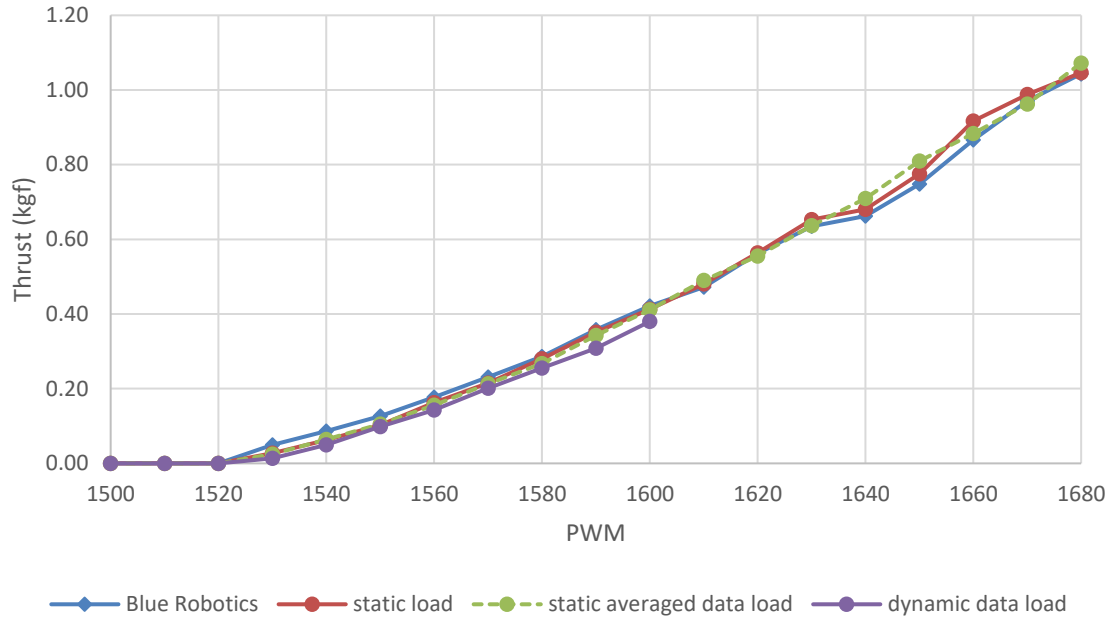


Figure 45 T200 PWM Thrust Data

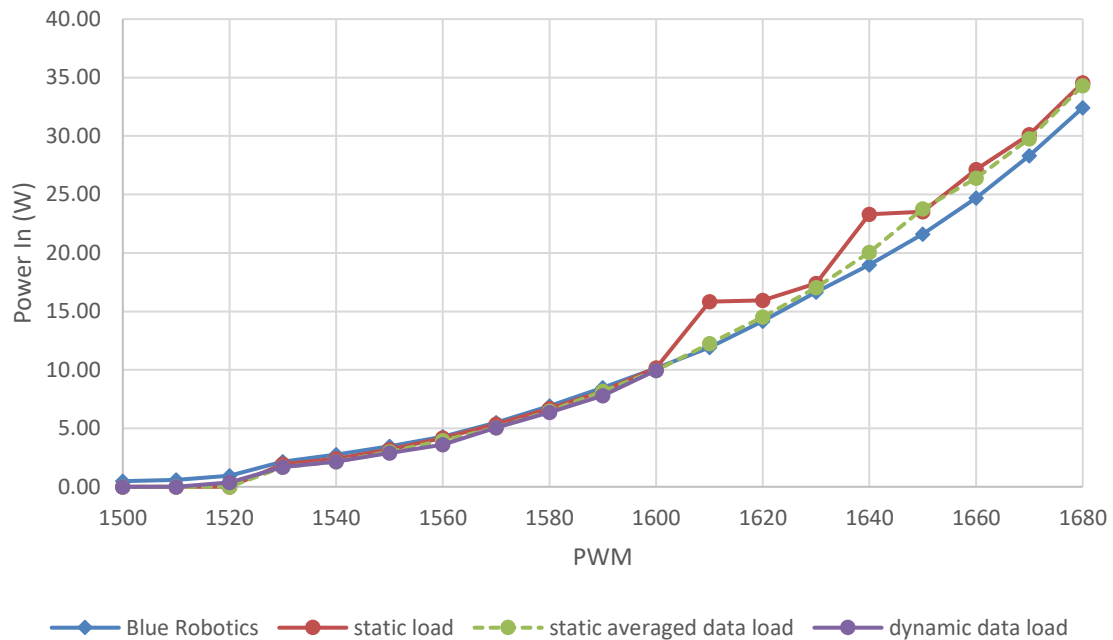


Figure 46: T200 PWM Power In Data

The next phase of experimentation dealt with the installation of the force balance into the wave tanks existing infrastructure and its ability to collect all the readings necessary. When comparing the manufacturers data to that of the measured runs, and taking the mechanical amplification of the measured data into account it is clear the data sets share not only the same general trend but magnitudes as well. A screw-type anemometer was used to determine the flow rate out of the thruster. Mechanical oscillations dictated that the screw-type anemometer was placed 0.32 m from the thruster so that it did not physically impact the thruster itself. This required the data collected by the anemometer to be adjusted to reflect flow speeds as close to the propeller as possible. To do this an assumption of constant mass flow rate while under thrust was made along with the application of the conservation of momentum, and the Bernoulli equation. Thrust produced by a propeller can be defined as the area of the propeller disk multiplied by the change in pressure across the disk. Measuring the pressure in front of and a distance behind the propeller allow for the determination of the change in pressure across the disk. The result of this is that the velocity at the propeller is the average of the velocity before and after the propeller. Data collected from both the static and dynamic tests are shown in Figure 45 and Figure 46 with the tabularized data listed in Appendix D, Table D2, Table D3, Table D4, and Table D5. The data is organized in the same manner as Table D1, with the measured data PWM, Voltage, Amperage, Wattage, and Load in Kilogram force catalogued. Data derived from the measured data, the Flow Rate, Load in Newtons, Power Output, and the systems overall efficiency are right justified and italicized.

It should be noted that in the dynamic test case, the maximum PWM value for the thruster was capped to 1600. This was done as operating the wave tank above these speeds caused significant fluid oscillation. However, as a PWM value of 1600 is above the region of interest of 1570 as stated in Chapter IV, it was felt that this was an acceptable trade-off.

The following figures contain data from Blue Robotics, the manufacturer of the T200 thruster, as well as both static cases, and the dynamic test case in which the wave tank was operated on a single pump to induce a flow of 0.015 meters per second. This is lower than the 0.4-0.5 meter per second range experienced by a seaglider in cruising operation. However, even at this speed oscillation in the system was beginning to skew data. The collection of thrust and power data was collected in order to verify that the experiment was providing accurate data vis-à-vis the performance of the T200 thruster. Of key interest is the correlation of the data in the 1500-1600 PWM range, as this is in the desired operating range for a slocum-type system. Figure 45 shows the correlation of the manufacturer's data with both static tests, with all three data sets being incredibly close throughout the PWM sweep. The exception to this is the dynamic data which has a lower thrust output through the tested PWM range due to the de-rating of the system which occurs in a dynamic flow field. This de-rating is due to the differential between the efflux velocity and incoming flow, as well as inefficiencies that are amplified by the moving fluid, including drag and tip effects. Simply put, a moving propeller changes the momentum of the fluid across itself producing thrust. The smaller the change in this momentum the less thrust produced. As a result of this relationship, a propeller will produce more thrust in a quiescent or quasi-static case than it will in a flow field. A

similar trend between the data is visible in Figure 46, where all power draw data including the data from the dynamic tests show the same general trend and magnitude up to a PWM value of 1600. After this value, the collected static data shows a slightly higher power draw.

The data in Figure 47 shows the relationship between commanded PWM value and power out. In this case, power out is the energy added to the flow of the thruster's efflux. Unlike Figure 45, and Figure 46 the values for the power out are calculated from measured data, not directly measured themselves. To calculate the mechanical power produced, the fluid velocity measured by the anemometer was multiplied the thrust measured by the force balance. This is the reason for the previously noted deviation in data between the manufacturer's data and the two static test cases. The no-slip condition applied in the calculation of the manufacturer's power out data implies that the overall losses in the system are lower than those measured. Despite this deviation occurring earlier than the desired PWM value of 1600, it is delayed enough that the region around PWM value of 1570 still show agreement.

Figure 48 highlights the efficiency-PWM curve for the T200 thruster from both manufacturers data and experimental results at both static and dynamic conditions. The overestimation of overall efficiency, evidenced Figure 48, is a result of the application of the non-slip condition assumption made from the manufacturer-supplied data. However, especially in the region of interest, below a PWM value of 1580, the manufacturer's data and both static cases do show agreement. With efficiencies for all three cases being in the 20% to 30% range. As is to be expected the dynamic case is below this.

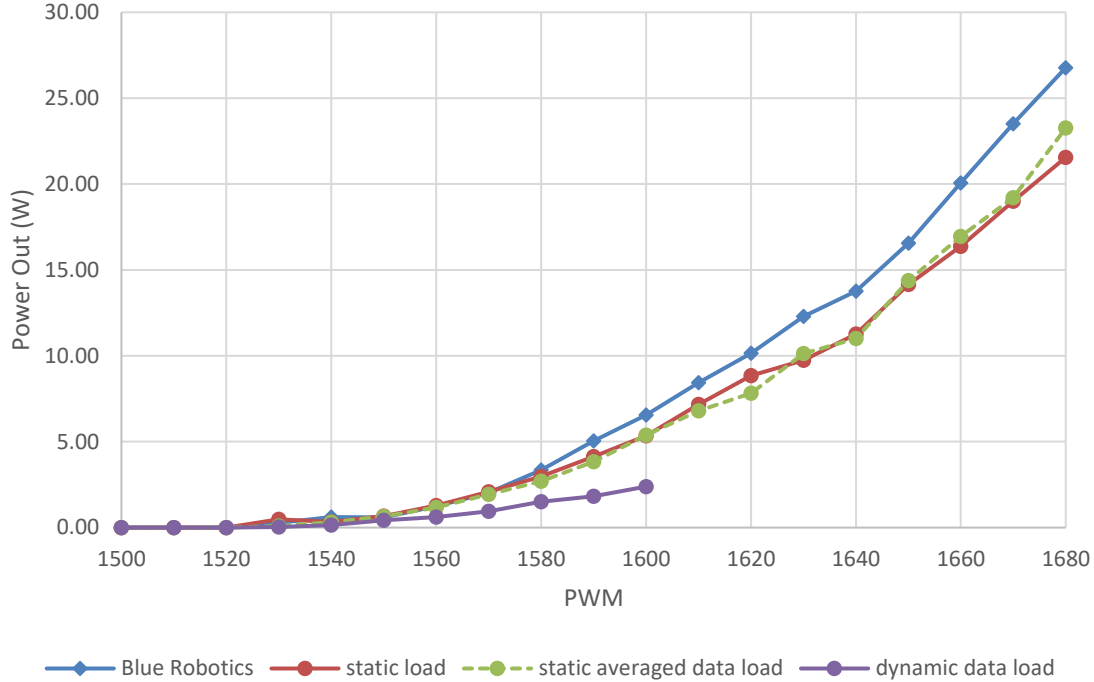


Figure 47: T200 PWM Power Out Data

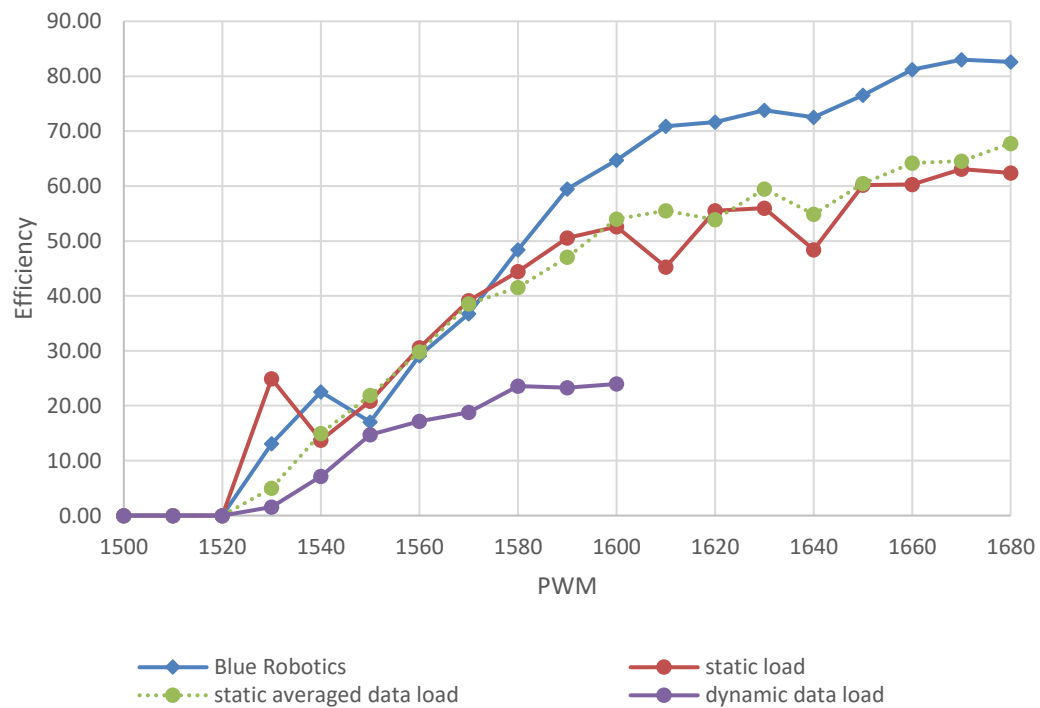


Figure 48: T200 PWM Efficiency Curves for Static and Dynamic Operation Cases

Similar to Figure 48, Figure 49 shows that for the static case, and at PWM values which produce a thrust in the desired one Newton (0.1kgf), range, the expected efficiency lies within the 20% to 30% range. Again as previously stated the exception to this is the dynamic data, which due to the added losses from motion, has a lower efficiency in the 15% to 20% range. These values are lower than the 45% required to compete with a buoyancy engine. However, this indicates that a COTS thruster is capable of achieving efficiencies required to compete with a buoyancy engine.

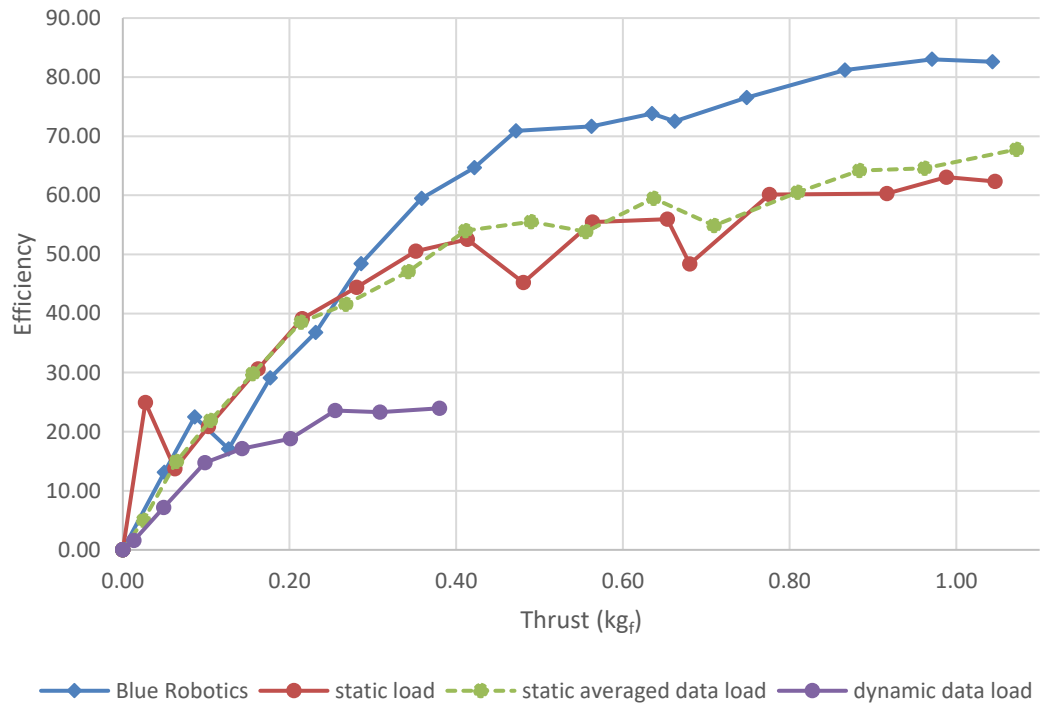


Figure 49: T200 Thrust Efficiency Data

5.10 Conclusion

The data produced in the course of the experiment agrees with the data provided by the manufacturer and reinforce the assumptions made in Chapter IV. This is especially

true in the performance range of interest. In the 1500-1600 PWM range, which corresponds to the low-thrust seaglider regime the T200's efficiency ranges between . Despite the efficiency, on the order of 35%, of the T200 thruster not meeting the required 45% efficiency value stated in Chapter IV to meet or exceed the performance of a buoyancy-driven system, there are a number of conclusions that can be drawn from the data. Key amongst these conclusions is that a commercial-off-the-shelf thruster can produce thrust consistently in the low ranges required to operate a slocum type seaglider. This data also shows that it is possible for a thruster of this type to achieve the efficiency values required to meet or exceed these performance targets. The overarching conclusion from the data presented is that, although the T200 is not the thruster to power an AUV capable of outperforming a buoyancy-driven seaglider, it is readily apparent one can be designed and built. An example of a system of similar size and capability to this desired propulsion system has already fielded in the form of the Tethys long range AUV [60].

Chapter 6: Conclusion and Future Work

6.1 Summary

The aim of this work was the investigation of enabling concepts and technologies for use in the development of a novel buoyancy driven winged submersible. These systems belong to a family of vehicles that rely on the modulation of buoyancy, and the hydrodynamic forces produced as a result as their primary means of propulsion. More commonly known as seagliders these platforms have proven to be a useful tool in the exploration of various oceanic biomes. Their relative simplicity from both an operational and functional standpoint have made them a go to asset in long-term oceanographic studies. These oceanic sensing missions can range anywhere from a days to weeks. This success is in part due to their endurance and low-noise characteristics. Inherent to their operation is a low-speed, low-drag mode shunned by the majority of surveying AUVs. These conventionally propelled AUVs typically operate at speeds over 1.5 m/s which is in excess of the 0.4-1.5 m/s seagliders are readily able to achieve. Despite the benefits low-speed operation affords seagliders it does preclude deployment in high current areas. Furthermore, the buoyancy engine itself has several weaknesses. These drawbacks include the reliance on depth for vertical excursions. A reduction in operational capability with decreasing depth was shown in section 4.9. Changes in the density of the working fluid, for example through changes in salinity, can render the seaglider unable to make forward progress. With these factors, the seagliders speed and depth limitations, it was decided that the best way to deliver a novel buoyancy driven winged submersible was to mitigate these shortcomings. The result of this decision led directly to the

investigation of different hull morphologies and the impact that has on overall seaglider performance.

Chapter 3 focused on select morphological changes made to the basic seaglider design and the resulting impact on performance. The investigation was broken down into the study of the same changes on two distinct types of seaglider. The two archetypes represented were the legacy or slocum type, a conventional streamlined body of revolution, and the flying wing type represented by the inverse Zimmerman Cranked Kite planform. The morphological changes were selected from concepts and technologies previously applied to existing aerospace systems. These systems were tested with both an annular wing, and a variable incidence wing. The approach taken for testing these changes was a simple experiment in which gliders of the same overall buoyancy were released in a test tank and their performance measured relative to one another. The results showed there is benefit to these systems, with improvements to both glide speed and glide path angle being possible. Both of these improvements would directly help mitigate the previously mentioned shortfalls in seaglider performance. Early in this branch of research it became clear that the morphological changes were always designing around the limitations of the buoyancy engine involved, be it the overall displacement of the engine, its efficiency, or the geometry of the system. This naturally led into the investigation of the buoyancy engine and its efficiencies as it relates to overall seaglider performance.

The buoyancy engine defines a seagliders performance. The buoyancy engines displacement relative to the seagliders overall displacement determines the available propulsive force available. Its overall volume, depth-rating, and efficiency are direct

drivers for speed, operational depth, and range. Given the seagliders unique operational regime, an interesting question arises: Can a conventional propulsion system compete with a buoyancy engine? Surprisingly this question has never been considered in the or documented in the available literature. Research had previously been done into hybridizing seagliders. This involves supplementing a seagliders buoyancy based propulsion system with a propeller to allow for higher speed operation, at the expense of endurance. The investigation of a conventionally propelled AUV operating in the low-speed low-drag regime favored by seagliders, and estimating its performance compared with a buoyancy based system had not been done. Chapter IV, covers the derivation of an energy-based first-principles approach to estimating seaglider performance. This method was then verified using real-world data showing that the theoretical results were within 3.5% of actual Slocum G2 seaglider performance numbers. This work was then expanded to estimate the required efficiency of a candidate propulsion system. To do this a notional vehicle was used, having the same physical properties as the Slocum G2. By comparing the energy usage of the two systems under the same conditions a target efficiency rating for the propulsion system was determined. For a 100% efficient buoyancy engine this efficiency rating was 86%. Finally a figure of merit was determined using an energy ratio. This FOM was used to simply show in the broadest case that a conventionally propelled AUV can compete with a buoyancy based propulsions system.

Chapter 5 focused on the experimentation used to confirm manufacture supplied data and assumptions made in Chapter IV. These experiments were conducted in the Wave Tank located at the Center for Nonlinear Waves in the College of Arts and Sciences

at the ERAU Daytona Beach Campus. This testing was carried out in phases beginning with design and manufacturing of a custom force balance. Static testing was then performed confirming values supplied by the manufacturer regarding thruster performance. In spite of the near quiescent velocities in which seagliders operate compared with other AUVs, propeller dynamic performance data was also tested. The results of this testing affirmed both the data from the manufacturer and the assumptions used in the development of the FOM in Chapter IV.

6.2 Conclusions

This research focused on improvement of seaglider performance. It did this through the investigation of both hull morphology and seaglider buoyancy engine efficiency. From this work several conclusions can be drawn. Regarding hull morphology, a variable angle of incidence wing, annular wing, and Inverse Zimmerman Cranked Kite planform were all investigated. The Zimmerman planform outperformed the legacy type, in terms of glide path angle and maximum velocity achievable. The annular wing proved to afford the platform a significant speed improvement but did so while operating at the steeper glider angles. Overall, an inverse Zimmerman planform, coupled with a conventional symmetric planar variable angle of incidence wing afforded the best combination of operation envelope expansion. This particular combination operated stably along glide path angles ranging from 20° to 57°.

Hull morphology is not the panacea to solving seaglider performance penalties regardless of the solution that is embraced. A key part of the performance potential of a seaglider comes from its buoyancy engine. Without a mission profile or particular

payload in mind the optimization of a hull to a notional mission is not truly solving the seagliders issues. Some of this can be offset using bespoke manufactured systems, or smaller, simpler designs. The other piece of the seaglider performance optimization lies in the buoyancy engine.

Investigation of the buoyancy engine and its efficiency formed the follow on line of inquiry after hull morphology. The key result from this research was that a non-buoyancy based propulsive system can compete with a buoyancy engine in the low-speed low-drag regime in which seagliders operate. A 100% efficient buoyancy engine can be equaled by an 86% efficient thruster. If the average buoyancy engine efficiency of the seagliders that publish this data of 50% is taken into account this number drops to 43%. The 43% target for the entire propulsion system is achievable. The Tethys long range AUV which is currently being operated in conditions near that of a seaglider has a measured propulsive efficiency of 55%.

6.3 Future work

One of the most important performance characteristics for a long range AUV is its endurance given an amount of stored energy, followed by the speed at which it can operate. Ideally these numbers will be as large as possible. This led to the current research of hull morphology and propulsive efficiency. Future work as an extension of this research includes the investigation of smaller bespoke manufactured systems, refinements to the seaglider modeling presented in Chapter IV, and the development of a low-speed optimized propulsion system. Further areas of research include the utilization of smart materials in the development of smaller more efficient buoyancy engines, the

investigation of methods for improving the overall performance of a seaglider through energy harvesting, and the addition of conformal PVT thrusters.

6.3.1 μAUV

The existing generation of AUVs are expensive, large, and difficult to deploy without external support equipment. Development of small, low cost Micro AUVs (μAUVs) alleviate a majority of these problems and are an area of interest for both civilian scientists and defensive applications alike. Small inexpensive systems, require lower thrusts to operate at the same low speeds favored by current generations of seagliders. These systems also allow for experimenting with novel planform and propulsion concepts. For these reasons the development of a μAUV would be worth investigating.

6.3.2 3D Printing/Bespoke Manufacturing

Moving from a concept validated by simulation and engineering analysis to a testable prototype is the crucial next step in the development and testing of any new platform. This often requires the accurate fabrication of complex shapes, often consisting of specific compound curves, and tight tolerances. Typically, this is accomplished using tooling for a design that may need extensive modifications which is expensive.

Mitigation of this through the use of CAD tools in conjunction with DDM is one potential solution. This disruptive technology has the potential to assist in the development of small-scale test components, subscale prototypes, or in the case of small AUVs and μAUVs full scale prototypes. Furthermore, if scaled correctly, tests of the

DDM subscale prototype can inform the user on concept performance long before large scale testing is required.

6.3.3 Energy Modeling

The development of a more detailed seaglider energy usage model would aid in the development of novel seaglider concepts. An accurate energy usage model would allow for a more rigorous testing of control algorithms, path planning strategies, sensor scheduling, mission planning, and system design. For thruster and hybrid AUVs a key aspect of refining this metric is the inclusion of minimum steerageway speed for AUVs. The steerageway speed is the velocity at which a vessel needs to operate at in order to maneuver. This metric is currently not considered in the energy model and has a sizeable impact on vessels requiring constant forward motion.

6.3.4 Propulsive Methodologies

Another area of investigation is the manner in which the buoyancy engine itself is implemented. The number, location, and displacement relative to the platform all have a marked influence on the performance of the glider. These areas looked at holistically have the potential to increase either the range, speed, or maneuverability of the system.

As previously stated in Chapter IV a conventional thruster can be competitive with a buoyancy engine. Further investigation of propulsive paradigms is key to furthering seaglider performance. The design and integration of a low-speed optimized high-efficiency propulsion system would be of interest. This work would focus on the entirety of the drive train. Fundamental to this effort would be the design and sizing of

the motor, bearings, shaft seals, aft body of the hull, and propeller. All these systems would have to be designed specifically for the system and its low-speed operating regime.

Taking inspiration from nature the PVT has been proposed as an alternate method of propulsion for a seaglider. Favored by Cephalopods and Medusozoan PVTs are a zero net mass exchange systems that are well suited for low speed and impulsive operations. These small thrusters require only a single external aperture which results in very little impact on the external hydrodynamic shape of the platform. A result of this is the option to install clusters of these bioinspired thrusters to aid in maneuvering, or station keeping of both conventionally sized seagliders, small AUVs, and μ AUVs.

Missions which previously would have been out of the operational envelope of a seaglider may become tractable with the proper augmentation of either the propulsive systems, maneuvering capabilities or the combination of the two. An example of this is the surveying of oceanic fronts, an area in which two different water masses interact. Currently a seaglider is unable to follow these regions of interaction due to the sweeping nature of seaglider turns. However, with the addition of lateral PVT maneuvering thruster this might be feasible.

6.3.5 Application of smart materials

Smart materials possess intrinsic properties that allow repeatable and reliable reaction to changes in their environment. These materials respond to a stimuli ranging from mechanical deformation to thermal changes as well as changes in the electrical domain and magnetic fields. The use of one such material, a Nickel Titanium alloy known as Nitonol, or shape memory alloy has been proposed for use in buoyancy

regulating devices [10], [11], and been the subject of limited testing. Leveraging this base research, a novel Nitonol based buoyancy engine could be developed.

6.3.6 Energy Harvesting

Another method for increasing seaglider performance is through energy harvesting. This concept has seen some limited trials with the advent of the Slocum Thermal Glider. Slocum gliders equipped with a thermal buoyancy engine already do this to great effect, with theoretical ranges far outstripping those of conventionally powered seagliders, [80]. These systems function through the use of a phase change material, in this case a wax. The interaction of this material with the environment and the resulting volumetric changes are leveraged to power the seagliders buoyancy engine with minimal input from the systems onboard energy storage. However, they are limited to operations in waters with a sufficient thermal gradient to allow the operation.

To mitigate this shortcoming other avenues of energy harvesting need to be addressed. Potential areas for research include the harvesting of waste energy in the wake of the seaglider and the use of a recovery device on the efflux of the buoyancy engine itself. Utilization of piezoelectric smart materials for energy harvesting have been investigated for numerous use cases [81]. Efflux energy harvesting could also be achieved through the use of a turbine, or via the onboard pump. This system would be akin to the regenerative breaking used in hybrid vehicles. The efficient storage of the recovered power is also an area of investigation. This synergistically overlaps with areas of research already happening at ERAU in both the clean energy track of the Mechanical Engineering program and the ongoing ECOCAR project.

6.4 Summary

The design and development of a novel buoyancy driven winged autonomous platform was initially proposed. This research took place in multiple phased steps to ensure success, and allow for the readjustment of focus as new areas of inquiry arose. The first stage of research was the familiarization of the author with seagliders. This included their history, initial research purpose, concepts in their design, operation, and shortcomings of buoyancy based propulsive systems. Following this research it was decided to investigate the exterior form or morphology of the seaglider to see if new concepts would lead to improvements in performance. This led to the development and testing of novel hull morphologies. These select concepts were culled from research previously applied to aerospace systems. They included variable angle of incidence wings, annular wings, and an Inverse Zimmermann Cranked Kite planform. Comparative testing of these designs yielded interesting results. However, by far the most interesting realization was the external hydrodynamic envelope of the system was only part of the problem. The capabilities and limitations imparted on the system by its buoyancy engine were far reaching and in need of investigation. This line of inquiry finally led to the question: Can A Conventional Propulsion System Match The Efficiency Of An Underwater Glider Buoyancy Engine? Surprisingly the answer is yes. A simple question, with a counterintuitive answer, which up to this point had not been asked. Conventional propulsion systems if designed correctly can compete with a buoyancy engine in the low-speed, low-drag regime favored by seagliders. This was proven using a first-principles energy based method with seagliders and the competing notional AUV operating in the sagittal plane. Verification and validation of the assumptions made in the development of

the thruster model and feasible efficiencies was later conducted using the non-linear wave tank. Looking at the entirety of the work conducted here led to new lines of inquiry for areas for future research. Key among these areas for investigation are the development of smaller bespoke seagliders, the utilization of smart materials for improvement in both buoyancy engine performance via energy harvesting and the use of PVTs. Of these areas, the investigation of both μ AUVs and energy harvesting are of key interest.

References

- [1] H. Strommel, "The Slocum Mission," *Oceanography*, pp. 22-25, 1989.
- [2] J. Tintore, G. Vizoso, B. Casas, S. Ruiz, S. Heslop, L. Renault, T. Oguz, B. Garau, A. Pascual, M. Martinez-Ledesma, L. Gomez-Pujol, A. Alvarez-Ellacuria, A. Orfila, F. Alemany, D. Alvarex-Berastegui, P. Reglero, E. Massuti, P. Velex-Belchi, J. Ruiz, M. Comez, E. Alvarez and M. Manriquez, "SOCIB: the impact of new marine infrastructures in understanding and forecasting in the Mediterranean Sea," in *Designing MED-SHIP: A Program for Repeated Oceanographic Surveys*, Supetar, CIESM, 2011, pp. 99-118.
- [3] J. A. Hilderbrand, G. L. D'Spain and M. A. Roch, "Glider-based Passive Acoustic Monitoring Techniques in the Southern California Region," Scripps Institution of Oceanography, San Diego, 2010.
- [4] S. J. R. W. M. District, "Fast facts about the Indian River Lagoon," 2018. [Online]. Available: <https://www.sjrwmd.com/waterways/indian-river-lagoon/facts/>. [Accessed 14 6 2018].
- [5] L. D. Mikey, "Marine Discovery Center," 29 February 2016. [Online]. Available: <http://www.marinediscoverycenter.org/algae-can-be-seen-from-space-2/>. [Accessed 8 April 2016].
- [6] R. Horrocks, Director, *Blue Planet II - One Ocean*. [Film]. BBC, 2017.
- [7] J. Graver, "Underwater Gliders: Dynamics, Control and Design," Joshua Graver, Princeton, 2005.
- [8] J. Cao, J. Cao, Z. Zeng and L. Lian, "Optimal Path Planning of Underwater Glider in 3D Dubins Motion with Minimal Energy Consumption," IEEE, 2016.
- [9] A. Wolek, T. Gode, C. A. Woolsey, J. Quenzer and K. A. Morgansen, "Design and Testing of a Pneumatically Propeled Underwater Glider for Shallow Water," Virginia Center for Autonomous Systems, Blacksburg, Virginia, USA, 2015.
- [10] A. J. Angilella, F. S. Gandhi and T. F. Miller, "Design and Testing of a Shape Memory Alloy buoyancy engine for Unmanned Underwater Vehicles," *Smart Materials and Structures*, 2015.
- [11] P. Molloy, "Smart Materials for Subsea Buoyancy Control," University of Glasgow, Glasgow, 2000.
- [12] Z. Chen, J. Yu and A. Zhang, "Impact of folding propeller spinning position for the transit efficiency of a hybrid-driven underwater glider," IEEE, 2016.
- [13] B. Claus, R. Bachmayer and C. D. Williams, "Development of an auxiliary propulsion module for an autonomous underwater glider," in *Proceedings of the Institution of Mechanical Engineers*, 2010.
- [14] H. C. Woithe, I. Chigirev, D. Aragon, M. Iqbal, Y. Shames, S. Glenn, O. Schofield, I. Seskar and U. Kremer, "Slocum Glider Energy Measurement and Simulation Infrastructure," in *IEEE Oceans 2010*, Sydney, 2010.

- [15] Teledyne Webb Research, "Slocum G2 Glider Operators Manual," Teledyne, East Falmouth, 2012.
- [16] J. Toland, The Great Dirigibles: Their Triumphs and Disasters, New York: Dover Publications, 1972.
- [17] "Library of Congress," 1906. [Online]. Available: <https://www.loc.gov/item/2001705774/>. [Accessed 18 July 2018].
- [18] C. C. Eriksen, "Autonomous Underwater Gliders," Autonomous and Lagrangian Platforms and Sensors (ALPS_ Workshop, La Jolla, 2003.
- [19] Y. Tomoda, K. Kawaguchi, T. Ura and H. Kobayashi, "Development and Sea Trials of a Shuttle Type AUV ALBAC," in *8th International Symposium on Unmanned Untethered Submersible Technology*, Durham, 1993.
- [20] SEQUOIA, "A LISST for gliders is in development," 17 October 2016. [Online]. Available: <https://www.sequoiasci.com/about/news/lisst-glider-development/>. [Accessed 29 October 2017].
- [21] AUVAC, "Scripps Spray Glider Configuration," [Online]. Available: <http://auvac.org/configurations/view/70>. [Accessed 17 October 2017].
- [22] KONGSBERG, "Full scale production of KONGSBERG Seaglider begins," 11 February 2014. [Online]. Available: <https://www.km.kongsberg.com/ks/web/nokbg0238.nsf/AllWeb/287D58C5F066C80AC1257C7C005B5BF4?OpenDocument>. [Accessed 16 October 2017].
- [23] I. H. Abbott and A. E. Von Doenhoff, Theory of Wing Sections Including a Summary of Airfoil Data, New York: Dover Publications, 1949.
- [24] J. D. Anderson, Fundamentals of Aerodynamics, New York: McGraw-Hill, 2001.
- [25] M. M. Monk, "Aerodynamics of Airships," *Aerodynamic Theory: A General Review of Progress, Under a Grant from the Guggenheim Fund for the Promotion of Aeronautics*, pp. 32-48, 1943.
- [26] S. Gudmundsson, General Aviation Aircraft Design: Applied Methods and Procedures, Waltham: Butterworth-Heinemann, 2014.
- [27] D. P. Raymer, Aircraft Design: A Conceptual Approach, Washington D.C.: American Institute of Aeronautics and Astronautics, 2012.
- [28] M. C. Y. Niu, Airframe Structural Design: Practical Design Information and Data on Aircraft Structures, Hong Kong: Commlit Press, 1995.
- [29] A. B. Philips, N. Gold, N. Linton, C. A. Harris, E. Richards, R. Templeton, S. Thune, J. Sitbon, M. Muller, I. Vincent and T. Sloane, "Agile Design of Low-Cost Autonomous Underwater Vehicles," in *IEEE Oceans 2017*, Aberdeen, 2017.
- [30] S. A. Jenkins, H. E. Douglas, J. Sherman, J. Osse, C. Jones, N. Leonard, J. Graver, R. Bachmayer, T. Clem, P. Carroll, P. Davis, J. Berry, p. Worley and J. Wasyl, "Underwater Glider Systems Study," Office of Naval Research, Arlington, 2003.
- [31] S. Wood, "Autonomous Underwater Gliders," in *Underwater Vehicles*, Vienna, I-Tech, 2008, pp. 499-524.

- [32] C. Waldmann, A. Kausche, M. Iversen, A. Pototzky, G. Looye, R. Bachmayer and D. Wilde, "MOTH-an underwater glider design study carried out as part of the HGF Alliance ROBEX," in *Autonomous Underwater Vehicles (AUV), IEEE/OES*, Oxford, 2014.
- [33] C. Sun, B. Song and P. Wang, "Parametric geometric model and shape optimization of an underwater glider with blended-wing-body," *International Journal of Naval Architecture and Ocean Engineering*, pp. 995-1006, 2015.
- [34] P. Brodsky and J. Lubby, "Final Report Flight Software Development for the Liberdade Flying Wing Glider," ONR, Arlington, 2013.
- [35] C. E. Skibski, "Design of a Autonomous Underwater Glider focusing on External Wing Control Surfaces and Sensor Integration," Florida Institute of Technology, Melbourne, Florida, USA, 2009.
- [36] Teledyne Marine, "Slocum G3 Glider," Teledyne Marine, March 2017. [Online]. Available: http://www.teledynemarine.com/Lists/Downloads/Teledyne%20Webb%20Research%20Brochure%20G3%202017_pages.pdf. [Accessed 14 June 2018].
- [37] Woods Hole Oceanographic Institution, "Spray Glider," 2018. [Online]. Available: <https://www.whoi.edu/main/spray-glider>. [Accessed 14 June 2018].
- [38] Kongsberg, "Kongsberg Seaglider Specification," May 2014. [Online]. Available: [https://www.km.kongsberg.com/ks/web/nokbg0397.nsf/AllWeb/3DB608B825D76BFBC1257B9F00392305/\\$file/Seaglider_product_specification.pdf](https://www.km.kongsberg.com/ks/web/nokbg0397.nsf/AllWeb/3DB608B825D76BFBC1257B9F00392305/$file/Seaglider_product_specification.pdf). [Accessed 14 June 2018].
- [39] Office of Naval Research, "Liberdade XRay Advanced Underwater Glider," [Online]. Available: http://auvac.org/uploads/platform_pdf/Liberdade%20advanced_underwater_glider.pdf. [Accessed 15 June 2018].
- [40] R. E. Davis, C. E. Eriksen and C. P. Jones, "Autonomous buoyancy-driven underwater gliders," in *Technology and applications of autonomous underwater vehicles*, Taylor and Francis, 2003, pp. 37-58.
- [41] D. C. Webb, P. J. Simonetti and C. P. Jones, "SLOCUM: An Underwater Glider Propelled by Environmental Energy," *Journal of Oceanic Engineering*, pp. 447-452, 2001.
- [42] D. L. Rudnick, "Ocean Research Enabled by Underwater Gliders," *Annual Review of Marine Science*, pp. 519-541, 2015.
- [43] J. G. Graver, R. Bachmayer, N. E. Leonard and D. M. Fratantoni, "Underwater Glider Model Parameter Identification," in *Proc. 13th Int. Symposium on Unmanned Untethered Submersible Technology*, Durham, NH, 2003.
- [44] J. G. Graver and N. E. Leonard, "Underwater Glider Dynamics and Control," *12th International Symposium on Unmanned Untethered Submersible Technology*, pp. 1710-1742, 2001.

- [45] B. Mitchell, E. Wilkening and N. Mahmoudian, "Low cost Underwater Gliders for LittleRoal Marine Research," *2013 American Control Conference*, vol. 2013, pp. 1412-1417, 2013.
- [46] C. G. Cameron, "The WET Buoyancy Engine Controlling Buoyancy via Electrochemistry," Defense R&D Canada, 2005.
- [47] M. Loc, H. Choi, J. Seo, S. Baek and J. Kim, "Development and Control of a New AUV," *International Journal of Control, Automation, and Systems*, vol. 12, pp. 886-894, 2014.
- [48] R. da Silva Tchilian, E. Rafikova, S. A. Gafurov and M. Rafikov, "Optimal control of an underwater glider vehicle," *Dynamics and Vibroacoustics of Machines*, vol. 176, pp. 732-740, 2016.
- [49] J. E. Poulin, "Concept Design of a Long Range AUV Propulsion System with an Onboard Electrical Generator," MIT, Cambridge, 2006.
- [50] S. Jo, H. Choi, S. Jeong and D. Jeong, "Design of a new high speed unmanned underwater glider and motion control," IEEE, 2016.
- [51] C. Sun, S. Baowei, P. Wang and X. Wang, "Shape optimization of blended-wing-body underwater glider by using gliding range as the optimization target," *International Journal of Naval Architecture and Ocean Engineering*, vol. xx, pp. 1-12, 2017.
- [52] A. B. Phillips, J. I. Blake, S. W. Boyd, S. Ward and G. Griffiths, "Nature in Engineering for Monitoring the Oceans (NEMO): An isopyncal soft boddie approach for deep diving autonomous underwater vehicles," in *IEEE/OES Autonomous Underwater Vehicles (AUV)*, Southampton, United Kingdom, 2012.
- [53] J. Tung, M. Gou, J. Guo, F. Chiu and S. Cheng, "Design of an Underwater Glider with Fore and Aft Buoyancy Engines," in *International Symposium on Underwater Technology*, Tokyo, Japan, 2007.
- [54] "Seaglide," 5 September 2016. [Online]. Available: www.seaglide.net.
- [55] B. Mitchell, E. Wilkening and N. Mahmoudian, "Developing an Underwater Glider for Educational Purposes," in *IEEE International Conference on Robotics and Automation*, Karlshruue, Germany, 2013.
- [56] C. Waldmann, A. Kausche, M. Iversen, R. Bachmayer, A. Pototzky, G. Looye, D. Wilde and S. Montenegro, "MOTH-an underwater glider design study carried out as part of the HGF Alliance ROBEX".
- [57] A. T. Bardole, "Contributions to Guidance and Control of Underwater Gliders," University of Southern Denmark, Odense, 2012.
- [58] Z. Wang, Y. Zhang, M. M. Zhang, Z. Yang and Z. Wu, "Design and flight performance of hybrid underwater glider with controllable wings," *International journal of Advanced Robotic Systems*, no. May-June, pp. 1-12, 2017.
- [59] H. Li, Y. Zhang, Y. Zhang, W. Niu and Y. Wang, "Optimizaiton Design of the Communication Attitude for Hybrid Underwater Gliders," in 2015

- Internatinoal Conference on Computer Science and Mechanical Automation*, 2015.
- [60] J. Yu, F. Zhang, A. Zhang, W. Jin and Y. Tian, "Motion Parameter Optimization and Sensor Scheduling for the Sea-Wing Underwater Glider," *IEEE Journal of Oceanic Engineering*, vol. 38, no. 2, pp. 243-254, 2013.
 - [61] J.-G. Wu, C.-y. Chen, H.-w. Zhang, C.-g. Xie and X.-m. Wang, "Study on Well-to-drag Efficiency of PEMFC Powered Glider," *ICIEA*, pp. 1970-1975, 2009.
 - [62] N. Garcia-Polanco and J. A. Palencia, "Aerodynamic Design of a Micro Air Vehicle: Study of Propeller-Engine Performance," SAE International, 2011.
 - [63] J. Allison, "Marine Water Jet Propulsion," *SNAME Transactions*, vol. 101, pp. 275-335, 1993.
 - [64] J. G. Bellingham, Y. Zhang, J. E. kerwin, J. Erikson, B. Hobson, B. Kieft, M. Godin, R. McEwen, T. Hoover, J. Paul, A. Hamilton, J. Franklin and A. Banka, "Efficient Propulsion for the Tethys Long-Range Autonomous Underwater Vehicle," in *2010 IEEE/OES*, Monterey, 2010.
 - [65] P. S. Krueger, A. A. Moslemi, J. T. Nichols, I. K. Bartol and W. J. Stewart, "Vortex Rings in Bio-inspired and Biological Jet Propulsion," *Advances in Science and Technology*, vol. 58, pp. 237-246, 2008.
 - [66] R. W. Whittlesey and J. O. Dabiri, "Optimal vortex formation in a self-propelled vehicle," *Journal of Fluid Mechanics*, vol. 737, pp. 78-104, 2013.
 - [67] A. P. Thomas, M. Milano, M. G. G'Sell, K. Fischer and J. Burdick, "Synthetic jet Propulsion for Small Underwater Vehicles," in *International Conference on Robotics and Automation*, Barcelona, 2005.
 - [68] M. W. Krieg, "Modeling and Thrust Optimization of a Bio-Inspired Pulsatile Jet Thruster," University of Colorado, Boulder, 2012.
 - [69] K. Mohseni, "Zero-Mass Pulsatile Jets for Unmanned Underwater Vehicle Maneuvering," in *AIAA 3rd "Unmanned Unlimited" Technical Conference*, Chicago, 2004.
 - [70] M. Krieg and K. Mohseni, "Dynamic Modeling and Control of Biologically Inspired Vortex Ring Thrusters for Underwater Robot Locomotion," *IEEE Transactions on Robotics*, 2010.
 - [71] M. Krieg and K. Mohseni, "On the Propulsive Efficiency of Unsteady Propulsors," in *Third International Symposium on Marine Propulsors*, Launceston, 2013.
 - [72] M. Krieg, P. Klein, R. Hodgkinson and K. Mohseni, "A Hybrid Class Underwater Vehicle: Bioinspired Propulsion, Embedded System, and Acoustic Communication and Localization System," *Marine Technology Society Journal*, vol. 45, no. 4, pp. 153-164, 2011.
 - [73] H. Quick, R. Widjaja, B. Anderson, B. Woodyatt, A. D. Snowden and S. Lam, "Phase I Experimental Testing of a Generic Submarine Model in the DSTO Low Speed Wind Tunnel," DSTP, Fishermans Bend, 2012.

- [74] L. Techy, R. Tomokiyo, J. Quenzer, T. Beauchamp and K. Morgansen, "Full-Scale Wind Tunnel Study of the Seaglider Underwater Glider," UWAA, Seattle, 2010.
- [75] Airfoil Tools, "NACA 65(2)-415," [Online]. Available: <http://airfoiltools.com/airfoil/details?airfoil=naca652415a05-il>. [Accessed 21 January 2017].
- [76] R. I. o. Technology, "MAV Prototype," [Online]. Available: http://edge.rit.edu/edge/OldEDGE/public/Archives/P0206F/mav_prototype.htm. [Accessed 13 June 2018].
- [77] G. E. Torres and T. J. Mueller, "Low-Aspect-Ratio Wing Aerodynamics at Low Reynolds Numbers," *AIAA Journal*, pp. 865-873, 2004.
- [78] "The Aviation History Online Museum," 1 June 2015. [Online]. Available: http://www.aviation-history.com/theory/angle_of_incidence.htm. [Accessed 26 August 2017].
- [79] J. R. Whittenbury, "Configuration Design Development of the Navy UCAS-D X-47-B," in "*100 Years of Achievement and Progress in Aviation Technology, integration, and Operations (ATIO)*", Virginia Beach, 2011.
- [80] A. Alvarez, "Redesigning the SLOCUM Glider for Torpedo Tube Launching," *Journal of Oceanic Engineering*, vol. 35, no. 4, pp. 984-991, 2010.
- [81] "Stanford Reports," [Online]. Available: <http://aero.stanford.edu/reports/nonplanarwings/ClosedSystems.html>. [Accessed 16 December 2017].
- [82] NATS, "Explaining Time Based Separation at Heathrow," 28 February 2014. [Online]. Available: <http://nats.aero/blog/2014/02/explaining-time-based-separation-heathrow/>. [Accessed 16 December 2017].
- [83] S. A. Jenkins and G. D'Spain, "Autonomous Underwater Gliders," in *Handbook of Ocean Engineering*, Springer, 2016, pp. 301-322.
- [84] D. Keerops, "The common forces: conservative or nonconservative?," *Physics Education*, vol. 41, no. 3, pp. 219-222, 2006.
- [85] J. D. Anderson, *Aircraft Performance and Design*, New York: McGraw-Hill, 1998.
- [86] C. D. Williams, R. Bachmayer and B. de Young, "Progress in Predicting the Performance of Ocean Glider from At-Sea Measurements".
- [87] M. Krieg and K. Mohseni, "On the Propulsive Efficiency of Unsteady Propulsors," in *Third International Symposium on Marine Propulsors*, Launceston, 2013.
- [88] Blue Robotics, "T200 Propeller Set," 11 4 2018. [Online]. Available: <https://bluerobotics.com/store/thrusters/t200-propeller-set-r1/>.
- [89] L. Lippsett and M. Carlowicz, "Green Energy Powers Undersea Glider," *Oceanus Magazine*, 25 September 2008.
- [90] D. T. Akcabay and Y. L. Young, "Hydroelastic response and energy harvesting potential of flexible piezoelectric beams in viscous flow," *Physics of Fluids*, vol. 24, no. 5, 2012.

- [91] "Sparkfun," 10 October 2016. [Online]. Available: <https://learn.sparkfun.com/tutorials/openscale-applications-and-hookup-guide>. [Accessed 14 May 2018].
- [92] "Robotshop," 13 May 2011. [Online]. Available: <https://www.robotshop.com/media/files/pdf/datasheet-3133.pdf>. [Accessed 14 May 2018].
- [93] "Robotshop," 13 May 2011. [Online]. Available: <https://www.robotshop.com/media/files/pdf/datasheet-3132.pdf>. [Accessed 14 May 2018].
- [94] L. Landweber and M. Gertler, "Mathmatical Formulation of Bodies of Revolution," Navy Department , Washington D.C., 1950.
- [95] W. Giles, T. Dinham-Peren, S. Amaratunga, A. Vrijdag and R. Partridge, "The Advanced WaterJet: Propulsor Performance and Effect on Ship Design," in *IMAREST 10th International Naval Engineering Conference and Exhibition*, Portsmouth, 2010.
- [96] R. E. Henderson, J. F. McMahon and G. F. Wislicenus, "A Method for the design of Pumpjets," Pennsylvania State University, University Park, 1964.
- [97] N. Fujisawa, "Measurements of Basic Performance for Waterjet Propulsion Systems in Water Tunnel," *International Journal of Rotating Machinery*, vol. 2, no. 1, pp. 43-50, 1995.
- [98] F. E. Fish, "Biomimetics: Determining engineering opportunites from nature," *Procedings of SPIE*, vol. 7401, no. Biomimetics and Bioinspiration, 2009.

Bibliography

- [1] H. Strommel, "The Slocum Mission," *Oceanography*, pp. 22-25, 1989.
- [2] J. Tintore, G. Vizoso, B. Casas, S. Ruiz, S. Heslop, L. Renault, T. Oguz, B. Garau, A. Pascual, M. Martinez-Ledesma, L. Gomez-Pujol, A. Alvarez-Ellacuria, A. Orfila, F. Alemany, D. Alvarex-Berastegui, P. Reglero, E. Massuti, P. Velex-Belchi, J. Ruiz, M. Comez, E. Alvarez and M. Manriquez, "SOCIB: the impact of new marine infrastructures in understanding and forecasting in the Mediterranean Sea," in *Designing MED-SHIP: A Program for Repeated Oceanographic Surveys*, Supetar, CIESM, 2011, pp. 99-118.
- [3] J. A. Hilderbrand, G. L. D'Spain and M. A. Roch, "Glider-based Passive Acoustic Monitoring Techniques in the Southern California Region," Scripps Institution of Oceanography, San Diego, 2010.
- [4] S. J. R. W. M. District, "Fast facts about the Indian River Lagoon," 2018. [Online]. Available: <https://www.sjrwmd.com/waterways/indian-river-lagoon/facts/>. [Accessed 14 6 2018].
- [5] L. D. Mikey, "Marine Discovery Center," 29 February 2016. [Online]. Available: <http://www.marinediscoverycenter.org/algae-can-be-seen-from-space-2/>. [Accessed 8 April 2016].
- [6] R. Horrocks, Director, *Blue Planet II - One Ocean*. [Film]. BBC, 2017.
- [7] J. Graver, "Underwater Gliders: Dynamics, Control and Design," Joshua Graver, Princeton, 2005.
- [8] J. Cao, J. Cao, Z. Zeng and L. Lian, "Optimal Path Planning of Underwater Glider in 3D Dubins Motion with Minimal Energy Consumption," IEEE, 2016.
- [9] A. Wolek, T. Gode, C. A. Woolsey, J. Quenzer and K. A. Morgansen, "Design and Testing of a Pneumatically Propeled Underwater Glider for Shallow Water," Virginia Center for Autonomous Systems, Blacksburg, Virginia, USA, 2015.
- [10] A. J. Angilella, F. S. Gandhi and T. F. Miller, "Design and Testing of a Shape Memory Alloy buoyancy engine for Unmanned Underwater Vehicles," *Smart Materials and Structures*, 2015.
- [11] P. Molloy, "Smart Materials for Subsea Buoyancy Control," University of Glasgow, Glasgow, 2000.
- [12] Z. Chen, J. Yu and A. Zhang, "Impact of folding propeller spinning position for the transit efficiency of a hybrid-driven underwater glider," IEEE, 2016.
- [13] B. Claus, R. Bachmayer and C. D. Williams, "Development of an auxiliary propulsion module for an autonomous underwater glider," in *Proceedings of the Institution of Mechanical Engineers*, 2010.
- [14] H. C. Woithe, I. Chigirev, D. Aragon, M. Iqbal, Y. Shames, S. Glenn, O. Schofield, I. Seskar and U. Kremer, "Slocum Glider Energy Measurement and Simulation Infrastructure," in *IEEE Oceans 2010*, Sydney, 2010.

- [15] Teledyne Webb Research, "Slocum G2 Glider Operators Manual," Teledyne, East Falmouth, 2012.
- [16] J. Toland, The Great Dirigibles: Their Triumphs and Disasters, New York: Dover Publications, 1972.
- [17] "Library of Congress," 1906. [Online]. Available: <https://www.loc.gov/item/2001705774/>. [Accessed 18 July 2018].
- [18] C. C. Eriksen, "Autonomous Underwater Gliders," Autonomous and Lagrangian Platforms and Sensors (ALPS_ Workshop, La Jolla, 2003.
- [19] Y. Tomoda, K. Kawaguchi, T. Ura and H. Kobayashi, "Development and Sea Trials of a Shuttle Type AUV ALBAC," in *8th International Symposium on Unmanned Untethered Submersible Technology*, Durham, 1993.
- [20] SEQUOIA, "A LISST for gliders is in development," 17 October 2016. [Online]. Available: <https://www.sequoiasci.com/about/news/lisst-glider-development/>. [Accessed 29 October 2017].
- [21] AUVAC, "Scripps Spray Glider Configuration," [Online]. Available: <http://auvac.org/configurations/view/70>. [Accessed 17 October 2017].
- [22] KONGSBERG, "Full scale production of KONGSBERG Seaglider begins," 11 February 2014. [Online]. Available: <https://www.km.kongsberg.com/ks/web/nokbg0238.nsf/AllWeb/287D58C5F066C80AC1257C7C005B5BF4?OpenDocument>. [Accessed 16 October 2017].
- [23] I. H. Abbott and A. E. Von Doenhoff, Theory of Wing Sections Including a Summary of Airfoil Data, New York: Dover Publications, 1949.
- [24] J. D. Anderson, Fundamentals of Aerodynamics, New York: McGraw-Hill, 2001.
- [25] M. M. Monk, "Aerodynamics of Airships," *Aerodynamic Theory: A General Review of Progress, Under a Grant from the Guggenheim Fund for the Promotion of Aeronautics*, pp. 32-48, 1943.
- [26] S. Gudmundsson, General Aviation Aircraft Design: Applied Methods and Procedures, Waltham: Butterworth-Heinemann, 2014.
- [27] D. P. Raymer, Aircraft Design: A Conceptual Approach, Washington D.C.: American Institute of Aeronautics and Astronautics, 2012.
- [28] M. C. Y. Niu, Airframe Structural Design: Practical Design Information and Data on Aircraft Structures, Hong Kong: Commlit Press, 1995.
- [29] A. B. Philips, N. Gold, N. Linton, C. A. Harris, E. Richards, R. Templeton, S. Thune, J. Sitbon, M. Muller, I. Vincent and T. Sloane, "Agile Design of Low-Cost Autonomous Underwater Vehicles," in *IEEE Oceans 2017*, Aberdeen, 2017.
- [30] S. A. Jenkins, H. E. Douglas, J. Sherman, J. Osse, C. Jones, N. Leonard, J. Graver, R. Bachmayer, T. Clem, P. Carroll, P. Davis, J. Berry, p. Worley and J. Wasyl, "Underwater Glider Systems Study," Office of Naval Research, Arlington, 2003.
- [31] S. Wood, "Autonomous Underwater Gliders," in *Underwater Vehicles*, Vienna, I-Tech, 2008, pp. 499-524.

- [32] C. Waldmann, A. Kausche, M. Iversen, A. Pototzky, G. Looye, R. Bachmayer and D. Wilde, "MOTH-an underwater glider design study carried out as part of the HGF Alliance ROBEX," in *Autonomous Underwater Vehicles (AUV), IEEE/OES*, Oxford, 2014.
- [33] C. Sun, B. Song and P. Wang, "Parametric geometric model and shape optimization of an underwater glider with blended-wing-body," *International Journal of Naval Architecture and Ocean Engineering*, pp. 995-1006, 2015.
- [34] P. Brodsky and J. Lubby, "Final Report Flight Software Development for the Liberdade Flying Wing Glider," ONR, Arlington, 2013.
- [35] C. E. Skibski, "Design of a Autonomous Underwater Glider focusing on External Wing Control Surfaces and Sensor Integration," Florida Institute of Technology, Melbourne, Florida, USA, 2009.
- [36] Teledyne Marine, "Slocum G3 Glider," Teledyne Marine, March 2017. [Online]. Available: http://www.teledynemarine.com/Lists/Downloads/Teledyne%20Webb%20Research%20Brochure%20G3%202017_pages.pdf. [Accessed 14 June 2018].
- [37] Woods Hole Oceanographic Institution, "Spray Glider," 2018. [Online]. Available: <https://www.whoi.edu/main/spray-glider>. [Accessed 14 June 2018].
- [38] Kongsberg, "Kongsberg Seaglider Specification," May 2014. [Online]. Available: [https://www.km.kongsberg.com/ks/web/nokbg0397.nsf/AllWeb/3DB608B825D76BFBC1257B9F00392305/\\$file/Seaglider_product_specification.pdf](https://www.km.kongsberg.com/ks/web/nokbg0397.nsf/AllWeb/3DB608B825D76BFBC1257B9F00392305/$file/Seaglider_product_specification.pdf). [Accessed 14 June 2018].
- [39] Office of Naval Research, "Liberdade XRay Advanced Underwater Glider," [Online]. Available: http://auvac.org/uploads/platform_pdf/Liberdade%20advanced_underwater_glider.pdf. [Accessed 15 June 2018].
- [40] R. E. Davis, C. E. Eriksen and C. P. Jones, "Autonomous buoyancy-driven underwater gliders," in *Technology and applications of autonomous underwater vehicles*, Taylor and Francis, 2003, pp. 37-58.
- [41] D. C. Webb, P. J. Simonetti and C. P. Jones, "SLOCUM: An Underwater Glider Propelled by Environmental Energy," *Journal of Oceanic Engineering*, pp. 447-452, 2001.
- [42] D. L. Rudnick, "Ocean Research Enabled by Underwater Gliders," *Annual Review of Marine Science*, pp. 519-541, 2015.
- [43] J. G. Graver, R. Bachmayer, N. E. Leonard and D. M. Fratantoni, "Underwater Glider Model Parameter Identification," in *Proc. 13th Int. Symposium on Unmanned Untethered Submersible Technology*, Durham, NH, 2003.
- [44] J. G. Graver and N. E. Leonard, "Underwater Glider Dynamics and Control," *12th International Symposium on Unmanned Untethered Submersible Technology*, pp. 1710-1742, 2001.

- [45] B. Mitchell, E. Wilkening and N. Mahmoudian, "Low cost Underwater Gliders for LittleRoal Marine Research," *2013 American Control Conference*, vol. 2013, pp. 1412-1417, 2013.
- [46] C. G. Cameron, "The WET Buoyancy Engine Controlling Buoyancy via Electrochemistry," Defense R&D Canada, 2005.
- [47] M. Loc, H. Choi, J. Seo, S. Baek and J. Kim, "Development and Control of a New AUV," *International Journal of Control, Automation, and Systems*, vol. 12, pp. 886-894, 2014.
- [48] R. da Silva Tchilian, E. Rafikova, S. A. Gafurov and M. Rafikov, "Optimal control of an underwater glider vehicle," *Dynamics and Vibroacoustics of Machines*, vol. 176, pp. 732-740, 2016.
- [49] J. E. Poulin, "Concept Design of a Long Range AUV Propulsion System with an Onboard Electrical Generator," MIT, Cambridge, 2006.
- [50] S. Jo, H. Choi, S. Jeong and D. Jeong, "Design of a new high speed unmanned underwater glider and motion control," IEEE, 2016.
- [51] C. Sun, S. Baowei, P. Wang and X. Wang, "Shape optimization of blended-wing-body underwater glider by using gliding range as the optimization target," *International Journal of Naval Architecture and Ocean Engineering*, vol. xx, pp. 1-12, 2017.
- [52] A. B. Phillips, J. I. Blake, S. W. Boyd, S. Ward and G. Griffiths, "Nature in Engineering for Monitoring the Oceans (NEMO): An isopyncal soft boddie approach for deep diving autonomous underwater vehicles," in *IEEE/OES Autonomous Underwater Vehicles (AUV)*, Southampton, United Kingdom, 2012.
- [53] J. Tung, M. Gou, J. Guo, F. Chiu and S. Cheng, "Design of an Underwater Glider with Fore and Aft Buoyancy Engines," in *International Symposium on Underwater Techonology*, Tokyo, Japan, 2007.
- [54] "Seaglide," 5 September 2016. [Online]. Available: www.seaglide.net.
- [55] B. Mitchell, E. Wilkening and N. Mahmoudian, "Developing an Underwater Glider for Educational Purposes," in *IEEE International Conference on Robotics and Automation*, Karlshruue, Germany, 2013.
- [56] C. Waldmann, A. Kausche, M. Iversen, R. Bachmayer, A. Pototzky, G. Looye, D. Wilde and S. Montenegro, "MOTH-an underwater glider design study carried out as part of the HGF Alliance ROBEX".
- [57] A. T. Bardole, "Contributions to Guidance and Control of Underwater Gliders," University of Southern Denmark, Odense, 2012.
- [58] Z. Wang, Y. Zhang, M. M. Zhang, Z. Yang and Z. Wu, "Design and flight performance of hybrid underwater glider with controllable wings," *International journal of Advanced Robotic Systems*, no. May-June, pp. 1-12, 2017.
- [59] H. Li, Y. Zhang, Y. Zhang, W. Niu and Y. Wang, "Optimizaiton Design of the Communication Attitude for Hybrid Underwater Gliders," in 2015

- Internatinoal Conference on Computer Science and Mechanical Automation*, 2015.
- [60] J. Yu, F. Zhang, A. Zhang, W. Jin and Y. Tian, "Motion Parameter Optimization and Sensor Scheduling for the Sea-Wing Underwater Glider," *IEEE Journal of Oceanic Engineering*, vol. 38, no. 2, pp. 243-254, 2013.
 - [61] J.-G. Wu, C.-y. Chen, H.-w. Zhang, C.-g. Xie and X.-m. Wang, "Study on Well-to-drag Efficiency of PEMFC Powered Glider," *ICIEA*, pp. 1970-1975, 2009.
 - [62] N. Garcia-Polanco and J. A. Palencia, "Aerodynamic Design of a Micro Air Vehicle: Study of Propeller-Engine Performance," SAE International, 2011.
 - [63] J. Allison, "Marine Water Jet Propulsion," *SNAME Transactions*, vol. 101, pp. 275-335, 1993.
 - [64] J. G. Bellingham, Y. Zhang, J. E. kerwin, J. Erikson, B. Hobson, B. Kieft, M. Godin, R. McEwen, T. Hoover, J. Paul, A. Hamilton, J. Franklin and A. Banka, "Efficient Propulsion for the Tethys Long-Range Autonomous Underwater Vehicle," in *2010 IEEE/OES*, Monterey, 2010.
 - [65] P. S. Krueger, A. A. Moslemi, J. T. Nichols, I. K. Bartol and W. J. Stewart, "Vortex Rings in Bio-inspired and Biological Jet Propulsion," *Advances in Science and Technology*, vol. 58, pp. 237-246, 2008.
 - [66] R. W. Whittlesey and J. O. Dabiri, "Optimal vortex formation in a self-propelled vehicle," *Journal of Fluid Mechanics*, vol. 737, pp. 78-104, 2013.
 - [67] A. P. Thomas, M. Milano, M. G. G'Sell, K. Fischer and J. Burdick, "Synthetic jet Propulsion for Small Underwater Vehicles," in *International Conference on Robotics and Automation*, Barcelona, 2005.
 - [68] M. W. Krieg, "Modeling and Thrust Optimization of a Bio-Inspired Pulsatile Jet Thruster," University of Colorado, Boulder, 2012.
 - [69] K. Mohseni, "Zero-Mass Pulsatile Jets for Unmanned Underwater Vehicle Maneuvering," in *AIAA 3rd "Unmanned Unlimited" Technical Conference*, Chicago, 2004.
 - [70] M. Krieg and K. Mohseni, "Dynamic Modeling and Control of Biologically Inspired Vortex Ring Thrusters for Underwater Robot Locomotion," *IEEE Transactions on Robotics*, 2010.
 - [71] M. Krieg and K. Mohseni, "On the Propulsive Efficiency of Unsteady Propulsors," in *Third International Symposium on Marine Propulsors*, Launceston, 2013.
 - [72] M. Krieg, P. Klein, R. Hodgkinson and K. Mohseni, "A Hybrid Class Underwater Vehicle: Bioinspired Propulsion, Embedded System, and Acoustic Communication and Localization System," *Marine Technology Society Journal*, vol. 45, no. 4, pp. 153-164, 2011.
 - [73] H. Quick, R. Widjaja, B. Anderson, B. Woodyatt, A. D. Snowden and S. Lam, "Phase I Experimental Testing of a Generic Submarine Model in the DSTO Low Speed Wind Tunnel," DSTP, Fishermans Bend, 2012.

- [74] L. Techy, R. Tomokiyo, J. Quenzer, T. Beauchamp and K. Morgansen, "Full-Scale Wind Tunnel Study of the Seaglider Underwater Glider," UWAA, Seattle, 2010.
- [75] Airfoil Tools, "NACA 65(2)-415," [Online]. Available: <http://airfoiltools.com/airfoil/details?airfoil=naca652415a05-il>. [Accessed 21 January 2017].
- [76] R. I. o. Technology, "MAV Prototype," [Online]. Available: http://edge.rit.edu/edge/OldEDGE/public/Archives/P0206F/mav_prototype.htm. [Accessed 13 June 2018].
- [77] G. E. Torres and T. J. Mueller, "Low-Aspect-Ratio Wing Aerodynamics at Low Reynolds Numbers," *AIAA Journal*, pp. 865-873, 2004.
- [78] "The Aviation History Online Museum," 1 June 2015. [Online]. Available: http://www.aviation-history.com/theory/angle_of_incidence.htm. [Accessed 26 August 2017].
- [79] J. R. Whittenbury, "Configuration Design Development of the Navy UCAS-D X-47-B," in "*100 Years of Achievement and Progress in Aviation Technology, integration, and Operations (ATIO)*", Virginia Beach, 2011.
- [80] A. Alvarez, "Redesigning the SLOCUM Glider for Torpedo Tube Launching," *Journal of Oceanic Engineering*, vol. 35, no. 4, pp. 984-991, 2010.
- [81] "Stanford Reports," [Online]. Available: <http://aero.stanford.edu/reports/nonplanarwings/ClosedSystems.html>. [Accessed 16 December 2017].
- [82] NATS, "Explaining Time Based Separation at Heathrow," 28 February 2014. [Online]. Available: <http://nats.aero/blog/2014/02/explaining-time-based-separation-heathrow/>. [Accessed 16 December 2017].
- [83] S. A. Jenkins and G. D'Spain, "Autonomous Underwater Gliders," in *Handbook of Ocean Engineering*, Springer, 2016, pp. 301-322.
- [84] D. Keerops, "The common forces: conservative or nonconservative?," *Physics Education*, vol. 41, no. 3, pp. 219-222, 2006.
- [85] J. D. Anderson, *Aircraft Performance and Design*, New York: McGraw-Hill, 1998.
- [86] C. D. Williams, R. Bachmayer and B. de Young, "Progress in Predicting the Performance of Ocean Glider from At-Sea Measurements".
- [87] M. Krieg and K. Mohseni, "On the Propulsive Efficiency of Unsteady Propulsors," in *Third International Symposium on Marine Propulsors*, Launceston, 2013.
- [88] Blue Robotics, "T200 Propeller Set," 11 4 2018. [Online]. Available: <https://bluerobotics.com/store/thrusters/t200-propeller-set-r1/>.
- [89] L. Lippsett and M. Carlowicz, "Green Energy Powers Undersea Glider," *Oceanus Magazine*, 25 September 2008.
- [90] D. T. Akcabay and Y. L. Young, "Hydroelastic response and energy harvesting potential of flexible piezoelectric beams in viscous flow," *Physics of Fluids*, vol. 24, no. 5, 2012.

- [91] "Sparkfun," 10 October 2016. [Online]. Available: <https://learn.sparkfun.com/tutorials/openscale-applications-and-hookup-guide>. [Accessed 14 May 2018].
- [92] "Robotshop," 13 May 2011. [Online]. Available: <https://www.robotshop.com/media/files/pdf/datasheet-3133.pdf>. [Accessed 14 May 2018].
- [93] "Robotshop," 13 May 2011. [Online]. Available: <https://www.robotshop.com/media/files/pdf/datasheet-3132.pdf>. [Accessed 14 May 2018].
- [94] L. Landweber and M. Gertler, "Mathmatical Formulation of Bodies of Revolution," Navy Department , Washington D.C., 1950.
- [95] W. Giles, T. Dinham-Peren, S. Amaratunga, A. Vrijdag and R. Partridge, "The Advanced WaterJet: Propulsor Performance and Effect on Ship Design," in *IMAREST 10th International Naval Engineering Conference and Exhibition*, Portsmouth, 2010.
- [96] R. E. Henderson, J. F. McMahon and G. F. Wislicenus, "A Method for the design of Pumpjets," Pennsylvania State University, University Park, 1964.
- [97] N. Fujisawa, "Measurements of Basic Performance for Waterjet Propulsion Systems in Water Tunnel," *International Journal of Rotating Machinery*, vol. 2, no. 1, pp. 43-50, 1995.
- [98] F. E. Fish, "Biomimetics: Determining engineering opportunites from nature," *Procedings of SPIE*, vol. 7401, no. Biomimetics and Bioinspiration, 2009.

Appendix A**Permission to Conduct Research**

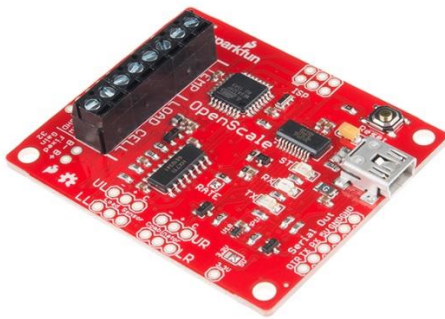
None was required for this research.

Appendix B

B1

SparkFun OpenScale [82]

The SparkFun OpenScale makes reading load cells easy. Attach a four-wire or five-wire load cell of any capacity, plug OpenScale into a USB port, open a terminal window at 9600bps, and you'll immediately see mass readings. To learn more about load cells see our tutorial on Getting Started with Load Cells. This board also has the Load Cell Combinator built in so you'll be able to read four load sensors as 1 load cell as well.



OpenScale combines the HX711 breakout board with an Atmega328P running Arduino and extensive pre-loaded configuration firmware to create an off-the-shelf solution for load cell reading.

OpenScale was designed for projects and applications where the load was static (for example a bee hive) or where constant readings are needed without user intervention (for example on a conveyor belt system). A load cell with OpenScale can remain in place for months without needing user interaction.

OpenScale makes it easy to zero and calibrate your scale via a simple to use configuration menu. Serial output and control is available through the mini-B USB port or through an FTDI compatible connection. This allows OpenScale to be attached seamlessly with a datalogger (OpenLog) or to a wireless Bluetooth transmitter (such as SparkFun Bluetooth Mate Silver). In the bee scale application , OpenScale is hooked up to Blynk Board and the data collected is pushed to data.sparkfun.com.

A precision digital temperature sensor is included on OpenScale to report the local temperature. An external connection is also available for a DS18B20 compatible temperature sensor to take temperature readings of the load cell. Please note that OpenScale reports the local and remote temperature readings but it does not alter the scale reading due to temperature fluctuations. It is up to the user to properly calibrate and post process these temperature readings to get the maximum scale accuracy.

OpenScale is fully open source hardware and software. OpenScale comes with a Arduino Uno compatible bootloader (STK500, 115200bps, 16MHz). Making modifications to the firmware is as easy as loading new code onto an Arduino. You can find the all the source in the OpenScale repository on github.

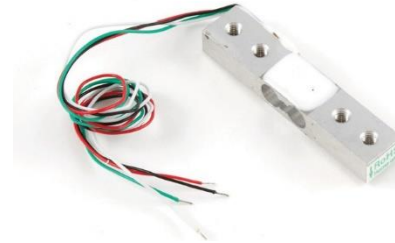
Interface Specifications

OpenScale communicates at TTL level 9600bps 8-N-1 by default. The baud rate is configurable from from 1200bps to 1,000,000bps. Most users will use the USB mini-B connection to connect to a computer. See How to Install FTDI Drivers tutorial for more information. Users may also communicate via the 6-pin serial interface:

B2 Micro Load Cell (0-780g) - CZL616C [83]

Contents

- What do you have to know?**
 - How does it work - For curious people**
 - Installation**
 - Calibration**
 - Product Specifications**
 - Glossary**
-



What do you have to know?

A load cell is a force sensing module - a carefully designed metal structure, with small elements called strain gauges mounted in precise locations on the structure. Load cells are designed to measure a specific force, and ignore other forces being applied. The electrical signal output by the load cell is very small and requires specialized amplification. Fortunately, the 1046 PhidgetBridge will perform all the amplification and measurement of the electrical output. Load cells are designed to measure force in one direction. They will often measure force in other directions, but the sensor sensitivity will be different, since parts of the load cell operating under compression are now in tension, and vice versa.

How does it work - For curious people

Strain-gauge load cells convert the load acting on them into electrical signals. The measuring is done with very small resistor patterns called strain gauges - effectively small, flexible circuit boards. The gauges are bonded onto a beam or structural member that deforms when weight is applied, in turn deforming the strain-gauge. As the strain gauge is deformed, its electrical resistance changes in proportion to the load.

The changes to the circuit caused by force is much smaller than the changes caused by variation in temperature. Higher quality load cells cancel out the effects of temperature using two techniques. By matching the expansion rate of the strain gauge to the expansion rate of the metal it's mounted on, undue strain on the gauges can be avoided as the load cell warms up and cools down. The most important method of temperature compensation involves using multiple strain gauges, which all respond to the change in temperature with the same change in resistance. Some load cell designs use gauges which are never subjected to any force, but only serve to counterbalance the temperature effects on the gauges that measuring force. Most designs use 4 strain gauges, some in compression, some under tension, which maximizes the sensitivity of the load cell, and automatically cancels the effect of temperature.

Installation

This Single Point Load Cell is used in small jewelry scales and kitchen scales. It's mounted by bolting down the end of the load cell where the wires are attached, and applying force on the other end in the direction of the arrow. Where the force is applied is not critical, as this load cell measures a shearing effect on the beam, not the bending of the beam. If you mount a small platform on the load cell, as would be done in a small scale, this load cell provides accurate readings regardless of the position of the load on the platform.



Calibration

A simple formula is usually used to convert the measured mv/V output from the load cell to the measured force:

*Measured Force = A * Measured mv/V + B (offset)* It's important to decide what unit your measured force is - grams, kilograms, pounds, etc.

This load cell has a rated output of $0.8 \pm 0.1 \text{mv/v}$ which corresponds to the sensor's capacity of 780g. To find A we use

$$\text{Capacity} = A * \text{Rated Output} \quad A = \text{Capacity} / \text{Rated Output} \quad A = 780 / 0.8 \\ A = 975$$

Since the Offset is quite variable between individual load cells, it's necessary to calculate the offset for each sensor. Measure the output of the load cell with no force on it and note the mv/V output measured by the PhidgetBridge.

$$\text{Offset} = 0 - 975 * \text{Measured Output}$$

Product Specifications

Mechanical	
Housing Material	Aluminum Alloy
Load Cell Type	Strain Gauge
Capacity	780g
Dimensions	45.16x9.32x6mm
Mounting Holes	M3 (Screw Size)
Cable Length	210mm
Cable Size	30 AWG (0.2mm)
Cable - no. of leads	4
Electrical	
Rated Output	$0.8 \pm 0.1 \text{ mv/V}$
Non-Linearity	0.05% FS
Hysteresis	0.05% FS
Non-Repeatability	0.05% FS
Creep (per 30 minutes)	0.1% FS
Temperature Effect on Zero (per 10°C)	0.05% FS
Temperature Effect on Span (per 10°C)	0.05% FS
Zero Balance	$\pm 1.5\%$ FS
Input Impedance	$1090 \pm 10 \text{ Ohm}$
Output Impedance	$1000 \pm 10 \text{ Ohm}$
Insulation Resistance (Under 50VDC)	$\geq 5000 \text{ MOhm}$
Excitation Voltage	5 VDC
Compensated Temperature Range	-10 to $\sim +40^\circ\text{C}$
Operating Temperature Range	-20 to $\sim +55^\circ\text{C}$
Safe Overload	120% Capacity
Ultimate Overload	150% Capacity

Glossary

Capacity

The maximum load the load cell is designed to measure within its specifications.

Creep

The change in sensor output occurring over 30 minutes, while under load at or near capacity and with all environmental conditions and other variables remaining constant.

FULL SCALE or FS

Used to qualify error - FULL SCALE is the change in output when the sensor is fully loaded. If a particular error (for example, Non-Linearity) is expressed as 0.1% F.S., and the output is 1.0mV/V, the maximum non-linearity that will be seen over the operating range of the sensor will be 0.001 mV/V. An important distinction is that this error doesn't have to only occur at the maximum load. If you are operating the sensor at a maximum of 10% of capacity, for this example, the non-linearity would still be 0.001mV/V, or 1% of the operating range that you are actually using.

Hysteresis

If a force equal to 50% of capacity is applied to a load cell which has been at no load, a given output will be measured. The same load cell is at full capacity, and some of the force is removed, resulting in the load cell operating at 50% capacity. The difference in output between the two test scenarios is called hysteresis.

Excitation Voltage

Specifies the voltage that can be applied to the power/ground terminals on the load cell. In practice, if you are using the load cell with the PhidgetBridge, you don't have to worry about this spec.

Input Impedance

Determines the power that will be consumed by the load cell. The lower this number is, the more current will be required, and the more heating will occur when the load cell is powered. In very noisy environments, a lower input impedance will reduce the effect of Electromagnetic interference on long wires between the load cell and PhidgetBridge.

Insulation Resistance

The electrical resistance measured between the metal structure of the load cell, and the wiring. The practical result of this is the metal structure of the load cells should not be energized with a voltage, particularly higher voltages, as it can arc into the PhidgetBridge. Commonly the load cell and the metal framework it is part of will be grounded to earth or to your system ground.

Maximum Overload

The maximum load which can be applied without producing a structural failure.

Non-Linearity

Ideally, the output of the sensor will be perfectly linear, and a simple 2-point calibration will exactly describe the behaviour of the sensor at other loads. In practice, the sensor is not perfect, and Non-linearity describes the maximum deviation from the linear curve. Theoretically, if a more complex calibration is used, some of the non-linearity can be calibrated out, but this will require a very high accuracy calibration with multiple points.

Non-Repeatability

The maximum difference the sensor will report when exactly the same weight is applied, at the same temperature, over multiple test runs.

Operating Temperature

The extremes of ambient temperature within which the load cell will operate without permanent adverse change to any of its performance characteristics.

Output Impedance

Roughly corresponds to the input impedance. If the Output Impedance is very high, measuring the bridge will distort the results. The PhidgetBridge carefully buffers the signals coming from the load cell, so in practice this is not a concern.

Rated Output

Is the difference in the output of the sensor between when it is fully loaded to its rated capacity, and when it's unloaded. Effectively, it's how sensitive the sensor is, and corresponds to the gain calculated when calibrating the sensor. More expensive sensors have an exact rated output based on an individual calibration done at the factory. **Safe Overload**

The maximum axial load which can be applied without producing a permanent shift in performance characteristics beyond those specified.

Compensated Temperature

The range of temperature over which the load cell is compensated to maintain output and zero balance within specified limits.

Temperature Effect on Span

Span is also called rated output. This value is the change in output due to a change in ambient temperature. It is measured over 10 degree C temperature interval.

Temperature Effect on Zero

The change in zero balance due to a change in ambient temperature. This value is measured over 10 degree C temperature interval.

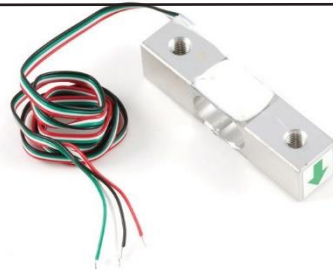
Zero Balance

Zero Balance defines the maximum difference between the +/- output wires when no load is applied. Realistically, each sensor will be individually calibrated, at least for the output when no load is applied. Zero Balance is more of a concern if the load cell is being interfaced to an amplification circuit - the PhidgetBridge can easily handle enormous differences between +/- . If the difference is very large, the PhidgetBridge will not be able to use the higher Gain settings.

B3 Micro Load Cell (0-5kg) - CZL635 [84]

Contents

- 1 What do you have to know?**
- 2 How does it work - For curious people**
- 3 Installation**
- 4 Calibration**
- 5 Product Specifications**
- 6 Glossary**



1 What do you have to know?

A load cell is a force sensing module - a carefully designed metal structure, with small elements called strain gauges mounted in precise locations on the structure. Load cells are designed to measure a specific force, and ignore other forces being applied. The electrical signal output by the load cell is very small and requires specialized amplification.

Fortunately, the 1046 PhidgetBridge will perform all the amplification and measurement of the electrical output.

Load cells are designed to measure force in one direction. They will often measure force in other directions, but the sensor sensitivity will be different, since parts of the load cell operating under compression are now in tension, and vice versa.

1 How does it work - For curious people

Strain-gauge load cells convert the load acting on them into electrical signals. The measuring is done with very small resistor patterns called strain gauges - effectively small, flexible circuit boards. The gauges are bonded onto a beam or structural member that deforms when weight is applied, in turn deforming the strain-gauge. As the strain gauge is deformed, its electrical resistance changes in proportion to the load.

The changes to the circuit caused by force is much smaller than the changes caused by variation in temperature. Higher quality load cells cancel out the effects of temperature using two techniques. By matching the expansion rate of the strain gauge to the expansion rate of the metal it's mounted on, undue strain on the gauges can be avoided as the load cell warms up and cools down. The most important method of temperature compensation involves using multiple strain gauges, which all respond to the change in temperature with the same change

in resistance. Some load cell designs use gauges which are never subjected to any force, but only serve to counterbalance the temperature effects on the gauges that measuring force. Most designs use 4 strain gauges, some in compression, some under tension, which maximizes the sensitivity of the load cell, and automatically cancels the effect of temperature.

2 Installation

This Single Point Load Cell is used in small jewelry scales and kitchen scales. It's mounted by bolting down the end of the load cell where the wires are attached, and applying force on the other end in the direction of the arrow. Where the force is applied is

not critical, as this load cell measures a shearing effect on the beam, not the bending of the beam. If you mount a small platform on the load cell, as would be done in a small scale, this load cell provides accurate readings regardless of the position of the load on the platform.

3 Calibration

A simple formula is usually used to convert the measured mv/V output from the load cell to the measured force:

Measured Force = A * Measured mV/V + B (offset) It's important to decide what unit your measured force is - grams, kilograms, pounds, etc.

This load cell has a rated output of $1.0 \pm 0.15 \text{mv/v}$ which corresponds to the sensor's capacity of 5kg.

To find A we use

$$\text{Capacity} = A * \text{Rated Output} \quad A = \text{Capacity} / \text{Rated Output} \quad A = 5 / 1.0$$

$$A = 5$$

Since the Offset is quite variable between individual load cells, it's necessary to calculate the offset for each sensor. Measure the output of the load cell with no force on it and note the mv/V output measured by the PhidgetBridge.

$$\text{Offset} = 0 - 5 * \text{Measured Output}$$



4 Product Specifications

Mechanical	
Housing Material	Aluminum Alloy
Load Cell Type	Strain Gauge
Capacity	5kg
Dimensions	55.25x12.7x12.7mm
Mounting Holes	M5 (Screw Size)
Cable Length	550mm
Cable Size	30 AWG (0.2mm)
Cable - no. of leads	4
Electrical	
Precision	0.05%
Rated Output	$1.0 \pm 0.15 \text{ mv/V}$
Non-Linearity	0.05% FS
Hysteresis	0.05% FS
Non-Repeatability	0.05% FS
Creep (per 30 minutes)	0.1% FS
Temperature Effect on Zero (per 10°C)	0.05% FS
Temperature Effect on Span (per 10°C)	0.05% FS
Zero Balance	$\pm 1.5\%$ FS
Input Impedance	$1130 \pm 10 \text{ Ohm}$
Output Impedance	$1000 \pm 10 \text{ Ohm}$
Insulation Resistance (Under 50VDC)	$\geq 5000 \text{ M} \Omega$
Excitation Voltage	5 VDC
Compensated Temperature Range	-10 to $\sim +40^\circ\text{C}$
Operating Temperature Range	-20 to $\sim +55^\circ\text{C}$
Safe Overload	120% Capacity
Ultimate Overload	150% Capacity

5 Glossary

Capacity

The maximum load the load cell is designed to measure within its specifications.

Creep

The change in sensor output occurring over 30 minutes, while under load at or near capacity and with all environmental conditions and other variables remaining constant.

FULL SCALE or FS

Used to qualify error - FULL SCALE is the change in output when the sensor is fully loaded. If a particular error (for example, Non-Linearity) is expressed as 0.1% F.S., and the output is 1.0mV/V, the maximum non-linearity that will be seen over the operating range of the sensor will be 0.001 mV/V. An important distinction is that this error doesn't have to only occur at the maximum load. If you are operating the sensor at a maximum of 10% of capacity, for this example, the non-linearity would still be 0.001mV/V, or 1% of the operating range that you are actually using.

Hysteresis

If a force equal to 50% of capacity is applied to a load cell which has been at no load, a given output will be measured. The same load cell is at full capacity, and some of the force is removed, resulting in the load cell operating at 50% capacity. The difference in output between the two test scenarios is called hysteresis.

Excitation Voltage

Specifies the voltage that can be applied to the power/ground terminals on the load cell. In practice, if you are using the load cell with the PhidgetBridge, you don't have to worry about this spec.

Input Impedance

Determines the power that will be consumed by the load cell. The lower this number is, the more current will be required, and the more heating will occur when the load cell is powered. In very noisy environments, a lower input impedance will reduce the effect of Electromagnetic interference on long wires between the load cell and PhidgetBridge.

Insulation Resistance

The electrical resistance measured between the metal structure of the load cell, and the wiring. The practical result of this is the metal structure of the load cells should not be energized with a voltage, particularly higher voltages, as it can arc into the PhidgetBridge. Commonly the load cell and the metal framework it is part of will be grounded to earth or to your system ground.

Maximum Overload

The maximum load which can be applied without producing a structural failure.

Non-Linearity

Ideally, the output of the sensor will be perfectly linear, and a simple 2-point calibration will exactly describe the behaviour of the sensor at other loads. In practice, the sensor is not perfect, and Non-linearity describes the maximum deviation from the linear curve. Theoretically, if a more complex calibration is used, some of the non-linearity can be calibrated out, but this will require a very high accuracy calibration with multiple points.

Non-Repeatability

The maximum difference the sensor will report when exactly the same weight is applied, at the same temperature, over multiple test runs.

Operating Temperature

The extremes of ambient temperature within which the load cell will operate without permanent adverse change to any of its performance characteristics.

Output Impedance

Roughly corresponds to the input impedance. If the Output Impedance is very high, measuring the bridge will distort the results. The PhidgetBridge carefully buffers the signals coming from the load cell, so in practice this is not a concern.

Rated Output

Is the difference in the output of the sensor between when it is fully loaded to its rated capacity, and when it's unloaded. Effectively, it's how sensitive the sensor is, and corresponds to the gain calculated when calibrating the sensor. More expensive sensors have an exact rated output based on an individual calibration done at the factory. **Safe Overload**

The maximum axial load which can be applied without producing a permanent shift in performance characteristics beyond those specified.

Compensated Temperature

The range of temperature over which the load cell is compensated to maintain output and zero balance within specified limits.

Temperature Effect on Span

Span is also called rated output. This value is the change in output due to a change in ambient temperature. It is measured over 10 degree C temperature interval.

Temperature Effect on Zero

The change in zero balance due to a change in ambient temperature. This value is measured over 10 degree C temperature interval.

Zero Balance

Zero Balance defines the maximum difference between the +/- output wires when no load is applied. Realistically, each sensor will be individually calibrated, at least for the output when no load is applied. Zero Balance is more of a concern if the load cell is being interfaced to an amplification circuit - the PhidgetBridge can easily handle enormous differences between +/- . If the difference is very large, the PhidgetBridge will not be able to use the higher Gain settings.

Appendix C

C1 Energy Analysis MATLAB Script

```

clear;
clc;
format long;

%%Energy Usage Comparison for Determination of Target Thruster Efficiency
%%in Order for a Conventionally Propelled AUG to have similar performance to
%%an AUG

%%Input variables
rho=1023.6; %water density at sea level
g=9.81; %acceleration due to gravity
theta=-22.77; %%Pitch angle in degrees
alpha=2.7; %%Angle of attack in degrees
hull=.22; %%Hull diameter in meters
Vol=.000488; %%Buoyancy engine total volume m^3
vinf=.388; %%velocity "u" m/s
v_horiz=.349; %%Horizontal velocity global m/s
CD=.27; %%Drag coefficient
Ponb=.2; %%Power onboard usage Watts
Psens=1; %%Power sensor usage Watts
Batt=8000000; %%Battery storage Joules
eta_p=0.5; %%Efficiency of pump at depth
h=1000; %%depth in meters
%%-----
%%Geometric_info
gamma=(theta+alpha); %%Glide Path Angle
gamma=abs(gamma) %%Value of Glide Path Angle
s.glide=h/sind(gamma) %%Distance covered on half a cycle
s.horiz=h/tand(gamma) %%Distance covered horizontally half cycle
s.glide_total=2*s.glide %%total distance gliding
s.horiz_total=2*s.horiz %%total distance horizontally
t_taken=s.horiz_total/vinf %%time taken from start to end of yo
S=pi*(hull)^2/4 %%Hull Frontal Area
%%-----
%%Forces
FB=rho*g*Vol/2 %%Buoyant Force
FBd=FB*sind(gamma) %%Buoyant Force in Drag Direction
FD=(1/2)*rho*vinf^2*S*CD %%Drag Force

```

```

FDd=FD*cosd(alpha) %%Drag Force in Drag Direction

PCTDiff=((abs(FBd-FD))/((FB+FD)/2))*100 %%Pct Difference between FD and
FB
%-%-----
%Work

Wbe=FB*s.glide; %%Work done travelling a half cycle
WbeTotal=2*Wbe; %%Work done travelling a whole cycle

%-%-----
%NRG

%%Bouyancy_Engine_NRG_Usage
EbeS=164; %%Energy used by pump at surface
EbeD=rho*g*h*Vol; %%Energy used by pump at depth
Ebe=EbeS+EbeD/eta_p %%Energy used by pump

%%Hotel_Load
Ehotel=(Ponb+Psens)*t_taken %%Hotel load

%%Thruster_NRG_Usage
Et.glide=FBd*2*s.glide %%Energy used by thruster to cover
2s.glide
Et.horiz=FBd*2*s.horiz %%Energy used by thruster to cover
2s.horiz

%-%-----
%%Performance

cycles=Batt/(Ebe+Ehotel) %%# of cycles used
range_g=cycles*s.glide_total; %%distance gliding in meter
range_h=cycles*s.horiz_total; %%distance horizontal in meter
range.glide=range_g/1000 %%distance gliding in kilometer
range.horiz=range_h/1000 %%distance horizontal in kilometer

%%Efficiency
EbeEta=EbeS+EbeD/eta_p %%Energy used by pump with
efficiency

%%Efficiency Targets
Eta_Target_Thruster.glide=Et.glide/EbeEta %%Target efficiency w/glide
Eta_Target_Thruster.horiz=Et.horiz/EbeEta %%Target efficiency w/vertical
Eta_Target_Thruster.depth=(FBd*h)/(Ebe/eta_p)*100

```

Appendix D

Tables

D1 Manufacturer Supplied Data For The Blue Robotics T200 Thruster

PWM	Voltage (V)	Amperage (A)	Power_{in} (W)	Load (kgf)	Flow Rate (m/s)	<i>Load</i> (N)	Power_{out} (W)	Eff. (%)*
1500	11.96	0.04	0.48	0.00	0.00	<i>0.00</i>	<i>0.00</i>	<i>0.00</i>
1510	11.96	0.05	0.60	0.00	0.00	<i>0.00</i>	<i>0.00</i>	<i>0.00</i>
1520	11.96	0.08	0.96	0.00	0.04	<i>0.00</i>	<i>0.00</i>	<i>0.00</i>
1530	11.95	0.18	2.15	0.05	0.58	<i>0.49</i>	<i>0.28</i>	<i>13.12</i>
1540	11.95	0.23	2.75	0.09	0.73	<i>0.85</i>	<i>0.62</i>	<i>22.51</i>
1550	11.94	0.29	3.46	0.13	0.47	<i>1.25</i>	<i>0.59</i>	<i>17.08</i>
1560	11.94	0.36	4.30	0.18	0.72	<i>1.74</i>	<i>1.25</i>	<i>29.10</i>
1570	11.94	0.46	5.49	0.23	0.89	<i>2.27</i>	<i>2.02</i>	<i>36.77</i>
1580	11.93	0.58	6.92	0.29	1.20	<i>2.80</i>	<i>3.35</i>	<i>48.43</i>
1590	11.93	0.71	8.47	0.36	1.43	<i>3.52</i>	<i>5.04</i>	<i>59.49</i>
1600	11.93	0.85	10.14	0.42	1.59	<i>4.14</i>	<i>6.56</i>	<i>64.70</i>
1610	11.91	1.00	11.91	0.47	1.83	<i>4.63</i>	<i>8.45</i>	<i>70.92</i>
1620	11.90	1.19	14.16	0.56	1.84	<i>5.52</i>	<i>10.15</i>	<i>71.67</i>
1630	11.89	1.40	16.65	0.64	1.97	<i>6.23</i>	<i>12.29</i>	<i>73.82</i>
1640	11.87	1.60	18.99	0.66	2.12	<i>6.50</i>	<i>13.77</i>	<i>72.51</i>
1650	11.88	1.82	21.62	0.75	2.25	<i>7.34</i>	<i>16.55</i>	<i>76.55</i>
1660	11.88	2.08	24.71	0.87	2.36	<i>8.50</i>	<i>20.07</i>	<i>81.20</i>
1670	11.90	2.38	28.32	0.97	2.47	<i>9.52</i>	<i>23.51</i>	<i>83.02</i>
1680	11.92	2.72	32.42	1.04	2.62	<i>10.23</i>	<i>26.78</i>	<i>82.59</i>

* Denotes the calculated efficiency of the system as a percentage

** Italicized and right aligned columns represent calculated values

D2 Static Run 1 of the Blue Robotics T200 Thruster***

PWM	Voltage (V)	Amperage (A)	Power_{in} (W)	Load (kgf)	Flow Rate (m/s)	Load (N)	Power_{out} (W)	Eff. (%)*
1500	12.00	0.00	0.00	0.00	0.00	<i>0.00</i>	<i>0.00</i>	<i>0.00</i>
1510	12.00	0.00	0.00	0.00	0.00	<i>0.00</i>	<i>0.00</i>	<i>0.00</i>
1520	12.00	0.00	0.00	0.00	0.00	<i>0.00</i>	<i>0.00</i>	<i>0.00</i>
1530	12.00	0.16	1.93	0.03	1.80	<i>0.27</i>	<i>0.48</i>	<i>24.93</i>
1540	12.00	0.20	2.40	0.06	0.54	<i>0.61</i>	<i>0.33</i>	<i>13.72</i>
1550	12.00	0.27	3.19	0.10	0.66	<i>1.01</i>	<i>0.67</i>	<i>20.86</i>
1560	12.00	0.35	4.16	0.16	0.80	<i>1.59</i>	<i>1.27</i>	<i>30.59</i>
1570	12.00	0.45	5.34	0.22	0.99	<i>2.11</i>	<i>2.09</i>	<i>39.12</i>
1580	12.00	0.56	6.68	0.28	1.08	<i>2.75</i>	<i>2.97</i>	<i>44.44</i>
1590	12.00	0.68	8.18	0.35	1.20	<i>3.45</i>	<i>4.14</i>	<i>50.56</i>
1600	12.00	0.85	10.18	0.41	1.32	<i>4.05</i>	<i>5.35</i>	<i>52.58</i>
1610	12.00	1.32	15.84	0.48	1.52	<i>4.72</i>	<i>7.17</i>	<i>45.25</i>
1620	12.00	1.33	15.94	0.56	1.60	<i>5.53</i>	<i>8.84</i>	<i>55.49</i>
1630	12.00	1.45	17.40	0.65	1.52	<i>6.41</i>	<i>9.74</i>	<i>55.98</i>
1640	12.00	1.94	23.30	0.68	1.69	<i>6.67</i>	<i>11.27</i>	<i>48.38</i>
1650	12.00	1.96	23.53	0.78	1.86	<i>7.61</i>	<i>14.16</i>	<i>60.16</i>
1660	12.00	2.26	27.14	0.92	1.82	<i>8.99</i>	<i>16.37</i>	<i>60.29</i>
1670	12.00	2.51	30.12	0.99	1.96	<i>9.69</i>	<i>19.00</i>	<i>63.08</i>
1680	12.00	2.88	34.56	1.05	2.10	<i>10.26</i>	<i>21.56</i>	<i>62.37</i>

* Denotes the calculated efficiency of the system as a percentage

** Italicized and right aligned columns represent calculated values

***This data was collected by manually reading off of the displayed data

D3 Static Run 2 of the Blue Robotics T200 Thruster***

PWM	Voltage (V)	Ampera ge (A)	Power_{in} (W)	Load (kgf)	Flow Rate (m/s)	Load (N)	Power_{out} (W)	Eff. (%)*
1500	12.00	0.03	0.36	0.00	0.00	<i>0.00</i>	<i>0.00</i>	<i>0.00</i>
1510	12.00	0.00	0.00	0.00	0.00	<i>0.00</i>	<i>0.00</i>	<i>0.00</i>
1520	12.00	0.00	0.00	0.00	0.00	<i>0.00</i>	<i>0.00</i>	<i>0.00</i>
1530	12.00	0.14	1.68	0.02	0.00	<i>0.22</i>	<i>0.00</i>	<i>0.00</i>
1540	12.00	0.18	2.16	0.06	0.52	<i>0.63</i>	<i>0.33</i>	<i>15.21</i>
1550	12.00	0.25	3.00	0.10	0.64	<i>1.01</i>	<i>0.65</i>	<i>21.52</i>
1560	12.00	0.33	3.96	0.15	0.72	<i>1.49</i>	<i>1.07</i>	<i>27.12</i>
1570	12.00	0.42	5.04	0.21	0.98	<i>2.11</i>	<i>2.06</i>	<i>40.94</i>
1580	12.00	0.54	6.48	0.27	1.12	<i>2.63</i>	<i>2.95</i>	<i>45.49</i>
1590	12.00	0.68	8.16	0.34	1.14	<i>3.33</i>	<i>3.80</i>	<i>46.58</i>
1600	12.00	0.83	9.96	0.42	1.32	<i>4.08</i>	<i>5.38</i>	<i>54.07</i>
1610	12.00	1.02	12.24	0.50	1.46	<i>4.87</i>	<i>7.11</i>	<i>58.08</i>
1620	12.00	1.21	14.52	0.56	1.52	<i>5.48</i>	<i>8.33</i>	<i>57.40</i>
1630	12.00	1.42	17.04	0.64	1.70	<i>6.32</i>	<i>10.74</i>	<i>63.02</i>
1640	12.00	1.67	20.04	0.71	1.60	<i>6.93</i>	<i>11.09</i>	<i>55.34</i>
1650	12.00	1.98	23.76	0.81	1.80	<i>7.94</i>	<i>14.29</i>	<i>60.15</i>
1660	12.00	2.20	26.40	0.88	1.94	<i>8.64</i>	<i>16.76</i>	<i>63.50</i>
1670	12.00	2.48	29.76	0.97	2.00	<i>9.48</i>	<i>18.95</i>	<i>63.68</i>
1680	12.00	2.86	34.32	1.07	2.20	<i>10.48</i>	<i>23.06</i>	<i>67.20</i>

* Denotes the calculated efficiency of the system as a percentage

** Italicized and right aligned columns represent calculated values

***This data was collected by manually reading off of the displayed data

D4 Static Run 3 of the Blue Robotics T200 Thruster***

PWM	Voltage (V)	Ampera ge (A)	Power_{in} (W)	Load (kgf)	Flow Rate (m/s)	Load (N)	Power_{out} (W)	Eff. (%)*
1500	12.00	0.00	0.00	0.00	0.00	<i>0.00</i>	<i>0.00</i>	<i>0.00</i>
1510	12.00	0.00	0.00	0.00	0.00	<i>0.00</i>	<i>0.00</i>	<i>0.00</i>
1520	12.00	0.00	0.00	0.00	0.00	<i>0.00</i>	<i>0.00</i>	<i>0.00</i>
1530	12.00	0.14	1.68	0.02	0.34	<i>0.24</i>	<i>0.08</i>	<i>4.98</i>
1540	12.00	0.18	2.16	0.06	0.51	<i>0.63</i>	<i>0.32</i>	<i>14.95</i>
1550	12.00	0.25	3.00	0.11	0.64	<i>1.03</i>	<i>0.66</i>	<i>21.89</i>
1560	12.00	0.33	3.96	0.16	0.77	<i>1.53</i>	<i>1.18</i>	<i>29.80</i>
1570	12.00	0.42	5.04	0.21	0.93	<i>2.10</i>	<i>1.94</i>	<i>38.53</i>
1580	12.00	0.54	6.48	0.27	1.03	<i>2.62</i>	<i>2.69</i>	<i>41.56</i>
1590	12.00	0.68	8.16	0.34	1.14	<i>3.36</i>	<i>3.84</i>	<i>47.07</i>
1600	12.00	0.83	9.96	0.41	1.33	<i>4.03</i>	<i>5.38</i>	<i>54.00</i>
1610	12.00	1.02	12.24	0.49	1.41	<i>4.80</i>	<i>6.79</i>	<i>55.50</i>
1620	12.00	1.21	14.52	0.56	1.43	<i>5.45</i>	<i>7.82</i>	<i>53.86</i>
1630	12.00	1.42	17.04	0.64	1.62	<i>6.25</i>	<i>10.14</i>	<i>59.49</i>
1640	12.00	1.67	20.04	0.71	1.58	<i>6.96</i>	<i>11.00</i>	<i>54.90</i>
1650	12.00	1.98	23.76	0.81	1.81	<i>7.94</i>	<i>14.37</i>	<i>60.49</i>
1660	12.00	2.20	26.40	0.88	1.95	<i>8.67</i>	<i>16.95</i>	<i>64.19</i>
1670	12.00	2.48	29.76	0.96	2.04	<i>9.44</i>	<i>19.21</i>	<i>64.56</i>
1680	12.00	2.86	34.32	1.07	2.21	<i>10.52</i>	<i>23.26</i>	<i>67.78</i>

* Denotes the calculated efficiency of the system as a percentage

** Italicized and right aligned columns represent calculated values

***This data was collected by averaging of the collected data at each PWM setting

D5 Dynamic Run 1 of the Blue Robotics T200 Thruster***

PWM	Voltage (V)	Ampera ge (A)	Power_{in} (W)	Load (kgf)	Flow Rate (m/s)	<i>Load (N)</i>	<i>Power_{out} (W)</i>	<i>Eff. (%)</i> *
1500	12.00	0.00	0.00	0.00	0.00	<i>0.00</i>	<i>0.00</i>	<i>0.00</i>
1510	12.00	0.00	0.00	0.00	0.00	<i>0.00</i>	<i>0.00</i>	<i>0.00</i>
1520	12.00	0.03	0.36	0.00	0.05	<i>0.00</i>	<i>0.00</i>	<i>0.00</i>
1530	12.00	0.14	1.68	0.01	0.20	<i>0.13</i>	<i>0.03</i>	<i>1.57</i>
1540	12.00	0.18	2.16	0.05	0.32	<i>0.48</i>	<i>0.15</i>	<i>7.15</i>
1550	12.00	0.24	2.88	0.10	0.44	<i>0.97</i>	<i>0.42</i>	<i>14.74</i>
1560	12.00	0.30	3.60	0.14	0.44	<i>1.40</i>	<i>0.62</i>	<i>17.16</i>
1570	12.00	0.42	5.04	0.20	0.48	<i>1.97</i>	<i>0.95</i>	<i>18.80</i>
1580	12.00	0.53	6.36	0.25	0.60	<i>2.50</i>	<i>1.50</i>	<i>23.59</i>
1590	12.00	0.65	7.80	0.31	0.60	<i>3.03</i>	<i>1.82</i>	<i>23.28</i>
1600	12.00	0.83	9.96	0.38	0.64	<i>3.73</i>	<i>2.39</i>	<i>23.96</i>

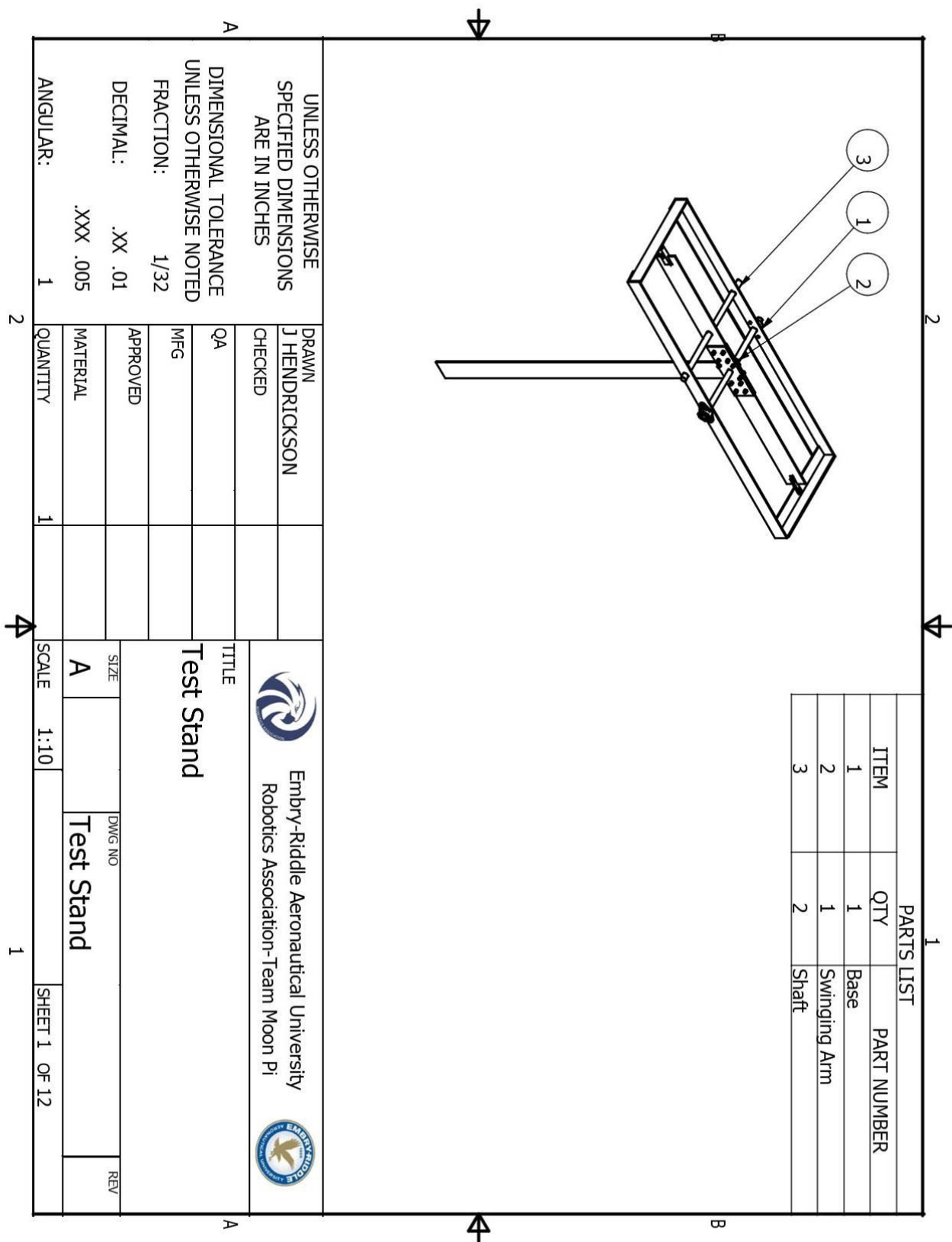
* Denotes the calculated efficiency of the system as a percentage

** Italicized and right aligned columns represent calculated values

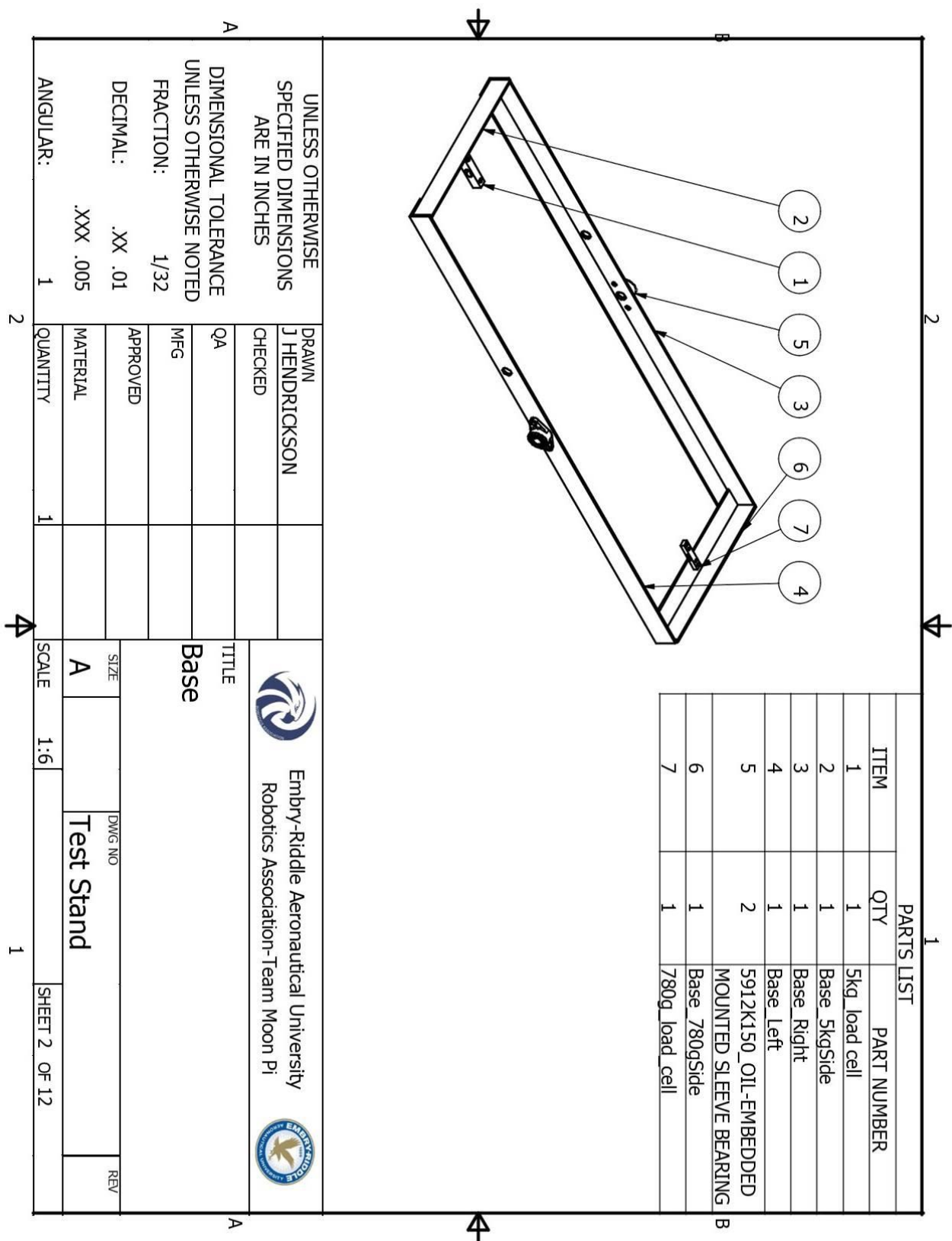
***This data was collected by averaging of the collected data at each PWM setting

Appendix E**Figures**

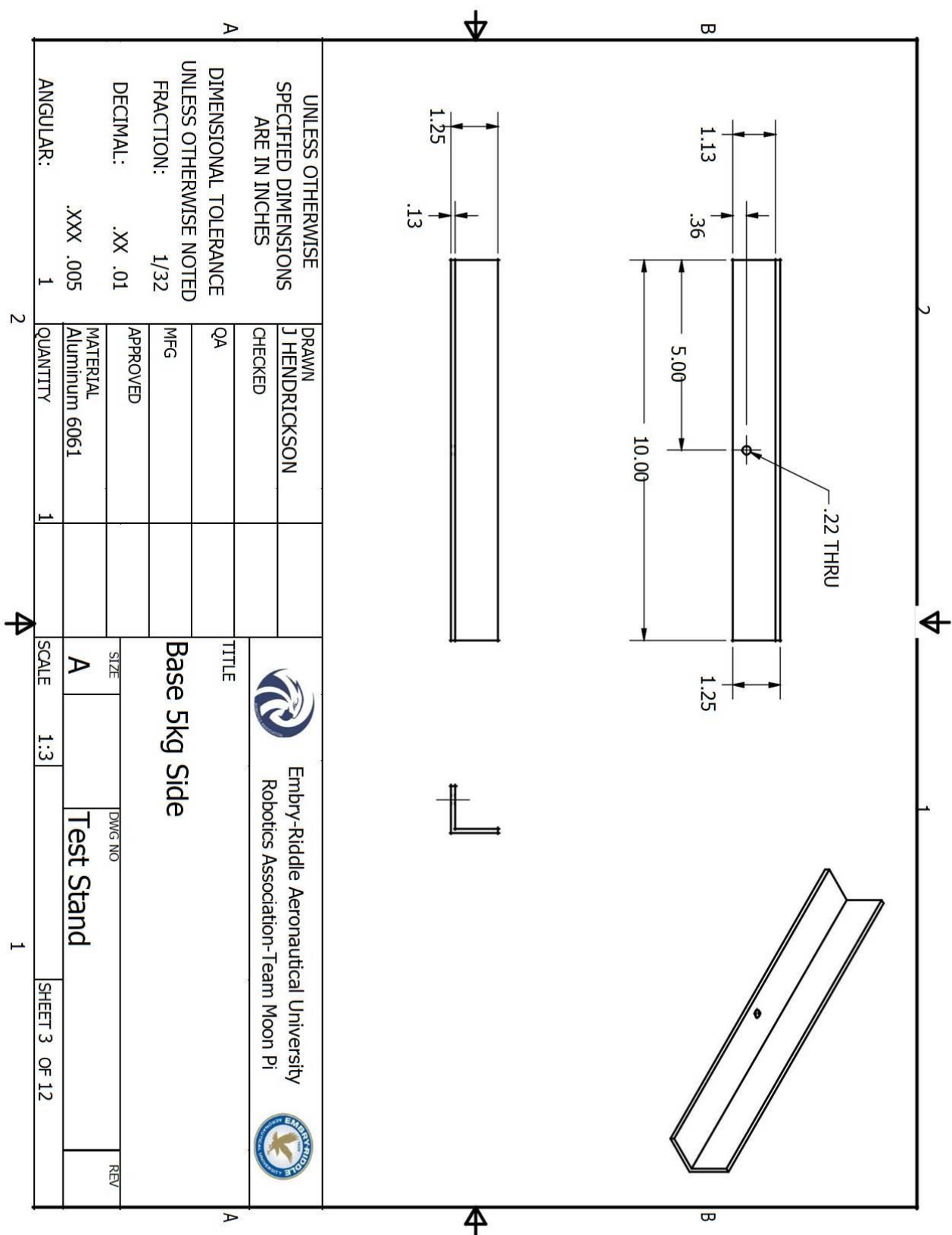
E1 Test Stand Assembly Overview



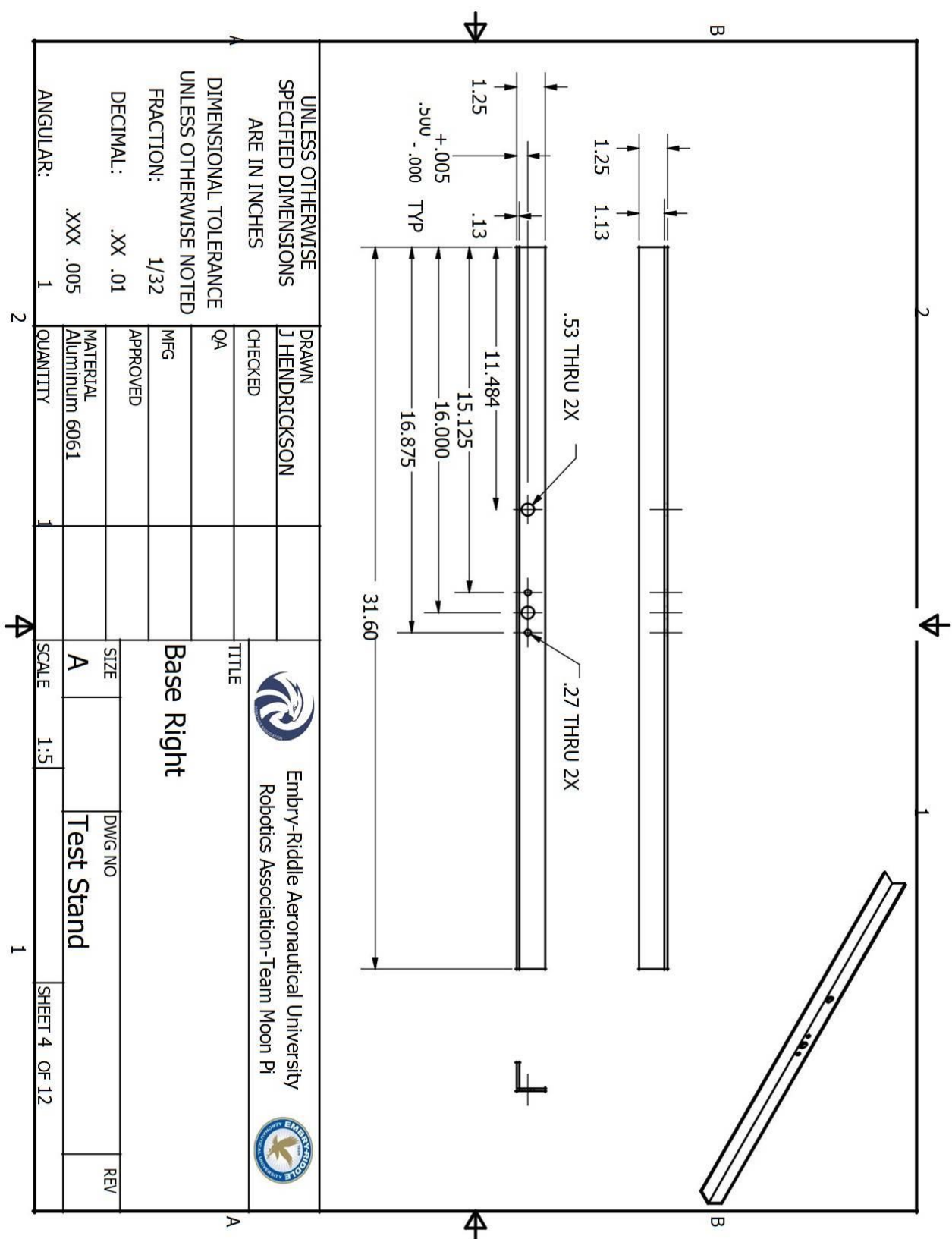
E2 Test Stand Base Assembly Overview



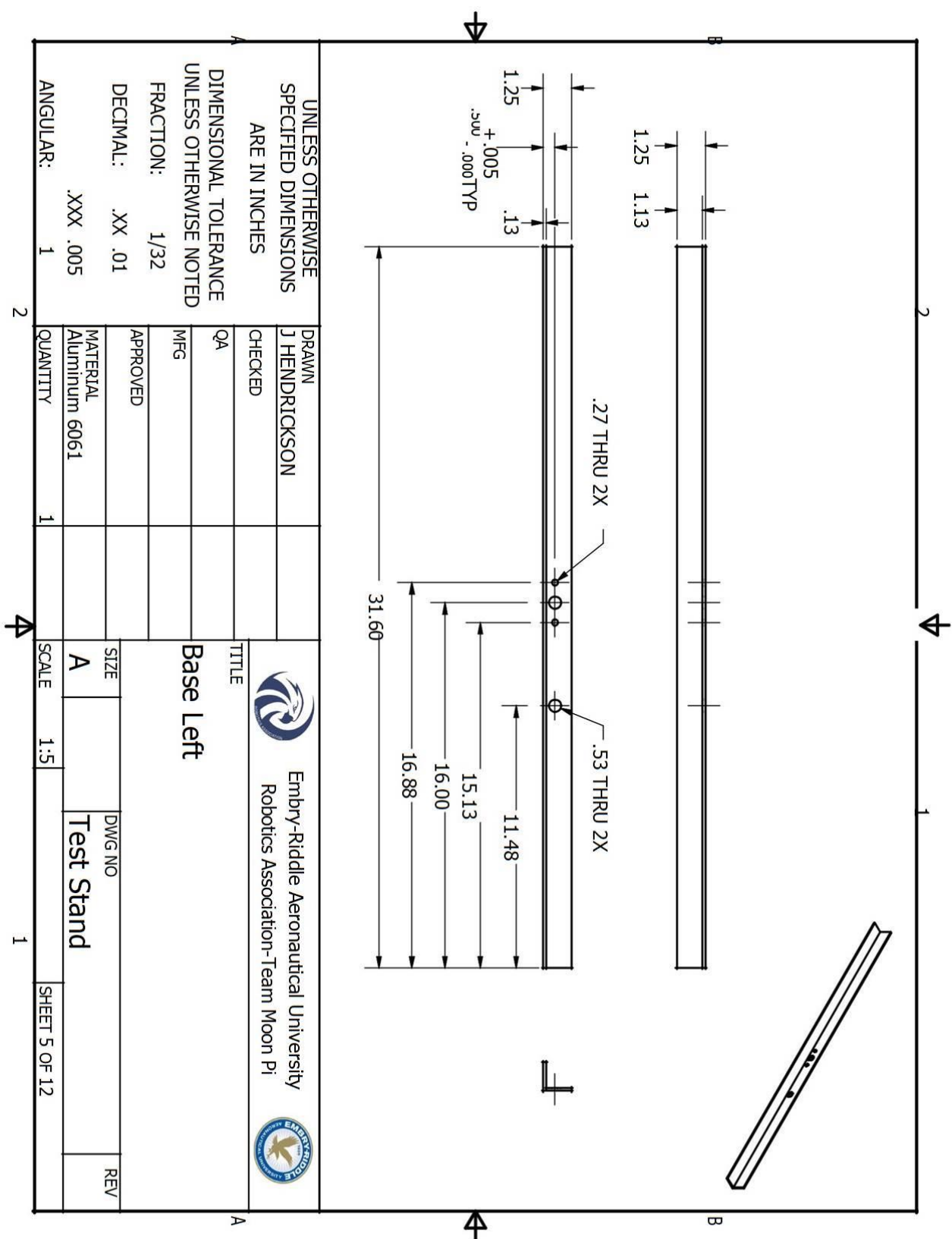
E3 Test Stand Base 5 kg Side Schematic



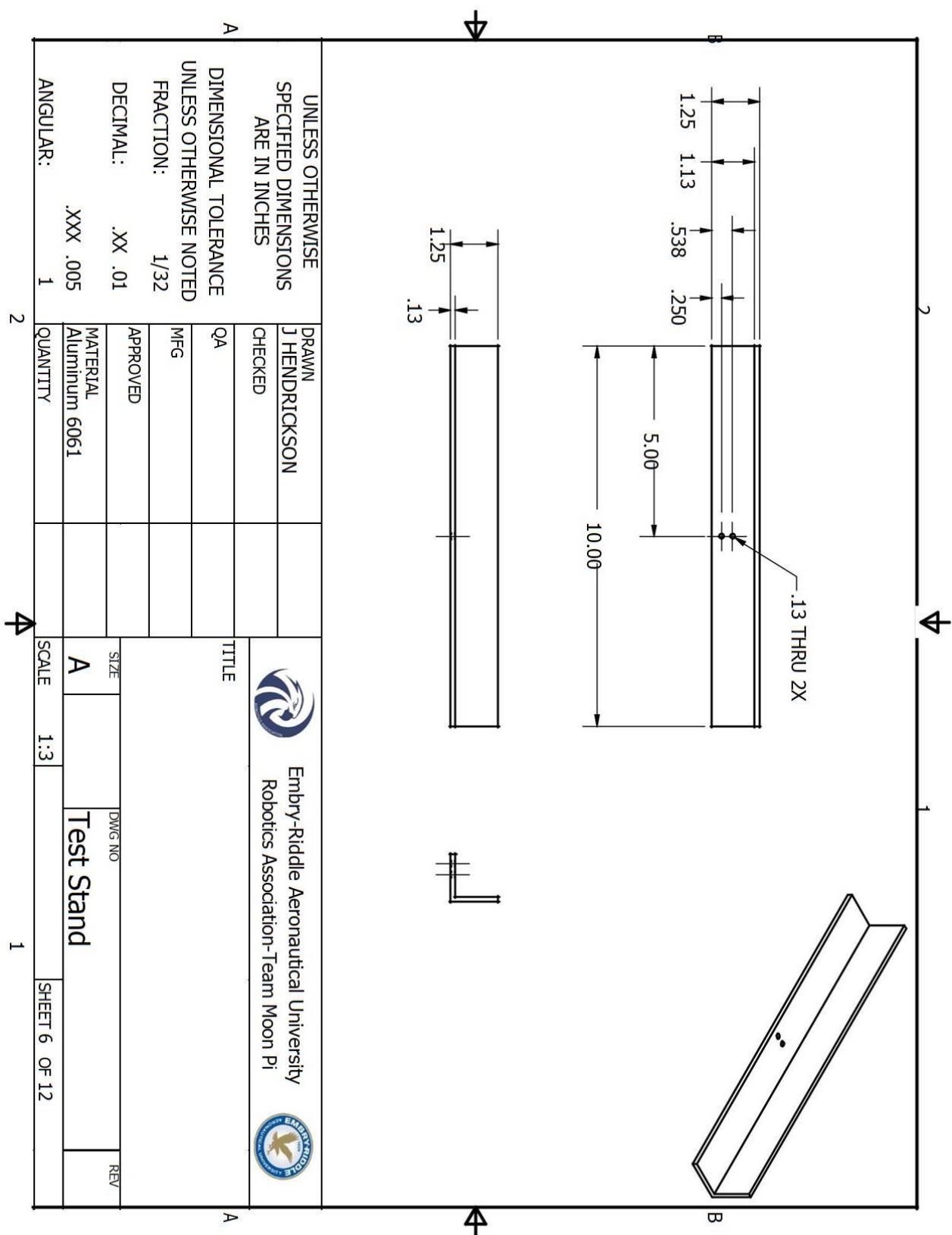
E4 Test Stand Base Right Side Schematic



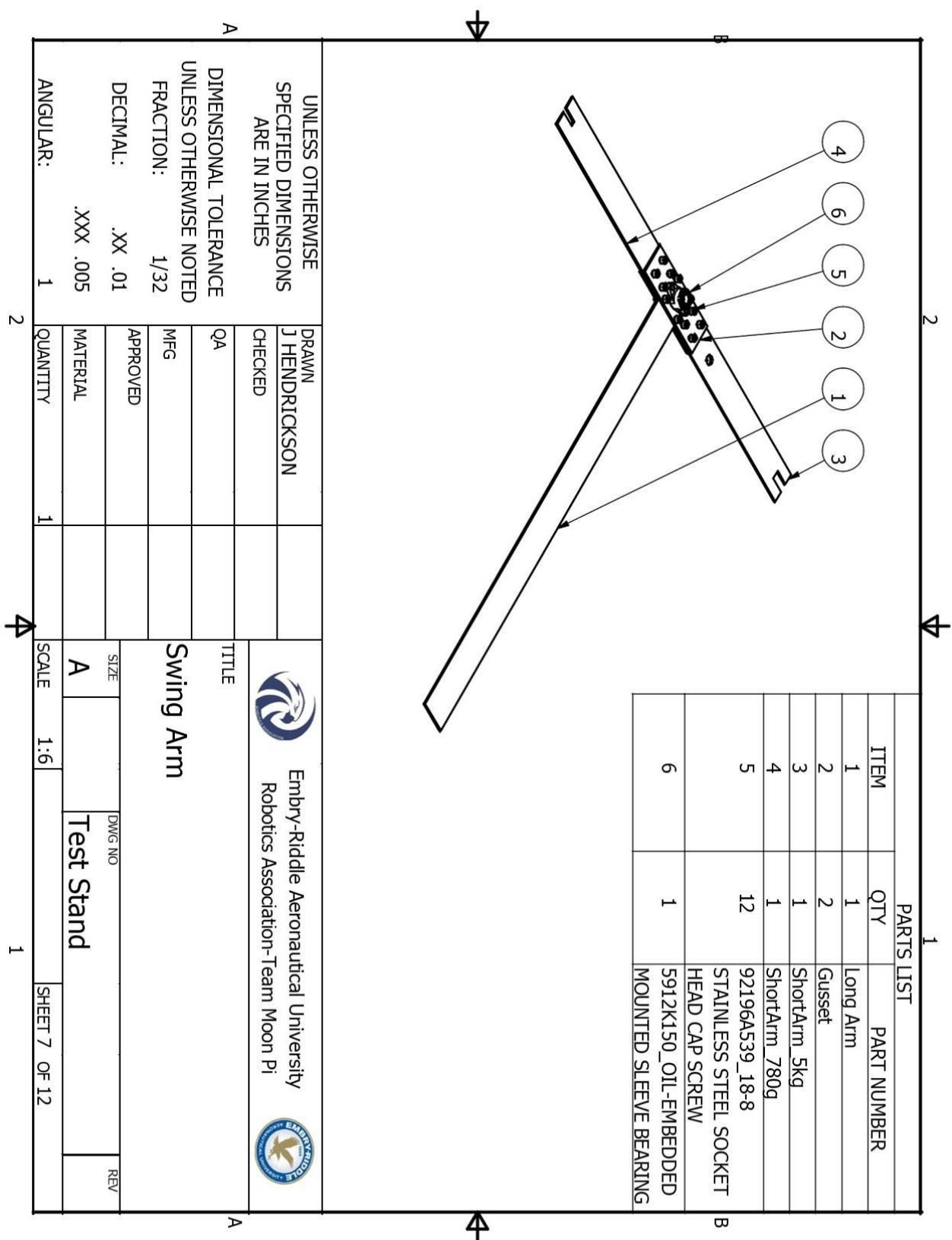
E5 Test Stand Base Left Side Schematic



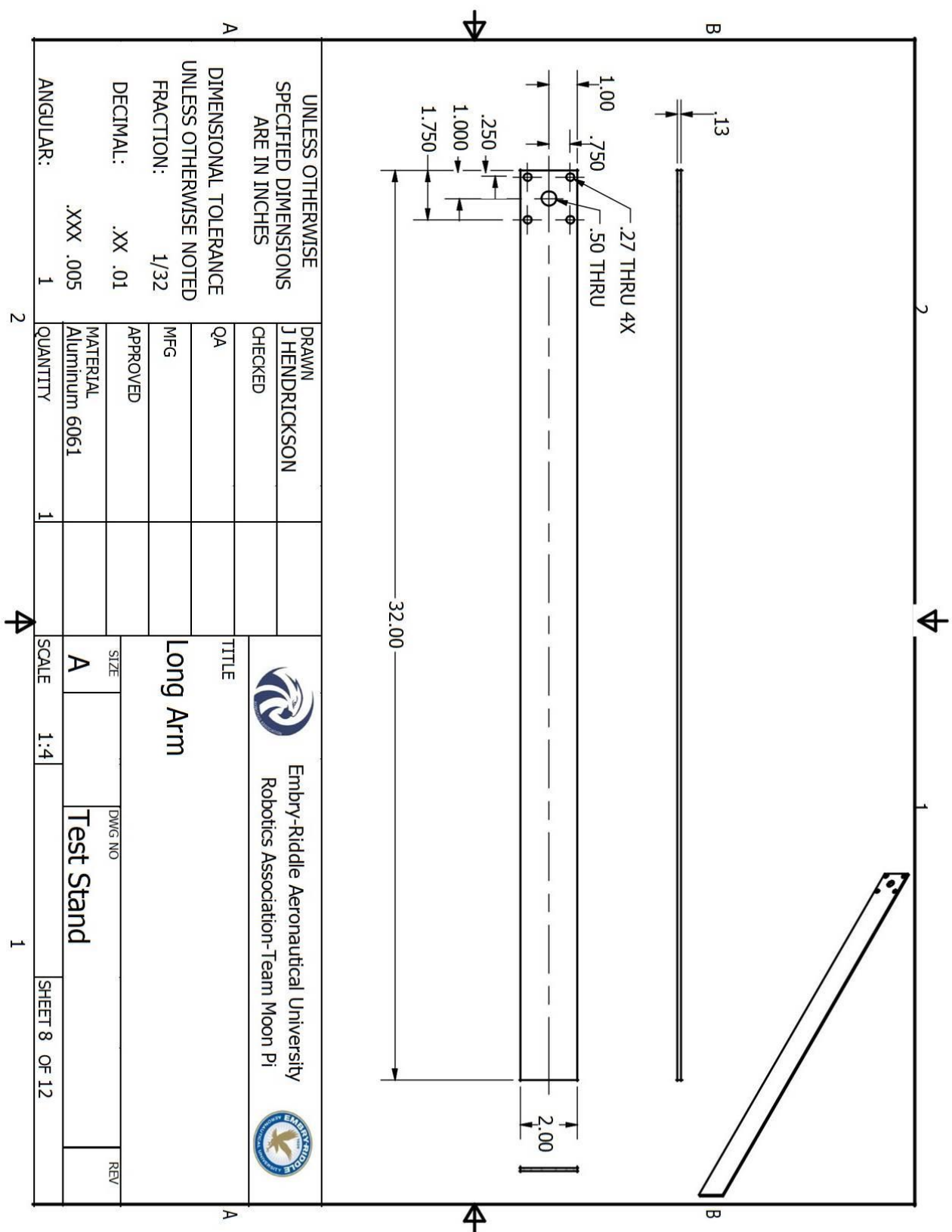
E6 Test Stand Base Top Schematic



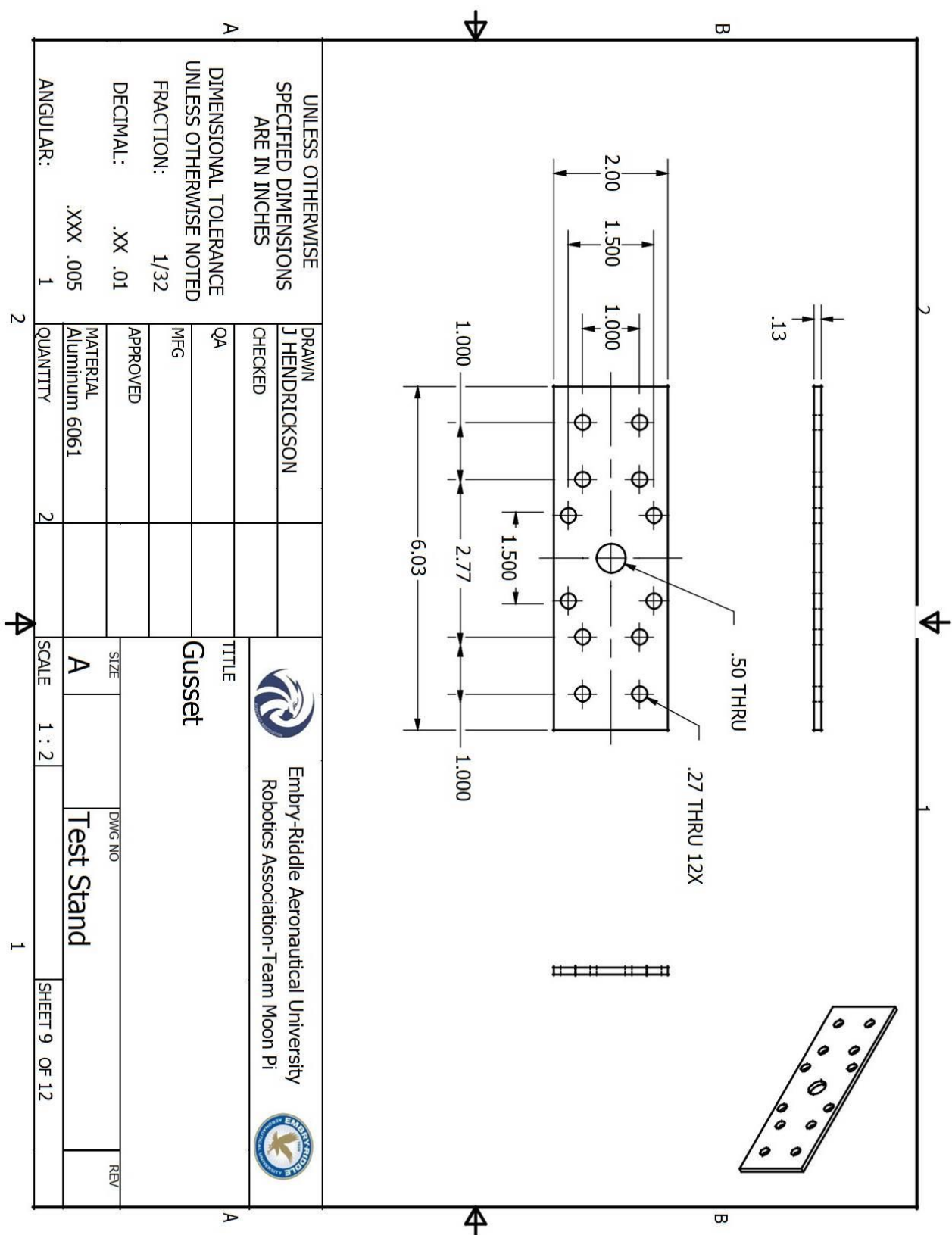
E7 Test Stand Swing Arm Overview



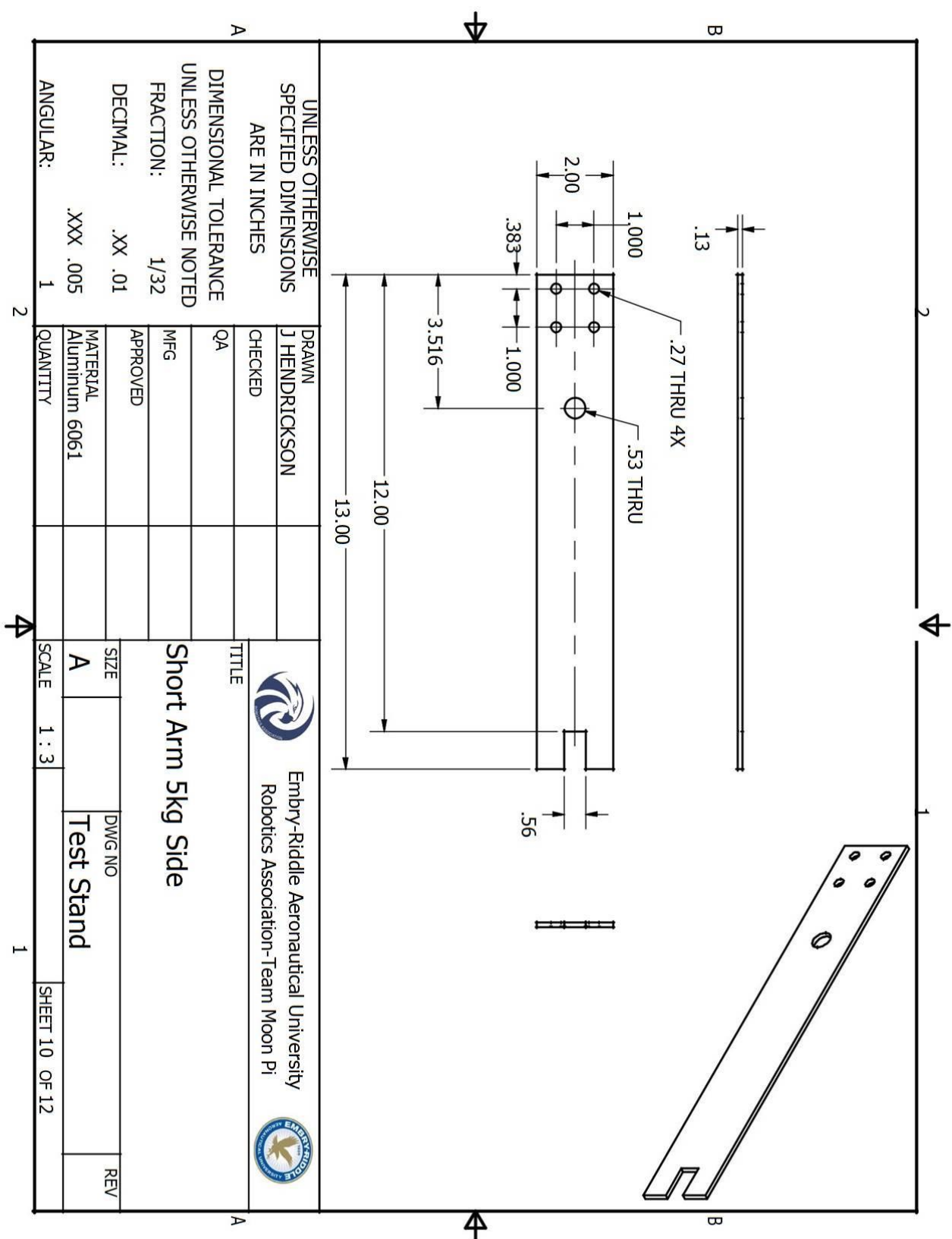
E8 Test Stand Swing Arm Schematic



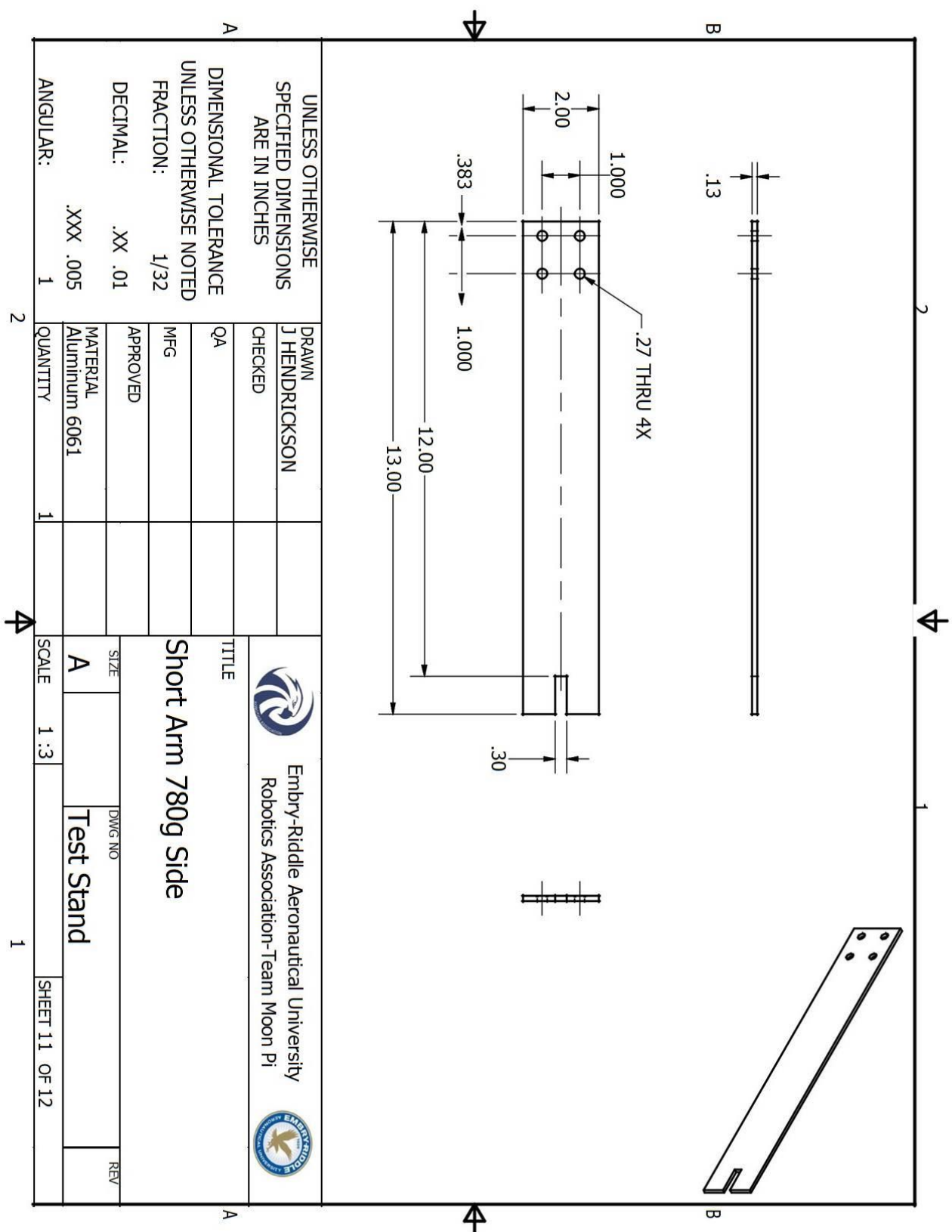
E9 Test Stand Swing Arm Gusset Schematic



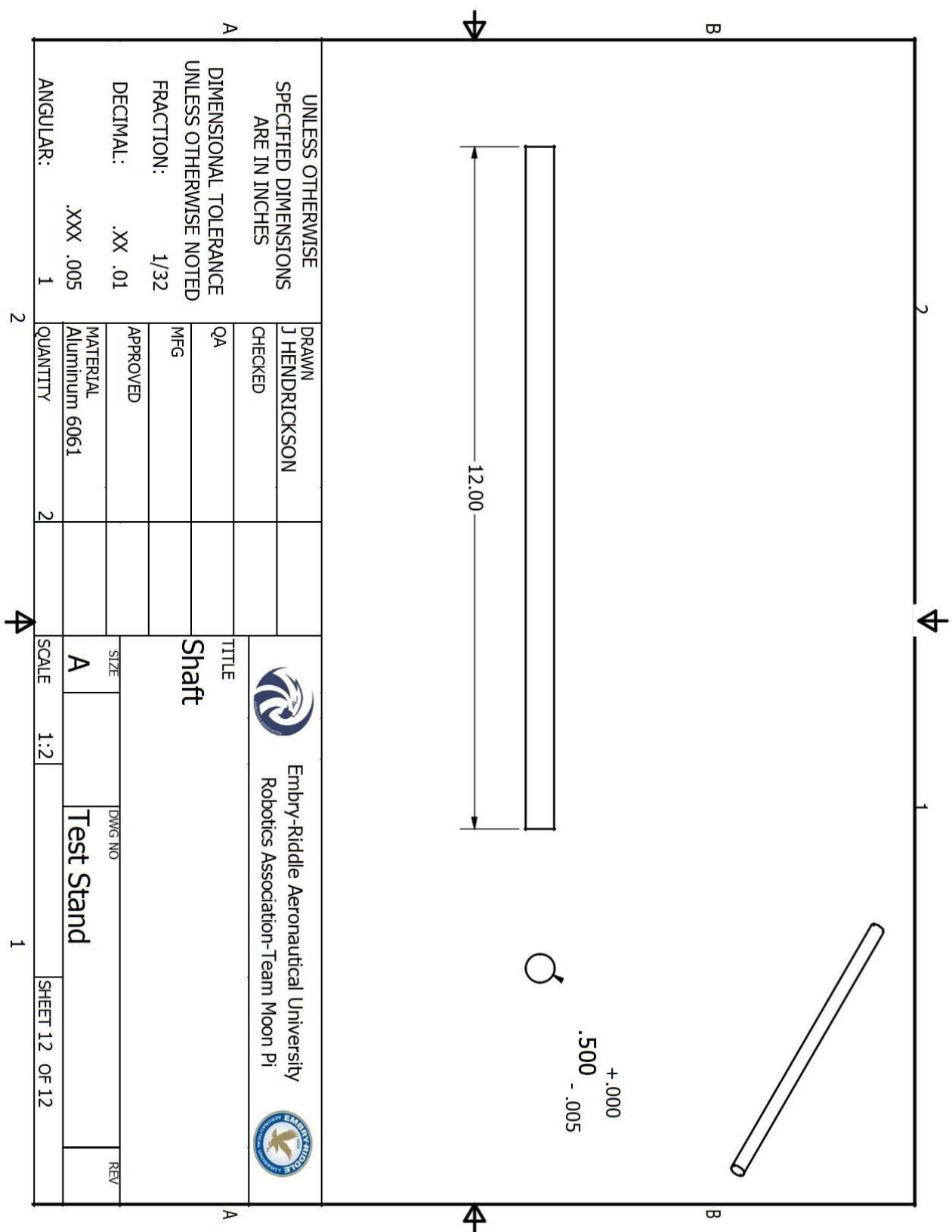
E10 Test Stand Swing Arm Top 5kg Side Schematic

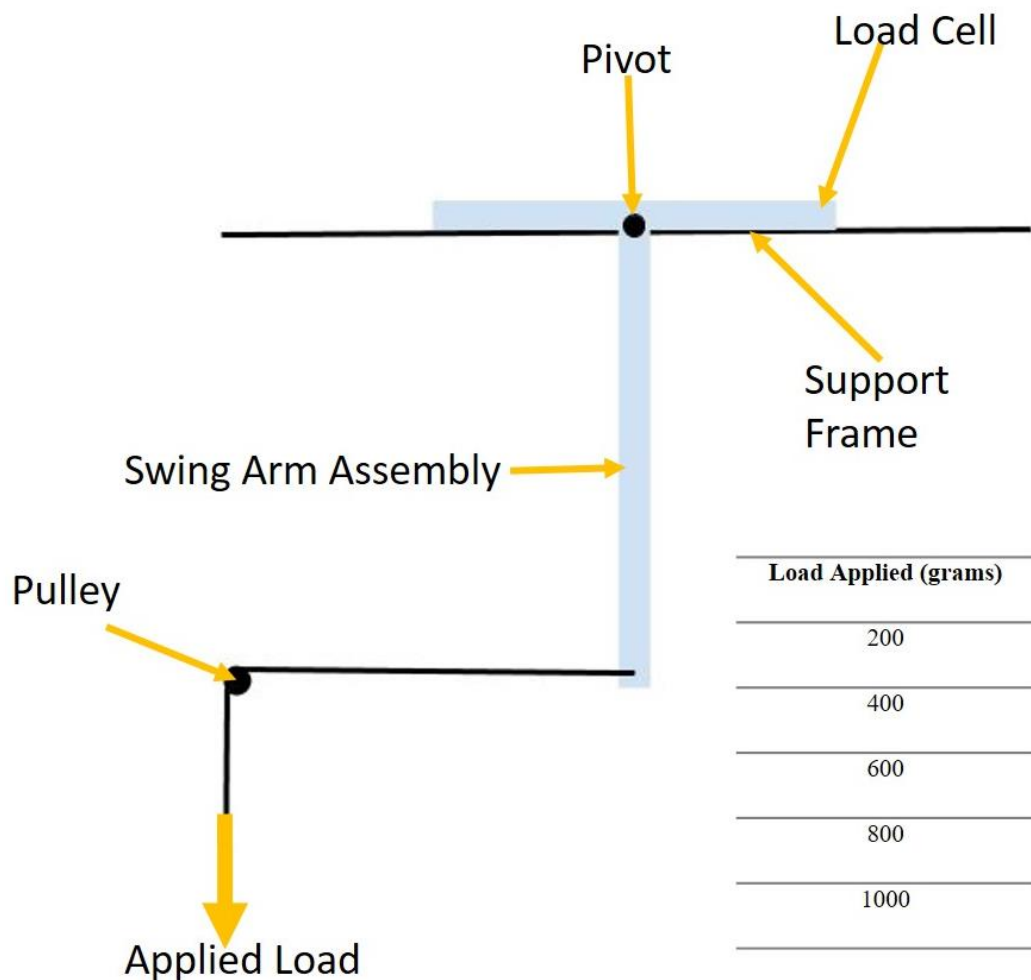


E11 Test Stand Swing Arm Top 0.780 kg Side Schematic

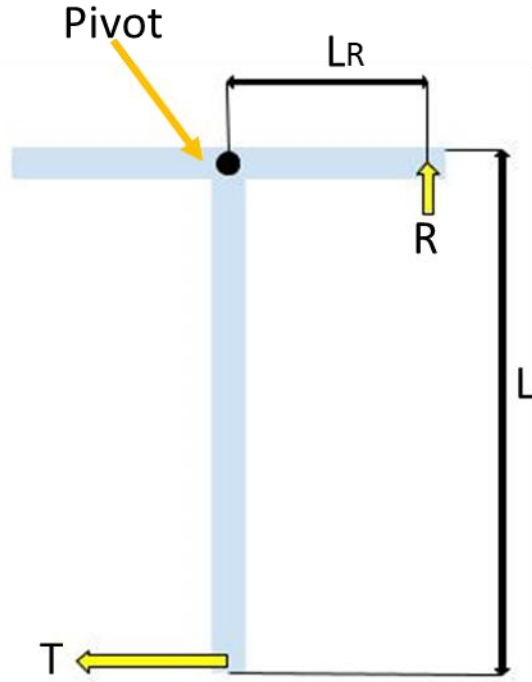


E12 Test Stand Main Shaft



E13 Test Stand Creep Testing Configuration

E14 Test Stand Structural Calculations



Assumptions:

- CCW moments are positive
- Material is 6061 AL
- Bending out of plane is minimal during static operations
- Only swing arm needs analysis as all other materials are thicker, more heavily supported and under lower loading

Physical Properties:

$$T=50.0139 \text{ Newton}$$

$$L=0.7874 \text{ m}$$

$$L_R=0.3302 \text{ m}$$

$$\text{Material Depth } h=y=0.508 \text{ m}$$

$$\text{Material Thickness } b=0.003175 \text{ m}$$

Bending on long arm:

$$\sigma_{max,bending} = \frac{(M_b)y}{I}$$

$$\sigma_{max,bending} = \frac{(TL)y}{\left(\frac{bh^3}{12}\right)}$$

$$\sigma_{max,bending} = \frac{(50.0139N)(0.7874m)(0.0508m)}{\left(\frac{(0.003175m)(0.0508m)^3}{12}\right)}$$

$$\sigma_{max,bending} = \frac{(2.0006Nm^2)}{\left(\frac{(4.16 \times 10^{-7})}{12}\right)}$$

$$\sigma_{max,bending} = \frac{(2.0006Nm^2)}{(3.469 \times 10^{-8}m^4)}$$

$$\sigma_{max,bending} = \frac{(2.0006Nm^2)}{(3.469 \times 10^{-8}m^4)}$$

$$\sigma_{max,bending} = 57.68 \text{ MPa}$$

$$\sigma_{yield,6061T6} = 241 \text{ MPa}$$

$$\text{Factor of Safety} = \frac{\text{yield stress}}{\text{working stress}}$$

$$\text{Factor of Safety} = \frac{241 \text{ MPa}}{57.68 \text{ MPa}}$$

$$\text{Factor of Safety} = 4.17$$

Moment equivalence to calculate reactions:

$$\sum_{pivot-CCW+} M = 0$$

$$\sum_{pivot-CCW+} M = -M_T + M_R$$

$$\therefore M_T = M_R$$

$$M_T = T \times L$$

$$M_R = R \times L_R$$

$$\therefore R = \frac{T \times L}{L_R}$$

$$R = \frac{(50.0139N)(0.7874m)}{0.3302m}$$

$$R = \frac{39.3809Nm}{0.3302m}$$

$$R = 119.264N$$

Bending on short arm

$$\sigma_{max,bending} = \frac{(M_b)y}{I}$$

$$\sigma_{max,bending} = \frac{(RL_R)y}{\left(\frac{bh^3}{12}\right)}$$

$$\sigma_{max_{bending}} = \frac{(50.0139N)(0.3302m)(0.0508m)}{\left(\frac{(0.003175m)(0.0508m)^3}{12}\right)}$$

$$\sigma_{max_{bending}} = \frac{(0.8389Nm^2)}{\left(\frac{(4.16 \times 10^{-7})}{12}\right)}$$

$$\sigma_{max_{bending}} = \frac{(0.8389Nm^2)}{(3.469 \times 10^{-8}m^4)}$$

$$\sigma_{max_{bending}} = 24.19 MPa$$

As the maximum bending moment is less than on the long arm which passes this to will pass.

E15 "Aereon" Lighter Than Air Ship. Retrieved from [17]

Dr. Solomon Andrew's airship "Aereon," in which he proposes ot [sic] cross ocean during Civil War, 1863 [Photograph of Lithograph].

